UNIVERSITY OF HYDERABAD

Tunable coherent perfect absorption in single & multi layered metal-dielectric composite media

by

SANJEEB DEY

A thesis submitted for partial fulfillment of the
Degree of Doctor of Philosophy

School of Physics,
University of Hyderabad,
Hyderabad - 500 046, India.

Declaration of Authorship

I, SANJEEB DEY, declare that this thesis titled, " *Tunable coherent perfect absorption in single & multi layered metal-dielectric composite media*" is the result of my investigation as Ph. D. scholar in the School of Physics, University of Hyderabad, India, under the supervision of Prof. Suneel Singh and the work presented in it are my own. I confirm that:

- This work was done wholly while in candidature for a research degree at this University.
- Where any part of this thesis has not previously been submitted for a degree or any other qualification at this University or any other institution.
- Where I have consulted the published work of others, it is always clearly attributed.
- I have acknowledged all main sources of help.

Signature : _____

Date : _____

Certificate of Authorship

This is to certify that the thesis entitled
"Tunable coherent perfect absorption in single & multilayered metal-dielectric composite media"
submitted by **Sanjeeb Dey** bearing registration number *10PHPH17* in partial fulfillment of the requirement for award of **Doctor of Philosophy** in the School of Physics is a bonafide work carried out by him under my supervision and guidance.

This thesis is free from plagiarism and has not been submitted previously in full or part to this or any other University or Institute for award of any degree or diploma

Parts of this thesis have been :

A.) Published in the following publications :

1. S. Dey, "Coherent perfect absorption using Gaussian beams", Opt. Comm. 356, 515-521, (2015), (ISSN : 0030-4018), Chapter III.
2. S. Dey, S. Singh and D. N. Rao, "Coherent perfect broadband absorption in composite medium", (Manuscript under preparation), Chapter IV.
3. S. Dey and S. Singh, "Concept of coherent perfect absorption", (Manuscript under preparation), Chapter V.
4. S. Dey, "Coherent perfect absorption in space-composite adjustable asymmetric layered media", (Under review), Chapter VI.

B.) Published in Conference proceedings :

1. S. Dey, S. Singh and D. N. Rao, "Coherent perfect absorption in multi-element composite medium", doi.org/10.1364/PHOTONICS.2016.W2C.3 (OSA conference), IIT-Kanpur (Photonics-2016).
2. Sanjeeb Dey and S. Singh, "Coherent perfect absorption with Gaussian beams", doi-10.10.131111 (IEEE explore), IIT-Delhi WRAP-2013.

C.) Oral Presentations :

1. S. Dey, "Coherent perfect absorption in multi-element composite medium", IIT-Kanpur (Photonics-2016) (International conference).

D.) Participation and Poster presentations :

1. S. Dey and S. Singh, "Coherent perfect absorption in composite medium", RAOS-2016 (Recent Advances in Optical Sciences - II), School of Physics, University of Hyderabad, (National).
2. S. Dey and S. Singh, "Coherent perfect absorption with Gaussian beams", IIT-Delhi WRAP- 2013 (International).
3. S. Dey and S. Singh,"Coherent perfect absorption in composite medium", Frontier in Physics - 2013, University of Hyderabad (National).
4. S. Dey and S. Singh, "Basic concept of Coherent perfect absorption", 3rd DAE-BRNS (2012)symposium on Atomic and Molecular Physics, IISER-Kolkata (International).
5. Participate at Indo-Japan International Workshop on Optical Fiber, Nano-photonics and Devices at CGCRI-Kolkata, (International).

Further, the student has passed the following courses towards fulfillment of coursework requirement for **Doctor of Philosophy (Ph. D.)** recommended by Doctoral Committee were the following courses passed.

Course Code	Course Name	Credits	Result
PY-801	Advanced Quantum Mechanics	4	Passed
PY-802	Advanced Statistical Mechanics	4	Passed
PY-803	Advanced Electro-magnetic Theory	4	Passed
PY-804	Advanced Research Methodology	4	Passed

Supervisor **Dean**

(Prof. Suneel Singh) **(Prof. Bindu A. Bambah)**

Date : Date :

School of Physics, University of Hyderabad, Hyderabad-500046, India.

"Go forward without a path,
Fearing nothing, caring for nothing!
Wandering alone, like the rhinoceros!
Even as a lion, not trembling at noises,
Even as the wind, not caught in the net,
Even as the lotus leaf, untainted by water,
Do thou wander alone, like the rhinoceros!"

Swami Vivekananda

Dedicated to

*. * . * . * . * . * . * . * . *

Late Smt. Anjali Dey (Mother)

&

Late Shree Satyendra Nath Dey (Father)

*. * . * . * . * . * . * . * . *

Acknowledgements

It is indeed my pleasure to thanks to all those who have directly or indirectly helped in the successful completion of my entire Ph. D course.

In the presence of the Almighty, in particular, my mother Late Smt. Anjali Dey, who suddenly was diagnosed with terminal illness, wished me to continue my Ph. D work, rather than take a break to serve her. I am indebted to my father Late Shri Satyendra Nath Dey, who took care of my mother during her illness so that I can continue my work to fulfill my mother's wish, and who took ill subsequently and left us. My heartfelt thanks to my brother Mr. Rajib Dey who shouldered additional responsibility on my behalf as well, in taking care of the both ailing parents, in their difficult moments.

But the hard days did not end. We brought my father to Hyderabad. He was diagnosed with having multiple myeloma. His treatment and my research were going side by side. His health deteriorated day by day and he finally left us last year.

I would like to express my profound sense of gratitude to Prof. Seyed E. Hasnain, the former Vice Chancellor, for granting me the University Fellowship, sparing me the financial hardship, during my most difficult times.

I would like to express my deep sense of gratitude to my thesis Advisor Prof. Suneel Singh, for his patient guidance, continued support and encourage through the course of my research. Without his invaluable suggestions and several helpful discussions, I would not have been able to see this day in my research career. I would also like to add that the encouragement and freedom he has given me to work independently on some problems of my interest, has helped me to become more confident at what I have been doing.

I would like to extend my gratitude to the former Deans, Prof. Bansal, Prof. Tewari, Prof. Chaturvedi, Prof. Rajender Singh and the current Dean, Prof. Bindu A. Bambah, for extending to me all the facilities of School of Physics.

I also would like to thank my doctoral Committee members Prof. Anantha Lakshmi and Dr. Ashoka Vudayagiri, for their valuable suggestions. I am also thankful to Prof. D. Narayana Rao, Prof. C.S. Sunandana and all the faculty members of Quantum Optics group of School of Physics, for their support at various stages.

I would also like to thank my former supervisor Prof. Subhasish Duttagupta for the training on basic modern optics.

I also thank Mr. Suresh Babu Sajja and Mr. K. Srinivas for helping in computing in many stages and Mr. T. Abraham & all supporting staff of School of Physics, Fellowship Section and Library for their help.

I am grateful to all my former teachers who have taught me at school, intermediate, undergraduate and postgraduate levels for inspiring me to learn the subject.

I would like to thank my colleagues and friends Dr. Sanjeev Kumar., Dr. Siva N. Chari, Dr. N. Shankaraiah, Dr. Ravikanth Verma, Dr. Sachin, Dr. Raju Botta, Dr. Ram Soorat and all my batchmates for their support during my stay in the University.

I am also grateful to Mr. Rajib Dey (brother), Smt. Debashri Dey (Garai) (wife) and Mr. Sourodeep Dey (son) for standing beside me in good and bad times.

My humble obeisance to GURUDEB RAMTHAKUR for all his Love and Grace.

Finally, I am much indebted to my PARENTS in many ways for their love, affection, support and encouragement in my life and career.

Sanjeeb Dey

List of Figures

Contents

Chapter 1

Introduction

One of the major pursuits of optical research over the years has been to achieve perfect absorption in novel materials that have been artificially developed from naturally occurring materials. Research in this field continues to elicit considerable interest in recent times as is evident from numerous studies devoted to development of strongly absorbing materials or devices. Many researchers have explored the possibility of perfect absorption in devices with plasmonic structures and meta-materials [1, 2, 3, 4, 5] in the past.

More recently, coherent perfect absorption using symmetric illumination of an absorber from both sides by identical light waves was proposed theoretically by Y. D. Chong and coworkers [4, 1] from Yale. Coherent perfect absorption (CPA), as the name suggests, is the process in which incident coherent electromagnetic radiation is completely absorbed in a medium. Such a medium is called a coherent perfect absorber. The absorbed electromagnetic energy may appear as some other form of internal energy such as thermal or electrical energy. As this function of the medium is exactly opposite to that of a laser – which converts some form of incoherent energy such as thermal or electrical energy into coherent light- the medium is also called an anti lasing device or anti-laser.

Subsequently, S. Longhi [8] proposed a fascinating feasibility of combining a laser and an anti-laser in a single device utilizing an optical medium that satisfies the PT (parity-time) symmetry condition for the dielectric constant. The device was then shown to perform simultaneously as a laser oscillator

by emitting coherent waves and as a coherent perfect absorber, fully absorbing incoming coherent waves with the right amplitudes and phases. The first practical demonstration of CPA was reported in 2011 by the same group - W. Wan and coworkers [2] from Yale, which proposed CPA in 2010. The initial proposals of CPA in a silicon wafer functioning as solid Fabry-Perot resonator were however limited to narrowband perfect absorption.

Since then CPA has been studied in several materials using various geometries for active device applications. S. Longhi further derived conditions for CPA, considering the time-reversed process of lasing in a homogeneously broadened two-level medium in an optical cavity. He demonstrated that the frequency of the field at which CPA occurs is generally different than the one of the lasing mode due to the breakdown of exact time-reversal symmetry [10]. J. W. Yoon et al. experimentally demonstrated total absorption of light mediated by surface-plasmon excited in Au grating on silicon substrate [11]. M. Pu et al. proposed an approach for designing a wide-angle perfect plasmonic nanostructure absorber at infrared frequencies [12]. M. Pu and coworkers also later utilized heavily doped silicon as tunable metal for broadband nearly perfect absorption in the terahertz frequency region with symmetrical coherent illumination [4]. H. Noh et al. demonstrated complete absorption and transfer of coherent light to surface plasmons in two- or three-dimensional metallic nanostructures by exciting it with the time-reversed mode of the corresponding surface plasmon laser ("spacer") [3]. T. Chen et al. demonstrated through classical electrodynamics based analysis of one- and two-beam coherent perfect absorbers, that the two-beam device can be configured to function as a phase-controlled three-state switch [15]. Making use of the properties of a slab with negative refraction and small losses, V. Klimov et al. have proposed an interesting concept of coherent perfect nano-absorbers (CPNAs) [16]. Ming Kang, et. al. reported the feasibility of polarization-independent coherent perfect absorption by simple dipole-like metasurface [17]. Y. D. Chong and coworkersinvestigated the noise properties of coherent perfect absorbers [18] to estimate the fundamental limits to its effectiveness as a background-free detector or interferometer imposed by finite signal or detector bandwidth. Based on the devices utilizing the properties of white-light cavities for broadband coherent perfect absorption, O. Kotlicki and J. Scheuer proposed new integrated-optics-based pulse absorber/terminator and optical modulator [19]. CPA has also been studied in nano-structured graphene and meta-surface

graphene [6, 7]. H. Park et. al. proposed a metal-insulator-metal waveguide based design of ultra-compact plasmonic coherent perfect absorber (CPA) operating in the near-infrared band [22]. Agarwal et al. have demonstrated the persistence of perfect photon absorption [23] in the nonlinear regime of the cavity quantum electrodynamics (CQED) below the threshold of optical bistability.

Recently T. Roger and coworkers experimentally demonstrated the occurrence of coherent perfect absorption process [24] in the single-photon regime in deeply subwavelength films. Their work opens up the possibility of a number of applications ranging for example from the development of single photon sensors in ultrathin film materials to highly efficient coupling of single photons to single plasmons for applications in quantum plasmonics.

Thus the tremendous interest in CPA phenomenon is seen to stem from its potential use in the development of numerous modern day applications such as, in designing generic detectors and switches (by means of perfect absorption interferometry) for efficient detection of coherent light signals of specific frequencies, nano-devices for quantum computation etc..

1.1 Coherent perfect absorption: concept

Physically coherent perfect absorption is a consequence of destructive interference between reflection and transmission (at interfaces) of two identical electromagnetic fields incident from 'left' and 'right' on two opposite faces of a dielectric slab in a symmetric illumination configuration. The incident beams from 'left' and 'right' multiply scatter within the slab with just the right amplitude and phase so that the total transmitted and reflected beams destructively interfere on both interfaces, leading to zero scattering through the interfaces or perfect absorption in the medium.

To illustrate this, let us consider first a plane electromagnetic wave incident (from left) at an angle θ (with respect to the normal to the interface) upon the 'left' interface of air (medium 1) and a dielectric slab (medium 2) of certain thickness. Part of the light is reflected back (in medium 1) at an angle θ and transmitted (in medium 2) at angle θ_t.

The transmitted field (in medium 2) undergoes multiple scattering within the dielectric slab and is partly transmitted through the other (right) interface of the dielectric slab (medium 2) and air (medium 3). The reflection coefficient r_L (at left interface) and transmission coefficient t_L (at right interface)

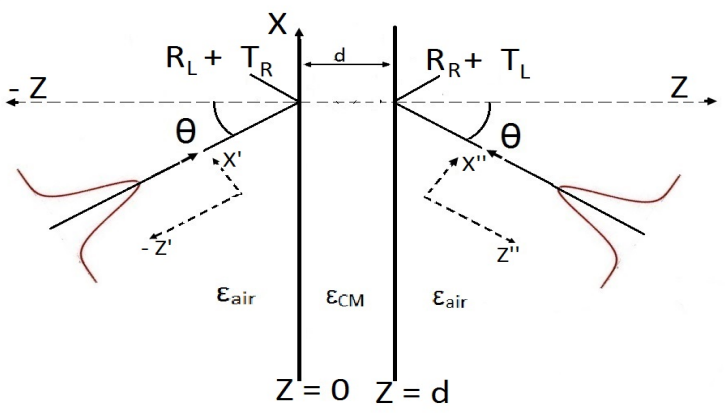

Figure 1.1: Two identical lights incident (at same angle θ) on the two air-CPA medium interfaces from both sides.

due to the (field from left) can be determined through appropriate boundary conditions on the electric and magnetic fields at the interfaces. It maybe noted that the subscripts 'L' in the reflection and transmission coefficients denote the electromagnetic field from 'left'.

Now consider another identical plane electromagnetic wave incident (from right) at an angle θ (with respect to the normal to the interface) upon the 'right' interface of the dielectric slab (medium 2) and air (medium 3). In the same manner outlined above, the reflection coefficient r_R (at right interface) and transmission coefficient t_R (at left interface) amplitudes for the (field from right) can be determined through appropriate boundary conditions on the electric and magnetic fields at the interfaces.

As the medium is linear, superposition principal holds and the net field at any of the two interfaces, for example, at 'left' interface, is the superposition of reflection coefficient r_L (of left field) and transmission coefficient t_R (of right field). The field scattering out of any interface is governed by the nature of interference between these two coefficient at that interface. Perfect absorption will occur if the net field at either interface is zero. That is if (at left interface, for example) the reflection coefficient r_L (of left field) and the transmission coefficient t_R (of right field) are equal in magnitude and opposite in phase. Similarly if (at right interface, for example) the reflection coefficient r_R (of right field) and the transmission coefficient t_L (of left field) are equal in magnitude and opposite in phase the the net scattering out of right interface

will vanish. Thus the fields multiply scatter within the slab leading to zero scattering through the interfaces or perfect absorption in the medium. This qualitatively is the essence of coherent perfect absorption. Detailed quantitative analysis is presented in subsequent chapters.

Therefore from preceding discussion it is obvious that owing to their tremendous scope for potential application, search for novel materials or devices that are strongly absorbing is of considerable interest in recent times. Of particular interest here is the prospect of utilizing composites materials for studying coherent perfect absorption.

1.2 Composite medium:

Optical properties of a material depend on the nature of interaction of its microscopic constituents (atom, molecules etc.) with electric and magnetic fields of applied electromagnetic radiation which may result in non-uniform distribution (at microscopic scales) of fields called local fields in the medium. In reality however, one need not go to microscopic level as the overall average response of a material, as a whole is expressed by the two macroscopic effective material parameters: **permittivity** ϵ and the **permeability** μ of the material. Moreover at optical frequencies, this complicated physics (occurring at microscopic scale) has macroscopic manifestation in the form of reflection, transmission and absorption /dispersion in the material. These macroscopic phenomena arising out of light-matter interactions (at microscopic scales) can be analyzed using Maxwell's equations which are the set of equations with interrelationship between fields, sources, and material properties.

The fields that appear in Maxwell's equations are the macroscopic fields where the microscopic features of structural homogeneities and the local fields are averaged out. This averaged response of the medium to the fields appears in form of following two constitutive relations between electric field E, the magnetic field H, the electric displacement field $\vec{D}$, and the magnetic flux density $\vec{B}$:

$$\vec{\mathbf{D}} = \epsilon\vec{\mathbf{E}} \tag{1.1}$$

$$\vec{\mathbf{B}} = \mu\vec{\mathbf{H}} \tag{1.2}$$

Thus the **permittivity** ϵ and the **permeability** μ establish relationship between the macroscopic field vectors in Maxwell's equations. The parameters

ϵ along with another related parameter – **refractive index**, "$n = (\sqrt{\epsilon\mu})$" provides a complete description of the response of a material to the electric field of an electromagnetic wave. In general the dielectric constant may be complex resulting in a complex value of the refractive index the imaginary part of which is used to describe the energy absorbed in the material. Moreover at optical frequencies, the relative permeability μ is taken normally to be unity hence in what follows we will assume μ =1.

Similar considerations apply to a composite material made by mixing two different materials possessing distinct **permittivities** ϵ_1 and ϵ_2. What is the response of such a material to the applied electromagnetic fields?

In this work we are interested in a composite medium arising out of a mixture of a dielectric (SiO_2) and one or more metals (Au, Ag etc.). In such a metal-dielectric composite material small (usually nanosized) metal clusters are formed as shown in the figure below.

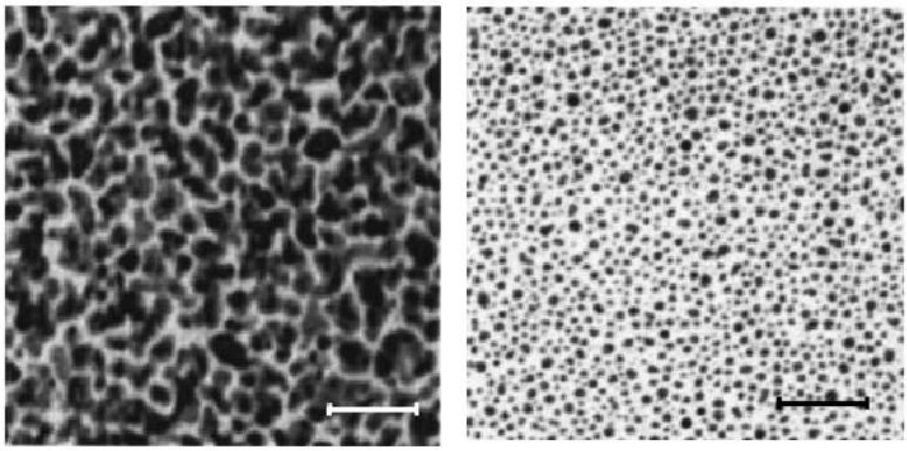

Figure 1.2: A typical composite medium [6] displaying metal (dark dots) and dielectric (light areas) components. First and second figure belong to high and low concentration respectively. Scale: bar is 200 nm

These metal clusters are segregated by dielectric (insulator). Hence the previously free electrons of the metal are localized (confined) to small (cluster) region and they can no longer move as freely through the medium as in bulk metal. Collective oscillation of these localized electrons is called localized plasmons and their frequency response is similar to that of simple harmonic oscillator model of (bound) electrons. Moreover at higher metal concentrations, there could be interaction between clusters as any optically excited

cluster is influenced by the field scattered by its neighbours. Consequently in a dielectric environment, any increase in the volume fraction of metal typically results in an increase in overall absorption and broadening and red-shift of the (localized) plasmon resonances.

If both the size of metal clusters and typical inter-cluster distances are much less than wavelength of visible radiation then it is possible to tackle the metal-dielectric mixture as an optically homogeneous material. For a disordered distribution where the metal and dielectric components are arranged randomly in the medium, generalized analytic approaches exist, that using the mean-field approximation estimate the average electromagnetic response of composite materials in terms effective dielectric function ϵ_{eff} of the macroscopically uniform medium. This effective dielectric function is given in terms of the permittivities of the individual components as well as their respective volume fractions.Two such popularly used effective medium theories are : Bruggeman effective medium theory ($BEMT$) [6, 11, 12] and Maxwell–Garnett theory (MGT) These two methods have different assumptions in regard to the composition and the material properties of each constituent in the mixture. Usually MGT is found to be valid for only low volumes of inclusions. Whereas $BEMT$ produces results identical to those of MGT at lower volumes of inclusions and thereafter it is capable of predicting many other interesting effects that MGT cannot as it fails at higher inclusion volumes. In the regime of our interest, we have found the Bruggeman effective medium theory is better suited for estimation of the effective permittivity of the composite.

1.3 Motivation:

Previous studies have shown that generally the optical properties of the composite can differ considerably from those of its individual constituents [6, 11, 12, 9, 13, 14, 15]. The biggest advantage of a composite medium lies in the fact that its optical properties can be tailored to suit the need of the experiment through variation of composition of its components or by changing its thickness. This property of composites renders them as ideal materials for realizing tunable CPA.

Although a few reports of investigation of CPA in composite materials [5] have appeared, there still remains a tremendous scope for further studies. For instance, most of the existing studies of CPA are restricted only to

plane electromagnetic wave approximation for the incident radiation. In real experiments the incident beams are not strictly plane waves but may have a certain intensity profile such as for example, a Gaussian intensity profile for beams derived from laser sources. There also is the issue of the bandwidth of absorption which is very narrow or is only restricted to specific frequencies whereas for many practical applications such as for harnessing solar energy it is imperative to have broadband absorption. In this context it would be of interest to undertake development, characterization and determination of optical properties of new composite materials for their use as perfect absorbers. This thesis is an endeavour in that direction. The organization of the thesis is as follows:

Chapter 2: The second chapter presents a theoretical scheme for developing composite materials that shall be used as medium for the study CPA in the later chapters. The aim here is to develop a formalism to numerically characterize the optical properties of composite materials as a function of various parameters such as the volume fraction of the constituents, wavelength of the incident radiation etc... The composites materials for CPA considered here are nonmagnetic (i.e. μ=1). Considering the composites materials as mixture of metals and dielectrics, various composite materials comprising two and three constituents - a dielectric (SiO2) and one or more metals (Au, Ag or Cu) of varying volume fractions are studied. Variation of the effective dielectric constant of the composite material as a function of the wavelength of the incident radiation and volume fraction of constituents is estimated numerically. For this purpose the more versatile Bruggemann effective medium theory is utilized since it imposes no restriction on the volume fraction and the number of constituents in the composite. The permittivity of metals for all wavelengths was obtained by interpolating numerically the "experimental data" of Johnson and Christy [8, 4]. The methodology developed here enables us to evaluate and optimize the permittivity of composites of arbitrary dielectric-metal composition.

Chapter 3: The third chapter consists of a numerical study of CPA in a composite material (CM) comprising two constituents - a dielectric (SiO2) and a metal (Au, Ag or Cu), the effective dielectric constant of which was estimated in the previous chapter using Bruggemann theory. Thereafter CPA is studied in this two-component composite material for the more realistic case

of Gaussian beams [8, 4]. This is because in real experiments, laser beams (with Gaussian profile) are used as incident electromagnetic radiation for illumination on both sides of a thin slab of composite medium. Thus in this way our study presented in this chapter differs from earlier works [5] which approximated incident radiation as plane electromagnetic waves. Our results indicate no adverse effects of beam profile, proving the existence of CPA even for Gaussian beams.

Chapter 4: In fourth chapter we explore numerically, the occurrence of CPA in a thin slab of three-component composite material - comprising a dielectric (SiO2) and two metals (Au and Ag) the optical properties of which were explored earlier in chapter 2. As stated earlier the aim here is to explore novel materials that can provide CPA, in addition of single frequency tunable, also over a broad range of wavelengths (or frequencies) as they may have many practical applications such as, in designing solar cells etc.. CPA in three elements (metal-metal-dielectric) CM is observed for both normal and as well as oblique incidences and a few more related issues are explored further in this chapter.

Chapter 5: In fifth chapter a theoretical formalism of CPA is presented. This theoretical treatment of CPA involves determining the reflection and transmission amplitudes at the two interfaces on either side of the CPA medium. This is accomplished by first obtaining the form of electromagnetic fields from solutions of Maxwell's equation in CPA and adjoining media. Thereafter boundary conditions on fields at each of the two interfaces namely, continuity of the tangential components of the electric and magnetic fields yields the reflection and transmission amplitudes at the two interfaces. Using these, an expression for the occurrence of CPA is derived. The numerically obtained parameters in the previous chapter when used in this expression are found to satisfy the CPA condition. Thus this expression provides us with a means to determine the range of parameter values for occurrence of CPA such as, wavelength of the incident radiation, the dielectric constant and thickness of the CM slab.

Chapter 6: Continuing our quest for new materials, in the sixth chapter we investigate CPA in a thin slab of layered medium under illumination on both sides by narrow laser beams at oblique incidence. The layered medium

is designed using a few layers of metal-dielectric composite and spacer (air) medium. The main advantage of this medium is that it is possible to create asymmetric slab structure by moving a composite layer into spacer layers. CPA in both asymmetric and symmetric structures were observed and the differences in results obtained were compared and contrasted to highlight the role of asymmetry in structure.

Chapter 7: Finally, we have summarized the main points of our study and highlighted our results in seventh Chapter.

Bibliography

[1] N. I. Landy, S. Sajuyigbe, J. J. Mock, D. R. Smith, and W. J. Padilla, "Perfect metamaterial absorber", Phys. Rev. Lett. 100 , 207402 (2008).

[2] T. V. Teperik, F. J. García de Abajo, A. G. Borisov, M. Abdelsalam, P. N. Bartlett, Y. Sugawara, and J. J. Baumberg, "Omnidirectional absorption in nanostructured metal surfaces", Nat. Photonics 2(5), 299 (2008).

[3] M. Diem, T. Koschny, and C. M. Soukoulis, "Wide-angle perfect absorber/thermal emitter in the terahertz regime", Phys. Rev. B 79 (3), 033101 (2009).

[4] E. E. Narimanov, and A. V. Kildishev, "Optical black hole: Broadband omnidirectional light absorber", Appl. Phys. Lett. 95, 041106 (2009).

[5] G. Nimtz and U. Panten, "Broad band electromagnetic wave absorbers designed with nano-metal films", Ann. Phys. 19, 53 (2010).

[6] Y. D. Chong, L. Ge, H. Cao and A. D. Stone, "Coherent Perfect Absorbers: Time-Reversed Lasers", Phys. Rev. Lett. 105, 053901 (2010).

[7] C. F. Gmachl, "Suckers for light", Nature 467, 39 (2010).

[8] S. Longhi, "PT-symmetric laser absorber", Phys. Rev. A 82, 031801(R) (2010).

[9] W. Wan, Y. D. Chong, L. Ge, H. Noh, A. D. Stone, and H. Cao, "Time-reversed lasing and interferometric control of absorption", Science 331, 889 (2011).

[10] S. Longhi, "Coherent perfect absorption in a homogeneously broadened two-level medium,", Phys. Rev. A 83, 055804 (2011).

[11] J. W. Yoon, W. J. Park, K. J. Lee, S. H. Song, and R. Magnusson, "Surface-plasmon mediated total absorption of light into silicon", Opt. Exp. 19, 20673 (2011).

[12] M. Pu, C. Hu, M. Wang, C. Huang, Z. Zhao, C. Wang, Q. Feng, and X. Luo, "Design principles for infrared wide-angle perfect absorber based on plasmonic structure", Opt. Express 19, 17413 (2011).

[13] M. Pu, Q. Feng, M. Wang, C. Hu, C. Huang, X. Ma, Z. Zhao, C. Wang, and X. Luo, "Ultrathin broadband nearly perfect absorber with symmetrical coherent illumination", Opt. Exp. 20, 2246 (2012).

[14] H. Noh, Y. Chong, A. D. Stone, and H. Cao, "Perfect coupling of light to surface plasmons by coherent absorption", Phys. Rev. Lett. 108, 186805 (2012).

[15] T. Chen, S. Duan, and Y. C. Chen, "Electrodynamics analysis on coherent perfect absorber and phase-controlled optical switch", J. Opt. Soc. Am. A 29, 689 (2012).

[16] V. Klimov, S. Sun and Guang-Yu Guo, "Coherent perfect nanoabsorbers based on negative refraction", Opt. Exp. 20, A13071 (2012).

[17] M. Kang, F. Liu, T. F. Li, Q. H. Guo, J. Li, and J. Chen, "Polarization-independent coherent perfect absorption by a dipole-like metasurface", Opt. Lett., 38, 3086 (2013).

[18] Y. D. Chong, Hui Cao and A. D. Stone, Physical Review A 87, 013843 (2013).

[19] O. Kotlicki and J. Scheuer, "Wideband coherent perfect absorber based on white-light cavity", Opt. Lett. 39, 6624 (2014).

[20] J. Zhang, "Coherent perfect absorption and transparency in a nano structured graphene film", Opt. Exp. 22, 12524 (2014).

[21] Y. Fan, "Tunable mid-infrared coherent perfect absorption in a graphene meta-surface", Sci. Rep. 5, 13956 (2015).

[22] H. Park, S. Y. Lee, J. Kim, B. Lee, and H. Kim, "Near-infrared coherent perfect absorption in plasmonic metal-insulator-metal waveguide", Opt. Exp. 23, 24464 (2015).

[23] G. S. Agarwal, Ke Di, L. Wang and Y. Zhu, "Perfect photon absorption in the nonlinear regime of cavity quantum electrodynamics", Phys. Rev. A 93, 063805 (2016).

[24] T.Roger, S. Vezzoli, E. Bolduc, J. Valente, J.J.F. Heitz, J. Jeffers, Cesare Soci,J. Leach1, C. Couteau2,5,6, N. I. Zheludev2,3 and D. Faccio, "Coherent perfect absorption in deeply subwavelength films in the single-photon regime", Nature Commun., 6:7031(2015).

[25] D. G. Sourya, O. J. F. Martin, S. Dutta Gupta, G. S. Agarwal, "Controllable coherent perfect absorption in a composite film", Opt. Exp. 20, 1330(2012).

[26] S. Dey, "Coherent perfect absorption using Gaussian beams", Opt. Comm. ,Vol.356 , pp. 515-521(2015).

[27] S. Dey and S. Singh, "Coherent perfect absorption with Gaussian beams", IIT-Delhi-WRAP2013-10.10.131111.

[28] P. B. Johnson and R. W. Christy, "Optical constants of the noble metals", Phys. Rev. B, Vol.6, pp. 4370–4379(1972).

[29] W. Cai and V. Shalaev, "Optical Metamaterials:Fundamentals and Applications", Springer, NewYork(2010), p.25.

[30] C. F. Bohren and D. R. Huffman, "Absorption and Scattering of Light by Small Particles", John Wiley & Sons, New York (1983) pp.77.

[31] G. L. Fischer, R. W. Boyd, R. J. Gehr, S. A. Jenekhe, J. A. Osaheni, J. E. Sipe, and L. A. Weller-Brophy, "Enhanced nonlinear optical response of composite materials", Phys. Rev. Lett. Vol.74, pp. 1871 (1995).

[32] G. S. Agarwal, and S. Dutta Gupta, "T-Matrix approach to the nonlinear susceptibilities of heterogeneous media", Phys. Rev. A, Vol.38, pp. 5678 (1988).

[33] S. Dutta Gupta, "Nonlinear optics of Stratified media", Progress in Optics, E.Wolf, ed.(Elsevier Science, 1998), Vol. 38, pp.1-84.

[34] M. Born and E. Wolf, "Principle of Optics", 7th ed., Cambridge University Press, NewYork(2005), p.75.

[35] L. Novotny and B. Hecht, "Principle of Nano-Optics", Cambridge University Press, NewYork(2006), p.45.

[36] H. Noh, Y. Chong, A. D. Stone, and H. Cao "Perfect coupling of light to surface plasmons by coherent absorption", Phys. Rev. Lett. Vol.108, 186805 (2012).

[37] S. Duttagupta, "Strong interaction mediated critical coupling at two distinct frequencies", Opt. Lett. Vol. 32, pp. 1483-1485 (2007).

[38] L. I. Perez, "Reflection and non-specular effect of 2D Gaussian beam in interfaces between isotropic and anisotropic media", J. Mod. Opt., Vol.47 pp.1645–1658 (2000).

[39] A. Yariv, "Quantum Electronics", 3rd ed., John Wiley & Sons, NewYork(1987), pp.106.

Chapter 2

Composite Medium

2.1 Introduction

As the aim of this thesis is to study the phenomenon of coherent perfect absorption (CPA) in novel optical materials, we must first find suitable materials for this purpose. Composite materials produced from a mixture of metals and dielectrics are well known example of such optical materials whose optical properties differ considerably from those of their individual constituents. In this chapter a formalism is presented which utilizes the existing effective medium schemes through numerical computation for developing and characterizing various two and three component (metal-dielectric) composite materials that shall be used for the study of CPA in the later chapters.

The organization of the chapter is as follows: In section two a brief review of the Bruggman effective medium theory for (metal-dielectric) composite materials is presented and compared with Maxwell Garnet theory. The main features and differences between both the theories are highlighted to indicate why the Bruggnman theory is usually preferable to the Maxwell Garnet theory. In section three expressions for the effective dielectric constant of two and three-component composite media are derived. The fourth section contains numerical results where we display graphically the effective dielectric constants as a function of wavelength and volume fraction for various two (metal-dielectric) and three-component (metal-metal-dielectric) composite media. Results for MGT are also presented for comparison and it is observed that both yield same results at low values of volume filling fractions but at higher volume

filling fraction values, BEMT differs considerably from MGT.

2.2 Composite medium

In a composite medium, if there is random distribution of components in such a manner that the two constituent materials(metal and dielectric)intermingle with each other, there is no distinction between the host and inclusion. In such a symmetric composite approximation, called Bruggmann effective medium theory (BEMT), each component is treated equally in the mixture so that it is possible to exchange the roles of metal and dielectric components. In other words, in BEMT both component are considered to be embedded in the effective medium, and there is no need to give preference to one component over the other. Fig. 2.1(a), depicts such a symmetric mixture where the host and inclusion are not distinguishable.

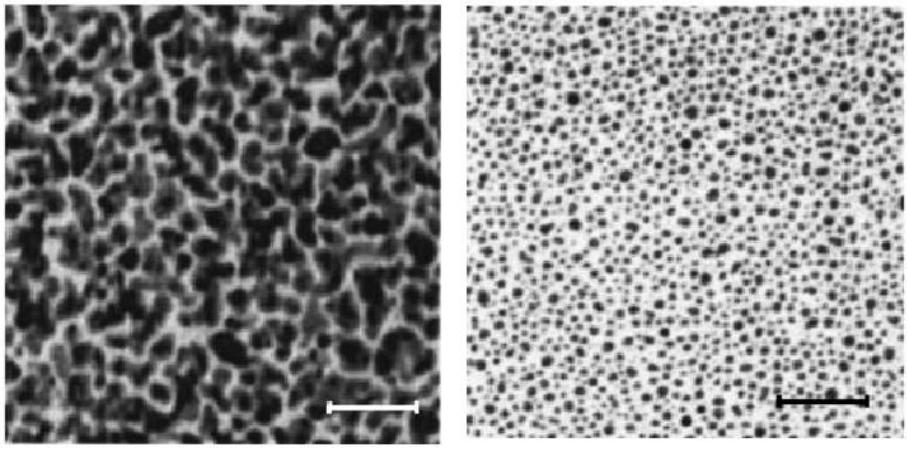

Figure 2.1: Typical schematic metal-dielectric composite medium [3] in (a) the Bruggeman geometry and (b) the Maxwell–Garnett geometry

On the other hand, Maxwell Garnett theory treats the system asymmetrically in that, it distinguishes between the host (dielectric) and the inclusion (metal). The material is to be visualized as inclusions (metal) evenly distributed in a host medium (dielectric). This can be seen in fig. 2.1(b) for the Maxwell–Garnett geometry where the inclusions (black dots) are embedded in the host material (white area) and appear as dots or spherical shapes.

Furthermore since in BEMT each component is treated equally in the mixture, it is quite straightforward to generalize the formalism to three and higher

number of components. In the next section the n component Bruggmann effective medium theory is discussed which is later used for determining the effective permittivity for specific cases of two and three component metal - dielectric composite media in subsequent sections.

2.3 Mathematical formula

2.3.1 n component composite

Let ϵ_{eff}, ϵ_h and ϵ_j respectively denote the permittivity of the effective, host and j^{th} component in a composite medium. Then, the Clausius-Mossotti relation can be written as follows:

$$\frac{\epsilon_{eff} - \epsilon_h}{\epsilon_{eff} + 2\epsilon_h} = \frac{1}{3\epsilon_0\epsilon_h} \sum_j N_j \alpha_j \tag{2.1}$$

where the $\alpha_j = \frac{3\epsilon_0\epsilon_h}{N_j} f_j(\frac{\epsilon_j - \epsilon_h}{\epsilon_j + 2\epsilon_h})$, $j = 1, 2....$ N_j is the average number of molecules and f_j is the volume fraction of the j^{th} elements per unit volume. After substituting for α_j in eq.(2.1) we have

$$\frac{\epsilon_{eff} - \epsilon_h}{\epsilon_{eff} + 2\epsilon_h} = \sum_j f_j \frac{\epsilon_j - \epsilon_h}{\epsilon_j + 2\epsilon_h} \tag{2.2}$$

We have ($f_1 + f_2 + .. + f_n = 1$) for n component CM. Now, according to Bruggeman geometry condition ϵ_h cannot be distinguished from effective dielectric function of CM therefore, $\epsilon_h = \epsilon_{eff}$. With this replacement in eq.(2.2) one arrives at the following Bruggeman formula for the effective medium theory:

$$\sum_j^n f_j \frac{\epsilon_j - \epsilon_{eff}}{\epsilon_j + 2\epsilon_{eff}} = 0, \quad \text{with} \quad \sum_j^n f_j = 1 \tag{2.3}$$

Note that in the above expression of n-component CM one can not differentiate between the inclusion and host. So this formula possesses symmetry in the sense it treats all inclusions as well the so called host (in MGT sense) on an equal footing.

2.3.2 Two component composite

For two component composite medium, the equation (2.3) of effective dielectric function reduces to the following equation :

$$\sum_{j=1}^{2} f_j \frac{\epsilon_j - \epsilon_{eff}}{\epsilon_j + 2\epsilon_{eff}} = 0, \quad \text{with} \quad f_2 = 1 - f_1$$
$$\Rightarrow f_1 \frac{\epsilon_1 - \epsilon_{eff}}{\epsilon_1 + 2\epsilon_{eff}} + f_2 \frac{\epsilon_2 - \epsilon_{eff}}{\epsilon_2 + 2\epsilon_{eff}} = 0 \tag{2.4}$$

Which is a quadratic equation of ϵ_{eff} with the following roots:

$$\epsilon_{eff} = \frac{1}{4}\{(3f_1 - 1)\epsilon_1 + (3f_2 - 1)\epsilon_2 \pm \sqrt{[(3f_1 - 1)\epsilon_1 + (3f_2 - 1)\epsilon_2]^2 + 8\epsilon_1\epsilon_2}\} \tag{2.5}$$

Here, ϵ_1, (f_1) and ϵ_2 $(f_2 = 1 - f_1)$ are permittivity (volume fraction) of metal

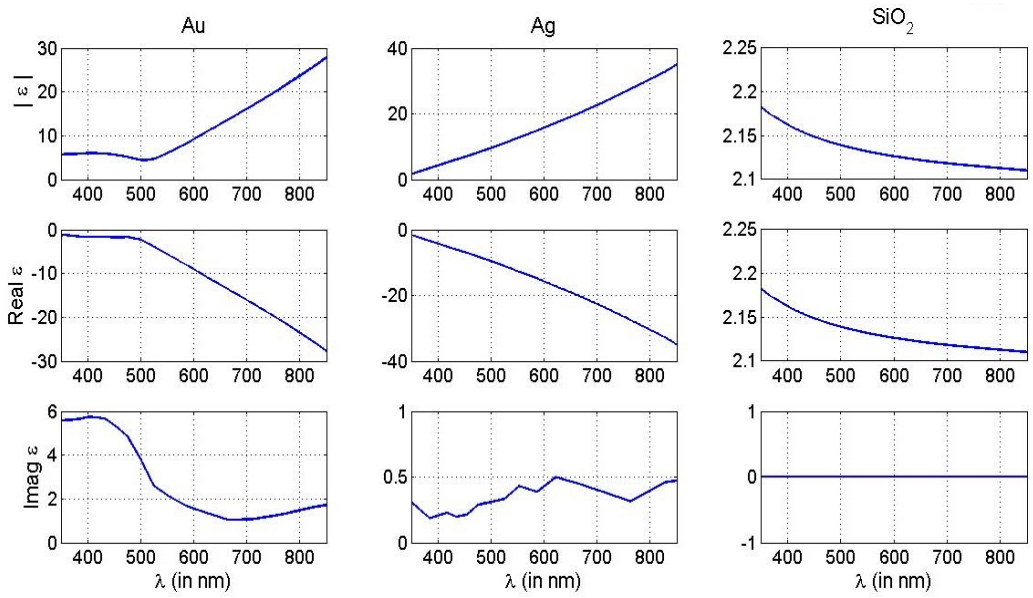

Figure 2.2: Fron left, first, second and third columns show respectively, the bulk permittivity of gold (Au), silver (Ag) and silica(SiO_2). From top first, second and third rows respectively, depict the absolute, real and imaginary values of the bulk permittivity.

and dielectric respectively. The sign of above eq. 2.5 should be chosen in such that the imaginary part of the solution should be positive.

2.3.3 Three component composite

Similarly, one can also obtain an expression for the effective dielectric constant for a three component composite from eq. (2.3).

$$\sum_{j=1}^{3} f_j \frac{\epsilon_j - \epsilon_{eff}}{\epsilon_j + 2\epsilon_{eff}} = 0, \quad \text{with} \quad f_1 + f_2 + f_3 = 1.$$

$$\Rightarrow f_1 \frac{\epsilon_1 - \epsilon_{eff}}{\epsilon_1 + 2\epsilon_{eff}} + f_2 \frac{\epsilon_2 - \epsilon_{eff}}{\epsilon_2 + 2\epsilon_{eff}} + f_3 \frac{\epsilon_3 - \epsilon_{eff}}{\epsilon_3 + 2\epsilon_{eff}} = 0, \tag{2.6}$$

wich is a cubic equation of ϵ_{eff} as,

$$\alpha\epsilon_{eff}^3 + \beta\epsilon_{eff}^2 + \gamma\epsilon_{eff} + \delta = 0 \tag{2.7}$$

the following coefficients a, b, c and d :

$$\alpha = 4 \tag{2.8}$$

$$\beta = 2\{\epsilon_1(1 - 3f_1) + \epsilon_2(1 - 3f_2) + \epsilon_3(1 - 3f_3)\} \tag{2.9}$$

$$\gamma = \epsilon_1\epsilon_2(3f_3 - 2) + \epsilon_2\epsilon_3(3f_1 - 2) + \epsilon_3\epsilon_1(3f_2 - 2) \tag{2.10}$$

$$\delta = -\epsilon_1\epsilon_2\epsilon_3 \tag{2.11}$$

The solution of the eq. (2.7) is as follows.

$$\epsilon_{eff}(k) = -\frac{1}{3\alpha}(\beta + \Omega\chi(k) + \frac{\Delta_0}{\Omega\chi(k)}) \quad \text{with} \quad k = 1, 2, 3 \tag{2.12}$$

Where $\chi(1) = 1$, $\chi(2) = \frac{-1+\iota\sqrt{3}}{2}$, $\chi(3) = \frac{-1-\iota\sqrt{3}}{2}$, $\Delta_0 = \beta^2 - 3\alpha\gamma$, $\Delta_1 = 2\beta^3 - 9\alpha\beta\gamma + 27\alpha^2\delta$ and $\Omega = \sqrt[3]{\frac{\Delta_1 + \sqrt{\Delta_1^2 - 4\Delta_0^3}}{2}}$. If Δ_0 is zero then Ω is also zero. Here among the three roots of the solution the root should be chosen such that the imaginary part of the solution is positive.

2.4 Maxwell-Garnett theory

Maxwell-Garnett theory [1, 3, 4] is based on the assumption that spherical particles of a material of permittivity ϵ are embedded in a host medium with permittivity ϵ_h. Then the 'effective permittivity', ϵ_{eff} of the composite medium can be expressed as follows :

$$\epsilon_{eff} = \epsilon_h \frac{1 + 2f\chi}{1 - f\chi} \tag{2.13}$$

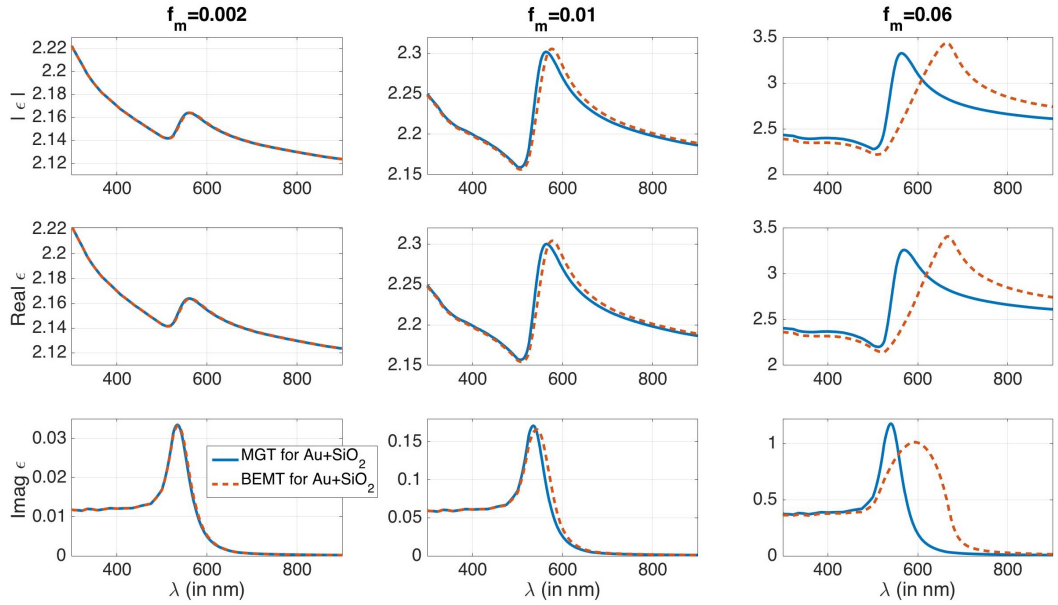

Figure 2.3: From top the first, second and third rows respectively, depict the absolute, real and imaginary parts of the permittivity of a gold-silica composite. From left, the first, second and third columns represent Au (gold) volume filling fraction, $f_G = 0.002$, 0.01 and 0.06 respectively. Dash lines depict BEMT results whereas solid lines are plotted using MGT.

where

$$\chi = \frac{\epsilon - \epsilon_h}{\epsilon + 2\epsilon_h} \tag{2.14}$$

and 'f' is the volume filling fraction of the inclusion with permittivity ϵ.

It is thus possible to evaluate the bulk effective permittivity of a composite in terms of the permittivity, ϵ, of the inclusion and the host permittivity, ϵ_h.

For a metal-dielectric composite, the metal is treated as an 'inclusion' whereas the dielectric component serves as the 'host'.

2.5 Numerical results

2.5.1 Two component composite

We now present the specific characteristics of metal-dielectric composite media (CM) that are considered as evenly distributed (homogeneous) mixtures of a metal (gold or silver) and silica (SiO_2). The permittivities of the components

used in calculations are obtained through numerical interpolation of the optical constants data of Johnson and Christy for metals (silver, gold) [7] and from ref.[8] for SiO_2 at all wavelengths in the 300 - 900 nm region. These are shown in fig.(5.2). Using the Bruggeman effective medium theory (BEMT) the effec-

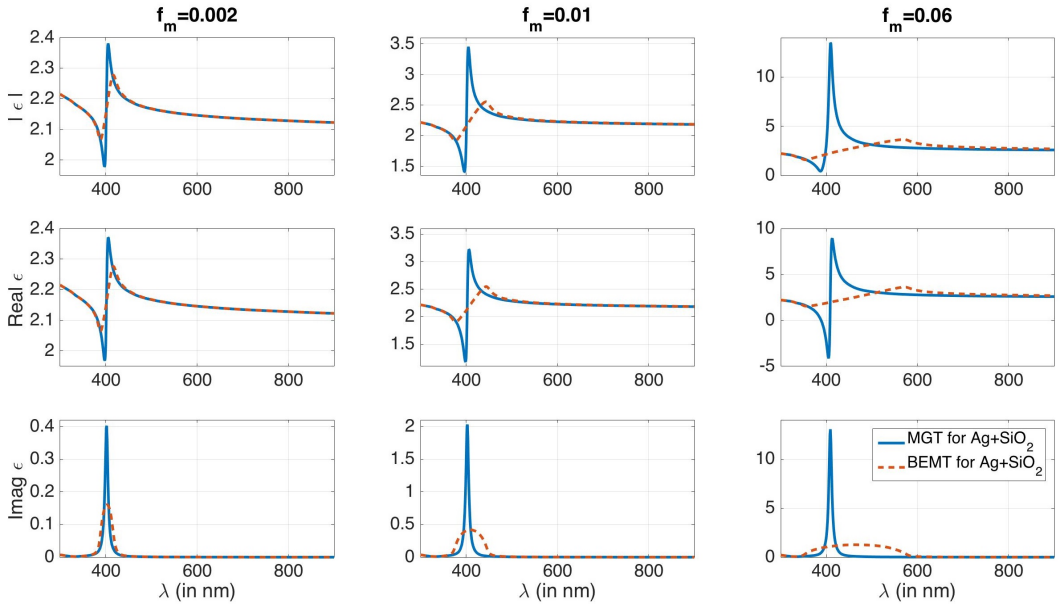

Figure 2.4: First, second and third rows of the figure depict respectively, the absolute, real and imaginary values of permittivity of a silver-silica composite. First, second and third columns correspond to Ag (silver) volume filling fraction, $f_S = 0.002, 0.01$ and 0.06 respectively. Dash lines depict BEMT results whereas solid lines are plotted using MGT.

tive permittivity of CM is evaluated numerically as a function of wavelength of the incident radiation and various volume filling fractions of the metals. For comparison and contrasting purpose, results of the Maxwell Garnet theory (MGT) are also presented. The results of the BEMT and MGT are shown in fig.(2.3) and fig.(2.4)where the absolute, real and imaginary values of the effective permittivity of composite media of different metals are plotted as a function of the wavelength for various volume fractions (f_m). It is clearly seen from the figure that results of both the theories match for low values of the volume filling factor till the inclusion reaches a value around 1%. Thereafter BEMT results show red shift and broadening of resonance in contrast to the (MGT) results. MGT resonances do not undergo shift and broadening but display absorption enhancement.

2.6 Three component composite

We now present the characteristics of three-componet CM considered as a homogeneous mixture of two metals and a dielectric. The effective permittivity

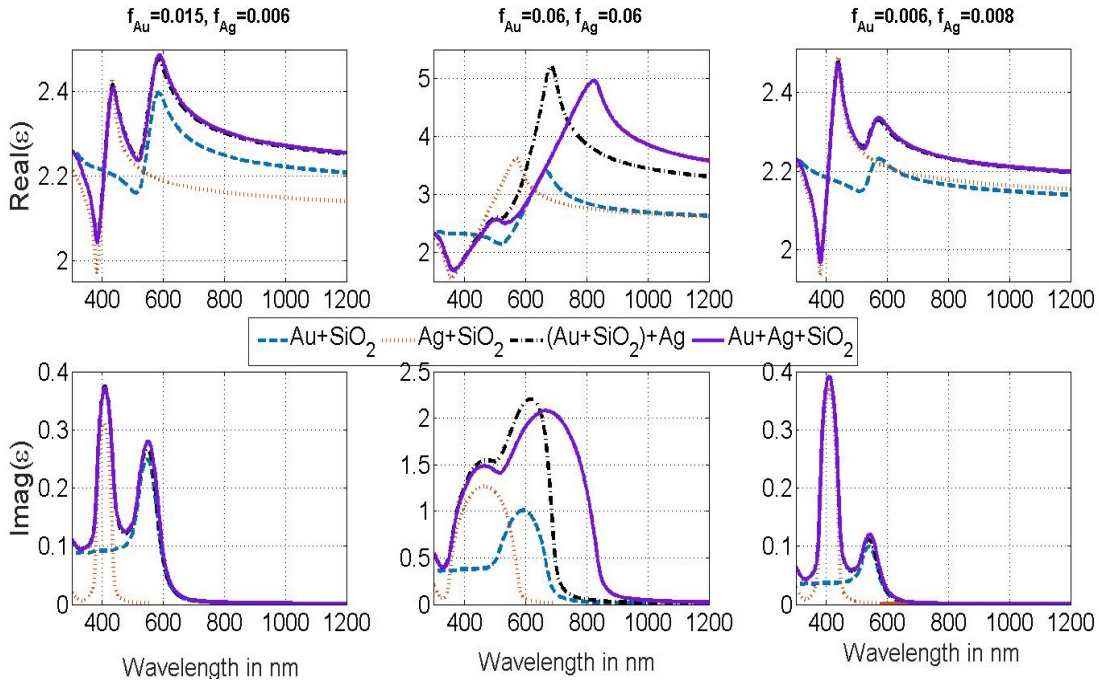

Figure 2.5: From top, the first and second rows respectively, depict the real and imaginary part of the permittivity of gold-silica, silver-silica and gold-silver-silica composite in the optical region. From left the first, second and third columns correspond respectively to the volume fractions (i)$f_{Au} = 0.015$, $f_{Ag} = 0.006$ (ii)$f_G = 0.06$, $f_S = 0.06$ and (iii)$f_G = 0.006$, $f_S = 0.008$ respectively.

of the three component CM is calculated from Bruggeman effective medium theory (BEMT) [2, 3, 4, 6] as a function of wavelength of incident radiation and various volume filling fractions of the metals. The permittivities for the metals have been obtained through numerical interpolation of Johnson and Christy's optical constants data of silver and gold [7] and for the dilectric (SiO_2) from ref[8] for all wavelengths in the visible region. We have then calculated real and imaginary value of CM using BEMT as in eq. 2.5 for wavelengths in the region 330nm to 900 nm and the results are plotted in the fig. (4.14). The permittivity of metals (Au or Ag) and dielectric (SiO_2) are used in BEMT equation to calculate numerically the permittivity of a com-

posite. The dash dot dash $(- \cdot -)$ line represent Au and SiO_2 composite or gold composite (GC), dash dash $(--)$ line represent Ag and SiO_2 composite or Silver composite (SC) and solid line $(-)$ represent Au, Ag and SiO_2 composite or gold-silver composite (GSC) respectively. The GSC was calculated using the BEMT twice as follows: initially GC was constructed using BEMT. Next BEMT was used again, taking Ag permittivity as ϵ_1 and GC permittivity as ϵ_2 respectively and their respective volume fractions as f_1 and f_2, to calculate the effective permittivity of GSC.

2.7 Conclusions and remarks

In this chapter we have presented a scheme for numerical construction and characterization of a few 2 and 3 component composite materials.

Two-component CM of several varieties including gold-silica and silver-silica have been experimentally fabricated and characterized previously. However most of them seem to focus on rather large volume filling fractions. Apart from two-component CM we have also attempted to develop three component metal-dielectric composites on which not much literature exists. A few existing work however deal with very large filling fractions and materials other than metal-dielectric composite media such as ceramic-metal (cermet) etc.

For our studies of coherent perfect absorption the CM can be weakly absorptive, that is high volume fraction of metals is not needed. hence we have restricted our studies/characterization to rather low values of volume fractions. In this regime of volume filling fractions one can use either BEMT or MGT as it was shown above that results of both the theories match for low values of the volume filling fraction till the inclusion reaches a value around 1%. Thereafter BEMT results show red shift and broadening of resonance in contrast to the (MGT) results. Thus BEMT is found to be more versatile theory as it provides a reasonable estimation of the effective permittivity at even higher values of the volume filling fractions.

Bibliography

[1] Maxwell and J. C. Garnett; "Colours in metal glasses and in metallic films"; Phil Trans R Soc Lond 203:385–420, 1904.

[2] D. A. G. Bruggeman; "Calculation of various physics constants in heterogenous substances I. Dielectricity constants and conductivity of mixed bodies from isotropic substances"; Annalen Der Physik 24:636–664, 1935.

[3] Wenshan Cai and Vladimir Shalaev; "Optical Metamaterials: Fundamentals and Applications"; Springer, New York, 2010.

[4] C. F. Bohren and D. R. Huffman; "Absorption and Scattering of Light by Small Particles" (John Wiley & Sons) p-77.

[5] J. E. Gubernatis; "Scattering theory and effective medium approximations to heterogeneous materials"; AIP Conference Proceedings, 40(1):84–98, 1978.

[6] John D. Jackson; "Classical Electrodynamics"; Wiley, Hoboken, NJ, 3rd edition, 1998.

[7] P. B. Johnson and R. W. Christy "Optical constants of the noble metals"; Physical Review B, 6(12):4370–4379, 1972.

[8] E. D. Palik; "Hand book of Optical Constant of Solids"; Academic Press, London, 1998.

Chapter 3

Coherent Perfect Absorption in metal-dielectric Composite

3.1 Introduction

The preceding chapter dealt with designing and characterization of the optical constants of two and three component metal-dielectric composite media. In this chapter we present a study of CPA in two-component (metal-dielectric) composites materials. In earlier studies of CPA [5, 6] it is clear that the calculations of CPA are performed using plane wave approximation. In reality however, the usual laser sources in the laboratory give out Gaussian beams as output. Furthermore, many applications in optics involve strong focusing of laser beams near planar surfaces.

Thus from a practical applications viewpoint it is imperative to investigate whether CPA like effects persist for such Gaussian input beams. In this paper we address this issue. Use of a Gaussian beam [13, 14] at oblique/normal incidence brings in complications, as it involves angular spectrum decomposition [18] which, is a Fourier transformation of the beam, require extensive numerical computation.

The organization of the chapter is as follows. In second section, a detailed description of the system and the illumination geometry are presented along with an outline of the necessary steps for the angular spectrum decomposition of the Gaussian beam. Assuming a certain polarization state (eg. s-polarization), the reflected and transmitted spectra are calculated for

both the incoming beams. An inverse Fourier transforms then leads to the output profiles for the scattered light. The third section contains numerical results and discussion. Optimization of system parameters for attaining CPA is performed. CPA in a metal-dielectric composite medum is then evaluated numerically for various beam waists of the Gaussian beam at oblique and normal incidences. The last section contains a summary of main results and conclusions.

3.2 Formulation and illumination geometry

The CPA medium (or CM) is a two component metal-dielectric composite slab of thickness "d" and is assumed to be non-magnetic i.e., μ =1. Two identical Gaussian beams are incident (along z' & z'' axes) from the opposite sides of the CM slab at the same incidence angle θ with the z axes (oriented along the normal to the flat surfaces of the CM as shown in Fig. 3.1). In the $x-z$ plane the planes of incidences at $z=0$ and $z=d$ are the two interfaces of the CPA medium. We henceforth use the label L and R for

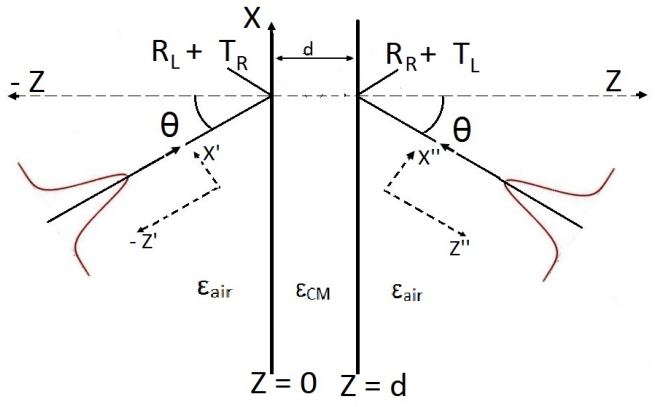

Figure 3.1: Two identical Gaussian beams focus on opposite interfaces of CM and air. Here, r_L (t_L) and r_R (t_R) are reflection (transmission) coefficient at the left and right side interface respectively. Various coordinate systems are also shown in the figure.

the propagating wave incident from left and right side respectively, so that the resulting reflected (transmitted) waves are denoted r_L, (t_L) and r_R (t_R) respectively. Since the medium of incidence and emergence are the same, the

symmetry of the structure implies that $r_L = r_R$ and $t_L = t_R$. Hence from symmetry considerations the total scattering amplitude at the interface $z = 0$ given by $r_L + t_R$ must be same as that at the interface $z = d$ given by $r_R + t_L$.

We now discuss the specific characteristics of metal-dielectric CM which is taken as a homogeneous mixture of gold (Au) and silica (SiO_2). The optical constants of gold [20] and dielectric [21] are interpolated [19] and the permittivity is calculated for all wavelengths in the visible region. The Bruggeman effective medium theory (BEMT) [16, 17] is used to evaluate the effective dielectric function (or permittivity) of CM as

$$\epsilon = \frac{1}{4}\{(3f_1 - 1)\epsilon_1 + (3f_2 - 1)\epsilon_2 \pm \sqrt{[(3f_1 - 1)\epsilon_1 + (3f_2 - 1)\epsilon_2]^2 + 8\epsilon_1\epsilon_2}\} \tag{3.1}$$

Here, ϵ_1, f_1, ϵ_2 and $f_2 = (1 - f_1)$ are permittivity and volume fraction of

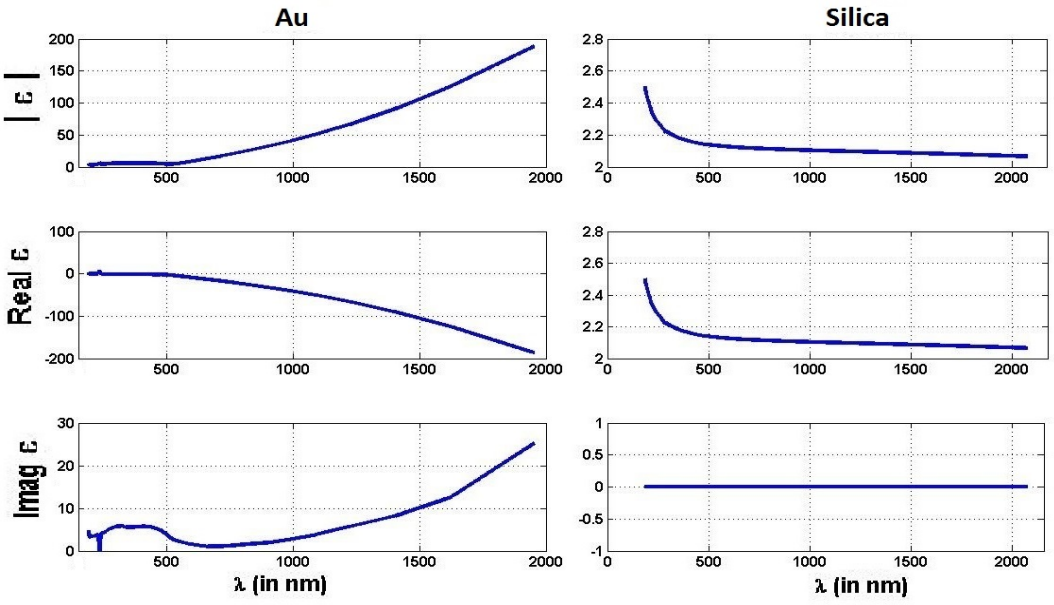

Figure 3.2: First, second and third row of the figure depict the absolute, real and imaginary values of permittivity of respective medium. First and second column show respectively, the permittivity of gold (Au) and silica (SiO_2).

metal and dielectric respectively. The results are shown in fig 3.1 where the absolute, real and imaginary values of permittivity for metal, dielectric and

CM with different volume fraction (f_m) are plotted as a function of the wavelength. Fig 3.3 illustrates the characteristic changes occurring in the absolute, real and imaginary parts of permittivity of CM for different volume fraction ($f_1 = 0.002, 0.006$ and 0.08) of gold (Au) in the range of 300 to 900 nanometers.

The CM slab is illuminated from both sides by two identical Gaussian

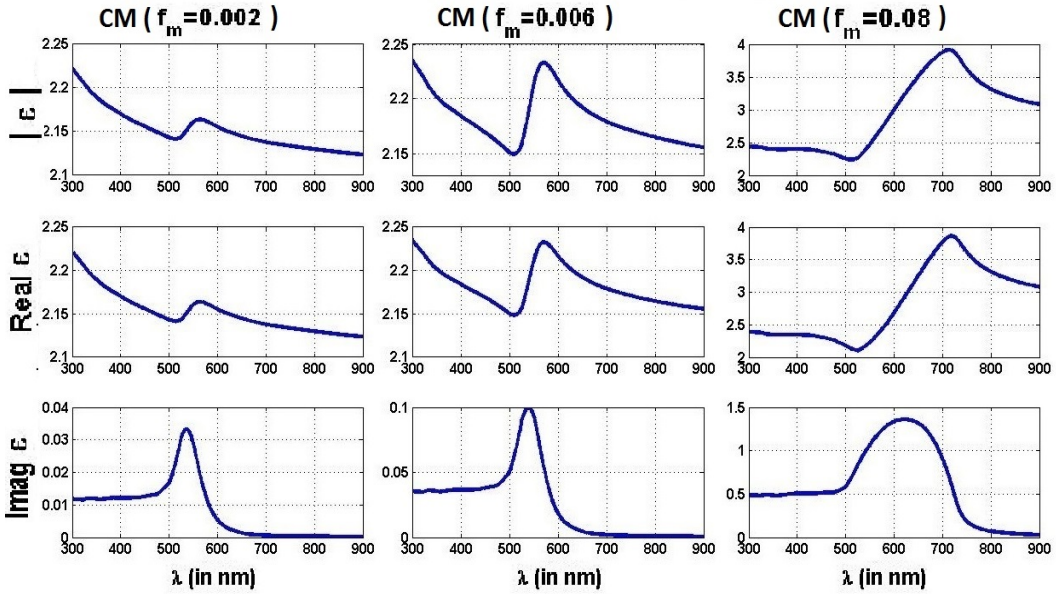

Figure 3.3: First, second and third row of the figure depict the absolute, real and imaginary values of permittivity of respective medium. First, second and third column are the permittivity of CM in the optical region when volume fractions are ($f_m =$) 0.002, 0.006 and 0.08 respectively.

beam sources with equal intensity, beam spot size, wavelength and angle of incidence. The un-primed axis at the air-CM interface $[x, y, z] = [0, 0, 0]$ ($[x, y, z] = [0, 0, d]$) and primed (double-primed) axis shown in the fig 3.1 are related through transformation matrix as

$$\begin{bmatrix} x' \\ y' \\ z' \end{bmatrix} = \begin{pmatrix} \cos\theta & 0 & -\sin\theta \\ 0 & 1 & 0 \\ \sin\theta & 0 & \cos\theta \end{pmatrix} \begin{bmatrix} x \\ y \\ z \end{bmatrix} \tag{3.2}$$

$$\begin{bmatrix} x'' \\ y'' \\ z'' \end{bmatrix} = \begin{pmatrix} \cos\theta & 0 & \sin\theta \\ 0 & 1 & 0 \\ -\sin\theta & 0 & \cos\theta \end{pmatrix} \begin{bmatrix} x \\ y \\ z - d \end{bmatrix} \tag{3.3}$$

Then the equations of Gaussian [13, 14] beams are propagating along z' and z'' axis can be represented as

$$E(x'(x,z);z'(x,z)) = \frac{w_0}{w(z')} e^{\frac{x'^2}{q'}} e^{ik_0 z'} e^{-i\eta(z')} \tag{3.4}$$

$$E(x''(x,z);z''(x,z)) = \frac{w_0}{w(-z'')} e^{\frac{x''^2}{q''}} e^{-ik_0 z''} e^{i\eta(z'')} \tag{3.5}$$

the above equations (4.3) and (3.5) are same in all dimension apart from their sign due to direction of propagation. The beam parameters are $\frac{1}{q'} = \frac{1}{w^2(z')} + \frac{ik_0}{2R(z')}$ and $\frac{1}{q''} = \frac{1}{w^2(-z'')} + \frac{ik_0}{2R(-z'')}$. By definition, irrespective of prime or double prime coordinate, the basic beam elements are as : wave vector, $k = \frac{2\pi}{\lambda}$; beam waist size, $w^2(z) = w_0^2(1 + \frac{z^2}{z_0^2})$; radius of curvature, $R(z) = z(1 + \frac{z_0^2}{z^2})$; Rayleigh range, $z_0 = w_0^2 \frac{\pi}{\lambda}$; Gouy phase, $\eta(z) = \tan^{-1}(\frac{z}{z_0})$.

For simplicity, the amplitude of E field of the beam is chosen to have a Gaussian spatial distribution only in the plane of incidence i.e., along the axis perpendicular to the direction of wave propagation and is independent of the coordinate perpendicular to the plane of incidence.

As is well known, for a paraxial Gaussian beam profile distribution along x' (x'') axis (fig 3.1), the wave front of the beam no longer remains planar but acquire a radius of curvature $R(z')$ ($R(z'')$) at a distance z' (z'') away from the beam waist located at $z' = 0$ ($z'' = d$). In other words, the Gaussian beam can be regarded as a collection of many plane waves having slightly differing (about a central) wave vectors. Then the Fourier transformation of it is the form of angular spectrum representations [18] of the Gaussian beam for fields $E(x'(x,z);z'(x,z))$ and $E(x''(x,z);z''(x,z))$ are of the following form:

$$\hat{E}(K_{x'};z') = \frac{1}{\sqrt{2\pi}} \int_{-\infty}^{\infty} e^{-iK_{x'}x'} dx' E(x';z') \tag{3.6}$$

$$\hat{E}(K_{x''};z'') = \frac{1}{\sqrt{2\pi}} \int_{-\infty}^{\infty} e^{-iK_{x''}x''} dx'' E(x'';z'') \tag{3.7}$$

Substituting eq (6.2), eq(4.3) in eq(3.6) and eq(6.3), eq(3.5) in eq(5.10) we obtain

$$\hat{E}(K_x;z) = \frac{w_0}{\sqrt{2\pi}} \int_{-\infty}^{\infty} dx e^{i(k_0 \sin\theta - K_x)x} \frac{e^{\frac{x^2 \sin^2\theta}{q}} e^{-i\eta(x\sin\theta)}}{w(x\sin\theta)} \tag{3.8}$$

The incident beams are focused at the respective slab-air interfaces (z = 0 and z = d). The above angular spectrum beam (represented as SA) is nothing but an infinite number of plane waves which is numerically evaluated.

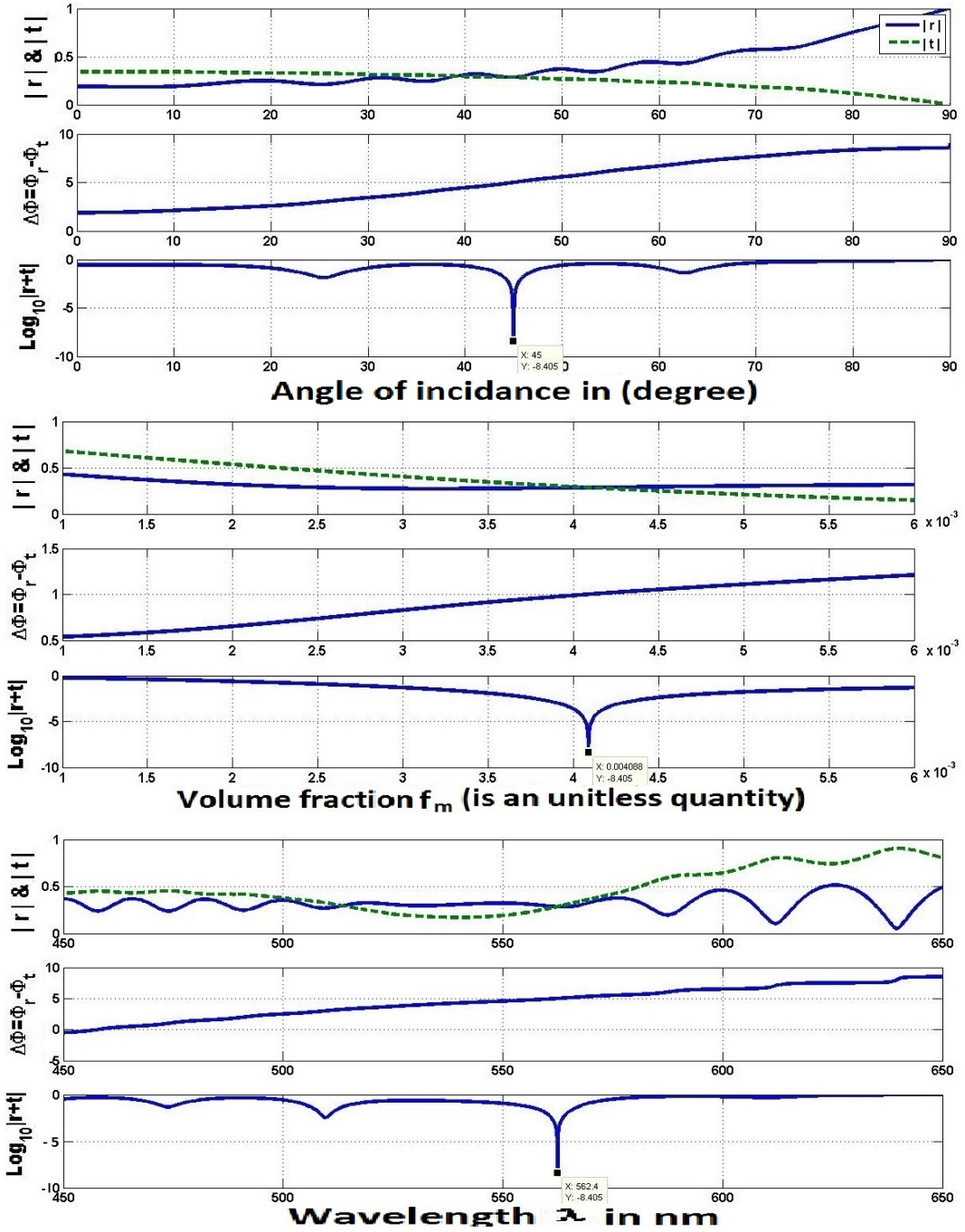

Figure 3.4: From first column of figures states at 45^o angle of incident, Second column of figures states at $f_1 = 0.0040884$ (unit less) volume fraction and third column of figures states at $\lambda = 562.4$ nm wavelength maximum absorption observed.

Thereafter each and every plane wave component goes through reflection and transmission [15, 22] at the interfaces. The reflected and the transmitted field amplitudes at the interfaces, z=0 (and z=d) can be obtained by using the Fresenel's coefficient of reflection and transmission for individual waves. Using the symmetry properties mentioned above the resultant amplitude is obtained by summing the reflection and transmission coefficients of one side. Finally, inverse Fourier transformation of SA gives the actual beam profile which is comes out can be written as

$$E(x;z) = \frac{1}{\sqrt{2\pi}} \int_{-\infty}^{\infty} [SA\, of\, \hat{E}(K_x;z)] e^{iK_x x} dK_x \tag{3.9}$$

The angular spectrum decomposition of the Gaussian beam using Fourier transformation leads to an infinite number of plane wave without altering the profile since Fourier transformation of a Gaussian is again a Gaussian. Each decomposed plane wave obeys Fresnel's reflection and transmission formalism [15, 22]. Now each element of reflected decomposed beam is coupled with either side's transmitted decomposed beam. Thereafter, all the resultant numerical amplitudes combine in inverse Fourier transform which leads to the resultant amplitude at $z = 0$ and $z = d$ respectively.

3.3 Numerical results and discussions

Before simulating the Gaussian beam, we have to determine the optimum system parameters for attaining CPA. The gold-silica CM gives maximum absorption for a thickness d ($= 5\mu m$) [5] when two s-polarized wave fall on CM from opposite side. The effective dielectric constant of the CM is calculated numerically using Bruggmann effective theory (eq (1)) using the following optimum parameters: a filing factor $f_1 = 0.0040884$ for gold, whose dielectric constant $\epsilon_1 (= -6.4552 + 1.9896i)$ at a wavelength, $\lambda = 562.4$ nm is obtained by interpolating experimental data of Johnson and Christy [20]. The dielectric constant of the dielectric (silica) is, $\epsilon_2 = 2.25$. The calculated permittivity of CM [16, 17] is $\epsilon_{CM} = 2.3225 + 0.0562i$ at the same wavelength. From fig 3.2, individual observation for angle of incidence is 45^o, volume fraction of CM $f_1 = 0.0040884$) and wavelength of two monochromatic plane wave (s-polarized) $\lambda = 562.4$ nm incident on CM from opposite side. It is observed that scattered amplitude out of the CM is around 10^{-8} times the incident amplitudes. We now study the same system replacing the plane waves by

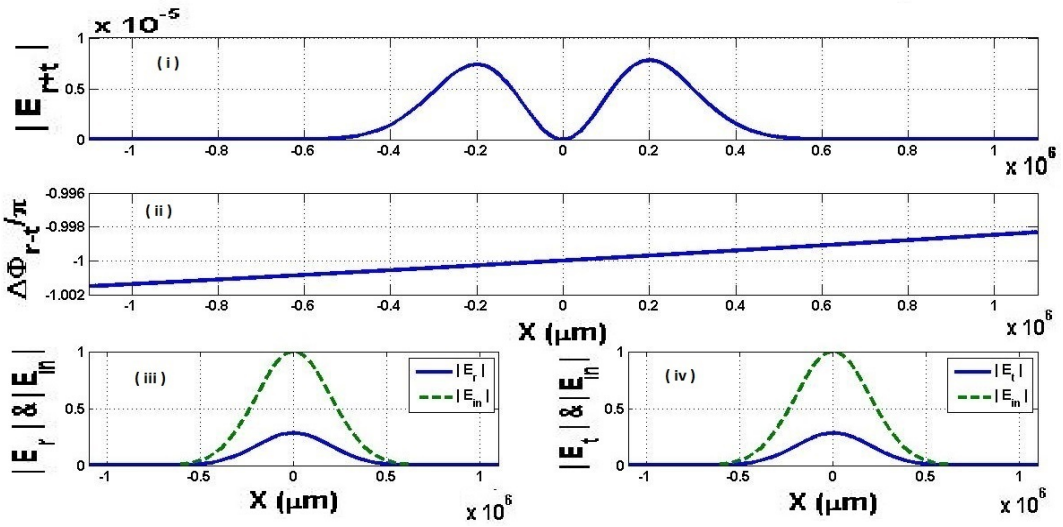

Figure 3.5: (i)Output or resultant beam profile when two identical Gaussian beams of wavelength 562.4 nm are focused on the slab from opposite side at 45^o angle of incidence. (ii) Phase change along the output beam profile. (iii) Incident and reflected beam profiles of one of the two incident Gaussian beam focusing at either $z = 0$ or $z = d$ on the CM slab. (iv) Incident and transmitted beam profile of single Gaussian beam incident on (any) one interface.

Gaussian beams.

Two identical Gaussian beams (Fig. 3.1)both having beam waist size $w_0 = 200$ μm, wavelength $\lambda = 562.4$ nm propagating along z' and $-z''$ axis are focused on the CM (at $z = 0$ and $z = d$) at same incidence angle of $\pm 45^o$ with z axis respectively. As we mentioned above since the beam distribution is symmetric in both x and y directions for simplicity we can consider only the beam distribution along x-axis. In the numerical calculations $K_{x^p} = \frac{2\pi}{\Delta x^p}$ and $\Delta x^p = 8\frac{w_0}{n}$, where $n = 2^{13}$. p stands for prime and double prime axes. The limiting points of x^p at focusing points are $-4w_0$ and $4w_0$ respectively. Fig 3.5(i) (in 2D) & fig. 3.6(b) (in 3D) is the output (or resultant) beam profile when two identical Gaussian beams ($\lambda = 562.4$ nm, $\epsilon_d = 2.25$, $w_0 = 200$ μm, $d = 5$ μm and $f_1 = 0.0040884$) focus from the opposite side on CM. One can see that the scattering amplitude is of the order of 10^{-6} compared to the incident amplitude. Fig 3.5(ii) shows phase difference between one side's reflected decomposed beam and other side's corresponding transmitted decomposed beam which is π. In fig 3.5 (iii) and (iv)we show reflection and transmission beam profile respectively (blue continuous line); these are also

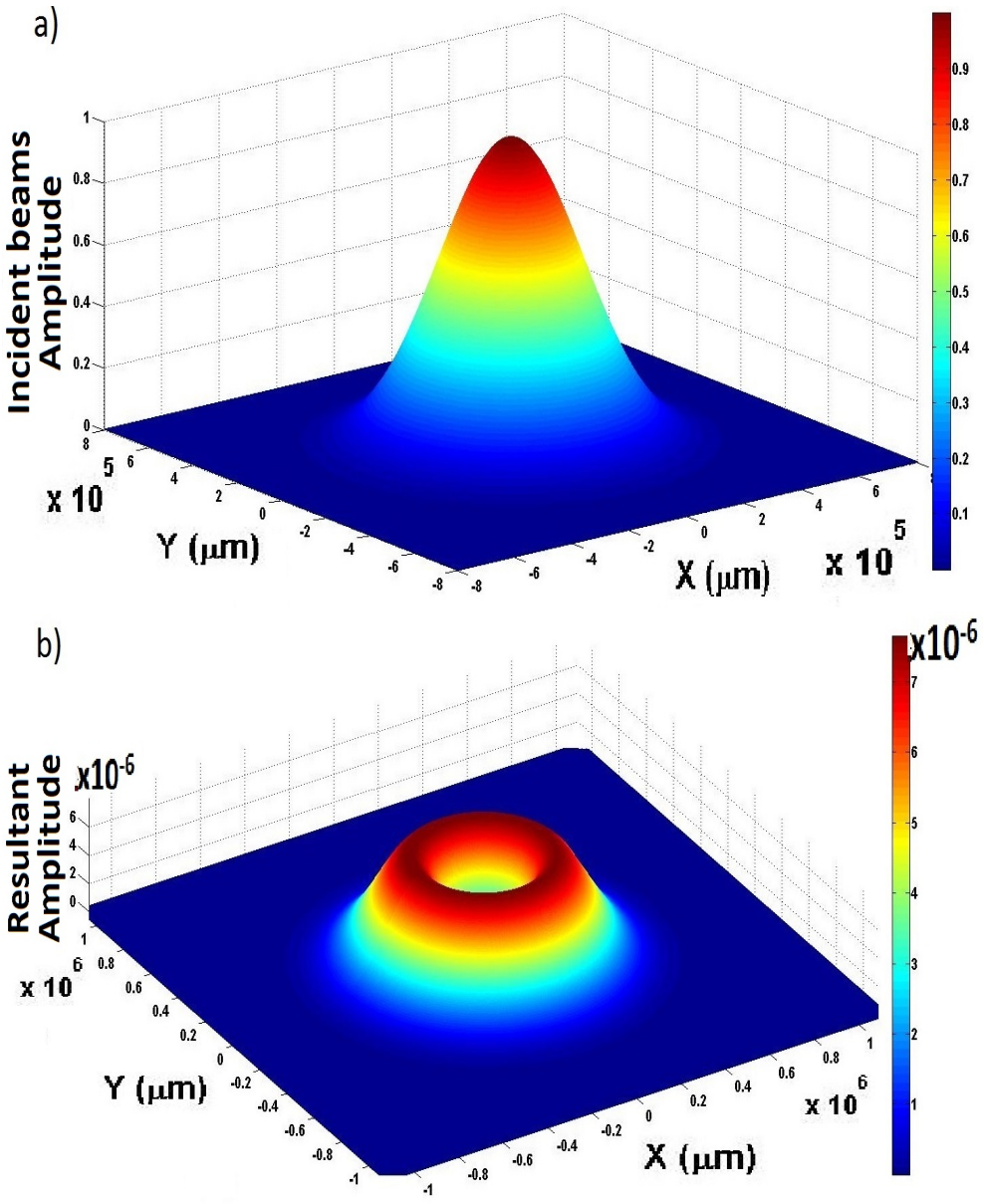

Figure 3.6: First figure is profile of two incident Gaussian beam focusing at $z = 0$ and $z = d$ on the wall of CM making an angle $\pm 45^o$ with z axes respectively where maximum amplitude is 1 unit. Second figure is resultant beam profile where the maximum amplitude is 7×10^{-6} unit

compared with incident beam profile (green dotted line) when the Gaussian beam is incident on CM from any one side. Fig. 3.6(a) shows the three-dimensional (3D) profile of two incident Gaussian beams that focus at $z = 0$ and $z = d$ interfaces of CM making an angle $\pm 45^o$ with z axes respectively

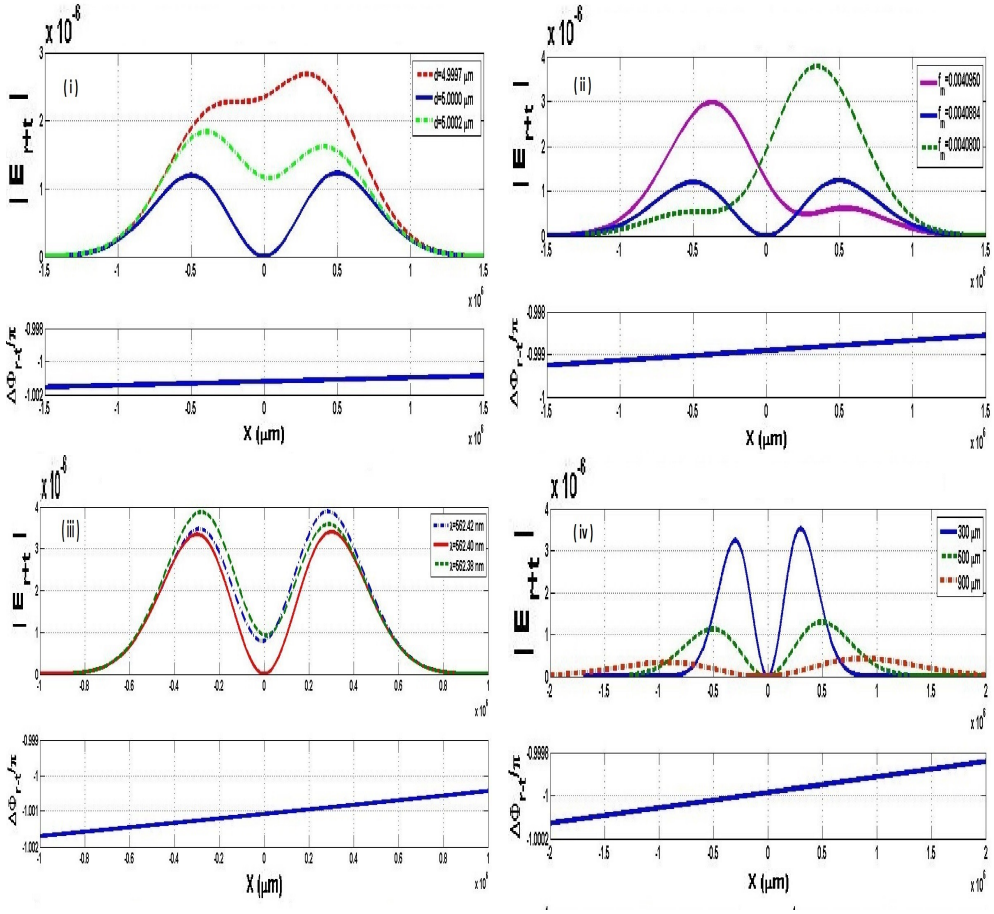

Figure 3.7: Observation of beam profile while making (i) small changes in thickness of slab d =4.9997, 5.0000 and 5.0002 μm (ii) small variation in volume fraction f_m =0.0040950, 0.0040884 and 0.0040800 , (iii) small variation in wavelength (λ =562.42, 562.40 and 562.38 in nm) and (iv) variation in beam waist size (w_0 =300, 500 and 900 μm)

where $w_0 = 200\ \mu$ and maximum amplitude is 1 unit. Now from fig. 3.5(i) & 3.6(b), resultant beam profile have the maximum amplitude of 7×10^{-6} unit. The basic optimized parameters of the CM(for achieving CPA) are: width of the medium ($d = 5\ \mu m$), volume fraction ($f_m = 0.0040884$), wavelength ($\lambda = 562.4$ nm) and beam waist ($w_0 = 200\ \mu m$) for an oblique incidence angle ($\pm 45^o$). To explore the experimental limitations we now investigate the variation in the output beam profile (fig 3.7) as well it's corresponding phase while simultaneously changing different basic parameters and keeping remaining optimized parameters fixed. We can observe the output profile of

beams (fig 3.7(i)) while widths of CM are d = 4.9997, 5.0000 and 5.0002 in μm and keeping remaining parameters are in calibrating state (CS). Next fig 3.7(ii), slightly changing in volume fraction f_1 (= 0.0040950, 0.0040884 and 0.0040800), the resultant beam profile keeping remaining parameters are fixed in CS. Figure 3.7(iii) shows the effect of slight variations in wavelength λ (=562.42, 562.40 and 562.38 nm) and when remaining parameters are constant in CS. And lastly (in fig 3.7(iv))the resultant wavefronts are observed for three different of beam waist size w_0 = (300, 500 and 900 μm) while the remaining parameters are keeping same in CS.

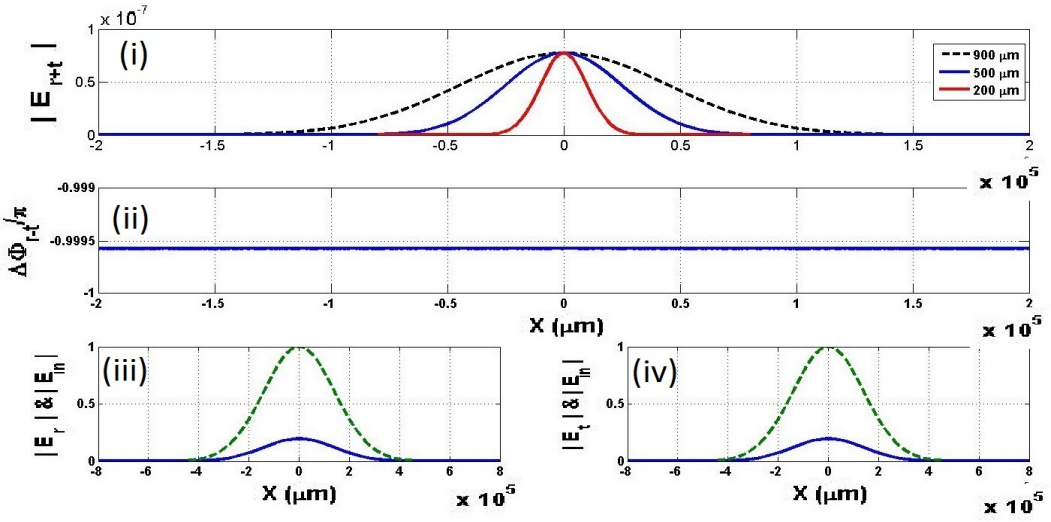

Figure 3.8: (i) Output or resultant beam profile when two identical Gaussian beams of wavelength 540 nm are focused on the CM slab from opposite side at 0^o angle of incidence. (ii) Phase change along the output beam profile. (iii) Incident and reflected beam profiles of one of the two incident Gaussian beam focusing at either $z = 0$ or $z = d$ on the CM slab. (iv) Incident and transmitted beam profile of single Gaussian beam incident on (any) one interface of CM.

Similarly, for normal incidence (i.e. 0^o along normal to z-axis) one can use a 5 μm CM (made of Gold and Silica) slab to show maximum absorption at wavelength (λ)=540 nm and volume fraction (f_m)=0.004408 with s-polarized or TE-mode plane wave. We now replace the plane wave with Gaussian beam in our calculations. Fig. 3.8, (c) and (d) show beam profile for incident beam (with black doted lines) and reflected and transmitted (blue lines) when only one of the Gaussian beam is incident on CM from any one of the sides. Now fig.3.8(a) shows the resultant beam profiles when two identical Gaussian beam

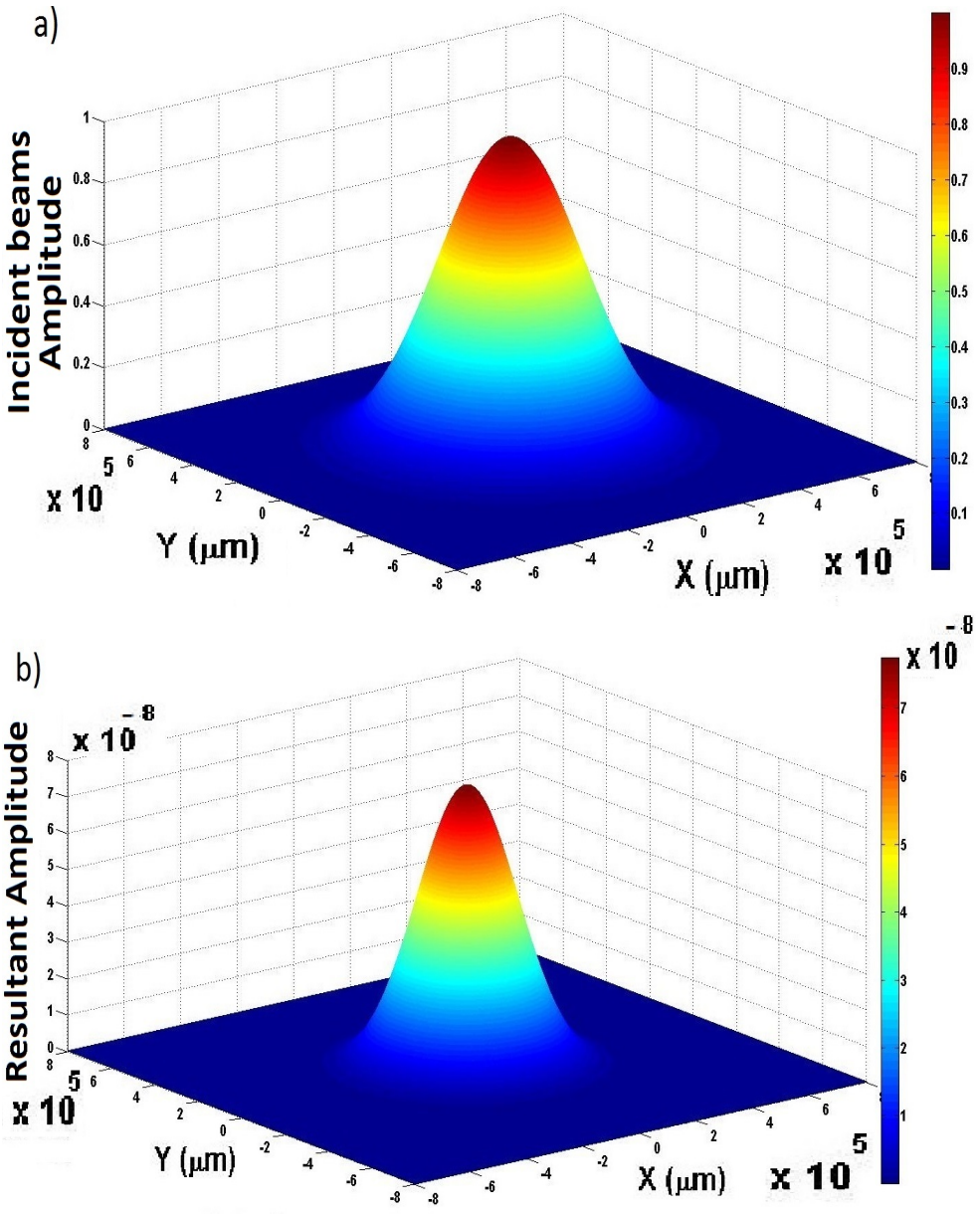

Figure 3.9: Three dimension representation of the profiles depicted in Figure 7. (a) Profile of one of the two incident Gaussian beam focused at either $z = 0$ or $z = d$ interface of the CM making an angle 0^o with z axes respectively where maximum amplitude is 1 unit. (b) Resultant beam profile where the maximum amplitude is 7.5×10^{-8} unit.

are incident from opposite sides on the CM along z-axes (i.e. normal incidence) with different beam waist size (200, 500 & 900 μm) in . Fig. 3.8(b) shows the phase difference between reflected and transmitted beam profiles.

First of fig. 3.9 is the 3D profile of both incident beams having beam waist size 200 μm and second one is the resultant output profile which has maximum amplitude 7.5×10^{-8} unit of incident amplitude. So, one can say this is complete absorption.

3.4 Summary and conclusion

in this chapter, coherent perfect absorption (CPA) is investigated using two identical Gaussian beams incident (at the same incident angle θ) on a gold-SiO_2 composite medium (CM) from the opposite ends. Our results show conclusively that CPA can be observed even with Gaussian beams as the slight imperfection of off-axis CPA is insignificant compared to the incident beam amplitudes. For oblique incidence (45^o), the central part and the peripheral parts of the beam is completely absorbed whereas the absorption is reduced in the middle parts of the resultant amplitude profile. From the figures 3.5(i) and 3.6(b), one can observe a resultant amplitudes of the order of 4×10^{-6} with respect to incident beams; which implies at least 99.999996% is absorbed from the incident beams due to critical coupling in the composite medium. In case of normal incidence (fig. 3.8(i) & 3.9 (b)) central parts have higher intensities compare to peripheral parts for several beam widths (900, 500, 200 μm) size. Both oblique (fig. 3.5(i) and 3.6(b)) and normal (fig. 3.8(i) & 3.9(b)) incidence cases have central amplitude of the order of 10^{-8} of beams at wavelength 562.4 and 540 nm respectively. Fig. 3.7 gives a sense of experimental limitations in various beam and CM parameters such as the thickness of the slab, volume fraction, coherent nature of beams and beam width. Fig. 3.7(iv) shows that for oblique incidence several beam widths exhibit different absorption patterns (specially in the middle part) but for normal incidence case (fig. 3.8) similar absorption patterns are obtained for different beam widths.

Hence this work essentially demonstrates that, CPA can occur even for moderately focused Gaussian beams which are typically generated in the laboratories and for experimental studies of optical problems.These results and observations could be useful in the analysis of any related physics and optical problems.

Bibliography

[1] Y. D. Chong, L. Ge, H. Cao and A. D. Stone; "Coherent Perfect Absorbers: Time-Reversed Lasers" Phys. Rev. Lett. 105, 053901 (2010).

[2] W. Wan, Y. D. Chong, L. Ge, H. Noh, A. D. Stone, and H. Cao, "Time-reversed lasing and interferometric control of absorption", Science 331, 889-892 (2011).

[3] S. Longhi, "Coherent perfect absorption in a homogeneously broadened two-level medium", Phys. Rev. A 83, 055804 (2011).

[4] S. Thongrattanasiri, F. H. L. Koppens, and F. J. GarciadeAbajo; "Complete Optical Absorption in Periodically Patterned Graphene", Phy. Rev. Lett. 108, 047401 (2012).

[5] D. G. Sourya, O. J. F. Martin, S. Dutta Gupta, and G. S. Agarwal, "Controllable coherent perfect absorption in a composite film", Optics Express 20, 1330 (2012).

[6] D. G. Sourya, R. Deshmukh, A. V. Gopal, O. J. F. Martin and S. Duttagupta; "Coherent perfect absorption mediated anomalous reflection and refraction", Optics Letters, Vol. 37, Issue 21, pp. 4452-4454 (2012).

[7] S. Longhi, "PT-symmetric laser absorber", Phys. Rev. A 82, 031801(R) (2010).

[8] M. Cai, O. Painter and K. j. Vahala; "Observation of Critical Coupling in a Fiber Taper to a Silica-Microspherefig Whispering-Gallery Mode System", PRL Vol. 85 no 74(4) (2000).

[9] Jonathan R. Tischler, M. Scott Bradley and Vladimir Bulovic; "Critically coupled resonators in vertical geometry using a planar mirror and a 5 nm thick absorbing film", Opt Lett, Vol. 31, 13, pp. 2045-2047 (2006).

[10] S. Dev, S. Duttagupta, J. Banerji and S. Duttagupta; "Critical coupling at oblique incident", J. Opt. A, Pure Appl. Opt. 9, 555-559 (2007).

[11] S. Duttagupta, "Strong interaction mediated critical coupling at two distinct frequencies", Opt Lett, Vol. 32, 11, pp. 1483-1485 (2007).

[12] H. Noh, Y. Chong, A. D. Stone, and H. Cao "Perfect coupling of light to surface plasmons by coherent absorption", PRL 108, 186805 (2012).

[13] L. I. Perez, "Reflection and non-specular effect of 2D Gaussian beam in interfaces between isotropic and anisotropic media",6 J. Modern Optics Vol. 47, Issue 10, 1645-58(2000).

[14] A. Yariv; "Quantum Electronics" (third Ed) (John Wiley & Sons) p-106.

[15] M. Born and E. Wolf; "Principle of Optics" (7th edition) (Cambridge university press) p-75.

[16] C. F. Bohren and D. R. Huffman; "Absorption and Scattering of Light by Small Particles" (John Wiley & Sons) p-77.

[17] W. Cai and V. Shalaev; "Optical Metamaterials: Fundamentals and Applications"(Springer) p-25.

[18] L. Novotny and B. Hecht; "Principle of nano optics" (Cambridge university press) p-45.

[19] S. Hassani; "Mathematical Method" (2nd edition)p-691 and Mathews & Fink; "Numerical methods using MATLAB"(3rd edition) p-186.

[20] P. B. Johnson and R. W. Christy; "Optical Constants of the Noble Metals" Phys. Rev. B 6, 4370-4379 (1972).

[21] E. D. Palik; "Handbook of Optical Constant of Solids", Academic press (1998).

[22] S. Dutta Gupta, "Nonlinear optics of Stratified media", Progress in Optics, E.Wolf, ed.(Elsevier Science, 1998), Vol. 38, p.1.

Chapter 4

Coherent Perfect Absorption in multi-metal-dielectric Composite

4.1 Introduction

The preceding chapter dealt with a study of coherent perfect absorption (CPA) in two component metal-dielectric composite medium. In this chapter we present a study of CPA in three-component (metal-metal-dielectric) composites materials.

Compared with two-component composite media, very few theoretical research and experimental investigation of three or more component composite materials have been performed. Even these use very high volume filling fractions are mostly limited to the study of metal-ceramics (cermets) [1], [2], [3].

In this chapter, we investigate CPA in a new composite medium using two metals, Gold (Au), Silver(Ag) and dielectric, Silica (SiO_2). Initially we determine all basic parameters to get CPA in two-component $Au - SiO_2$ and $Ag - Sio_2$ composites for two very close wavelengths, say λ_1 and λ_2 respectively. We then construct a new CM comprising $Au + Ag + SiO_2$ with similar volume fractions and investigate the occurrence of CPA as a function of wavelength and thickness of the composite.

The organizations of the chapter is as follows: In the next section we formulate the problem and state the geometry of the system. Third section

contain numerical results and discussion. In section four we summarize the results and draw conclusions from them.

4.2 Formulation and Geometry

The medium made of metal-dielectric composite of thickness "d" is assumed to be non magnetic i. e. relative permeability is 1. Two identical plane waves (PW)/Gaussian beams (GB) are incident on the opposite interfaces of the composite medium (CM) along Z' and Z'' axes. Here Z' and Z'' axes are inclined to Z axes at angle of incidence "θ" and "$-\theta$" at $Z = 0$ and $Z = d$ respectively as shown in the fig. 4.1. We use the label L and R for left and right side respective incident propagating waves. Hence, the resulting reflected (transmitted) waves are denoted as r_L (t_L) and r_R (t_R) respectively. So that total scattering amplitude at $Z = 0$ and $Z = d$ are $r_L + t_R$ and $r_R + t_L$ respectively. The composite medium is illuminated from both sides

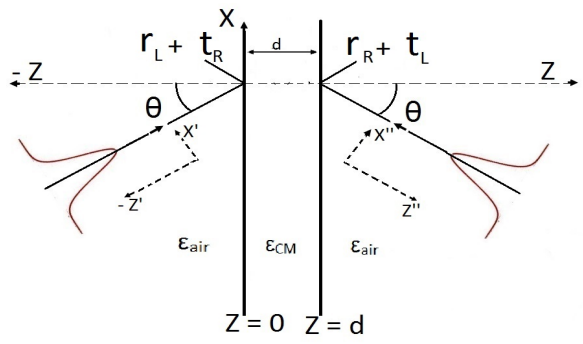

Figure 4.1: Two identical plane/Gaussian beams focus on opposite interfaces of CM and air. Here, r_L (t_L) and r_R (t_R) are reflection (transmission) coefficient at the left and right side interface respectively. Various coordinate systems are also shown in the figure.

by two identical laser sources of equal intensity, width, wavelength and angle of incidence at $[x, y, z] = [0, 0, 0]$ and $[x, y, z] = [0, 0, d]$ as shown in the fig. 4.1. From the figure, one can find clear relations among all axes; i. e. $x' = x\cos\theta - z\sin\theta$, $y' = y$, $z' = x\sin\theta + z\cos\theta$, $x'' = x\cos\theta + (z-d)\sin\theta$, $y'' = y$ and $z'' = (z-d)\cos\theta - x\sin\theta$. Where θ is angle of incidence.

Considering the three-component composite medium as a homogeneous mixture of metals and dielectric, the effective permittivity of CM is calculated

from Bruggeman effective medium theory (BEMT) [11, 12] using the optical constants of metals (Au and Ag) [16] and dielectric (SiO_2)[24] by interpolation for all wavelengths in the visible region as described in chapter 2. The incident beam falls on the air-CM interface along prime/double prime (representing by p) axes. Then equations of a Gaussian [5, 17, 18] beam propagating along p axes can be represented as :

$$E(x^p, z^p) = \frac{w_0}{w(z^p)} e^{\frac{x^{p2}}{q^p}} e^{\pm ik_0 z^p} e^{\mp i\eta(z^p)} \tag{4.1}$$

In the above eq. 6.2 + and − sign comes due to (opposite) direction of propagation. The beam parameters are $\frac{1}{q^p} = \frac{1}{w^2(\pm z^p)} + \frac{ik_0}{2R(\pm z^p)}$. By definition, irrespective of prime or double prime coordinate, the basic beam elements are as : wave vector, $k = \frac{2\pi}{\lambda}$; beam waist size, $w^2(z) = w_0^2(1 + \frac{z^2}{z_0^2})$; radius of curvature, $R(z) = z(1 + \frac{z_0^2}{z^2})$; Rayleigh range, $z_0 = w_0^2 \frac{\pi}{\lambda}$; Gouy phase, $\eta(z) = \tan^{-1}(\frac{z}{z_0})$. Angular spectrum representations [5, 14] formalism is used in whicb the Gaussian beam is regarded as a collection of many plane waves having different wave vector.

$$\hat{E}(K_x; z) = \frac{w_0}{\sqrt{2\pi}} \int_{-\infty}^{\infty} [e^{i(k_0 \sin\theta - K_x)x} \frac{e^{\frac{x^2 \sin^2\theta}{q}} e^{-i\eta(x\sin\theta)}}{w(x\sin\theta)}] dx \tag{4.2}$$

The incident beams are focused on two opposite interfaces (i. e. z = 0 and z = d) of the CM and air . The angular spectrum beam is ideally an infinite number of plane waves that is numerically evaluated using Fourier trasform. Then each plane wave correspond to reflection (r) and transmission (t) at the interfaces. The r and t field amplitudes are obtain by using the coefficients of reflection and transmission [13, 15] as outlined in chapter 1. Finally, the scattering amplitude (SA) obtained from ($r_L + t_R$) or ($r_R + t_L$) for all the plain waves are to be inversely Fourier transformed to obtain the resultant beam profile which can be written as

$$E(x; z) = \frac{1}{\sqrt{2\pi}} \int_{-\infty}^{\infty} [SA\, of\, \hat{E}(K_x; z)] e^{iK_x x} dK_x \tag{4.3}$$

4.3 Numerical results and discussions

All the numerical results are simulated for TE (or s-) polarised light. The construction of three component composites was done as follows: Initially, for a given thickness of the composite medium and the angle of incidence, we

determine the optimum parameters for attaining CPA in the two component , gold-silica and silver-silica composites, around a common wavelength.

In these simulations the angle of incidence is fixed at $\theta_i = 45^o$ and the thickness of the composite medium is initially fixed at, d = 100 μm. The influence of 'd' on CPA is also studied later by varying the thickness from 10 μm to 300 μm.

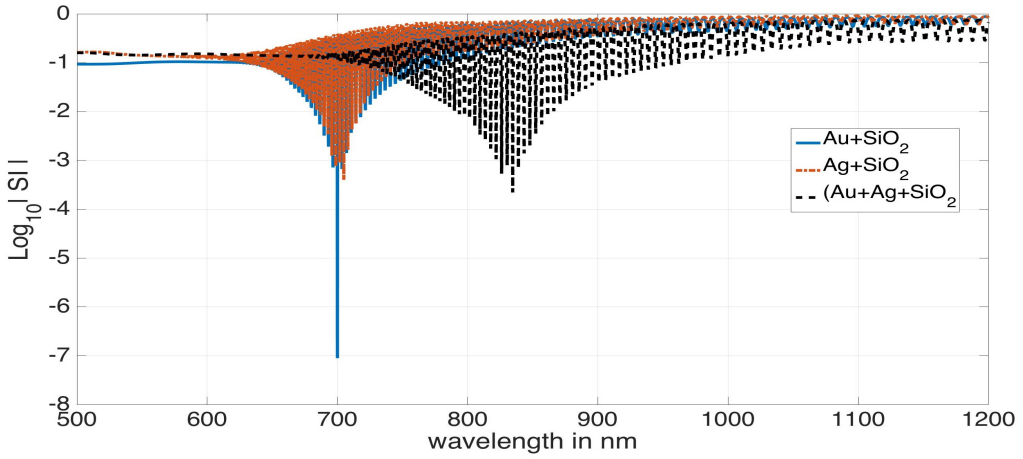

Figure 4.2: Log of scattering amplitude is measured with respect to wavelengths. Solid $(-)$, dash dot dash $(-\cdot-)$ dash $(--)$ and lines are for CPA in GC $(Au + SiO_2)$, SC $(Ag + SiO_2)$ and GSC $(Au + Ag + SiO_2)$ respectively.

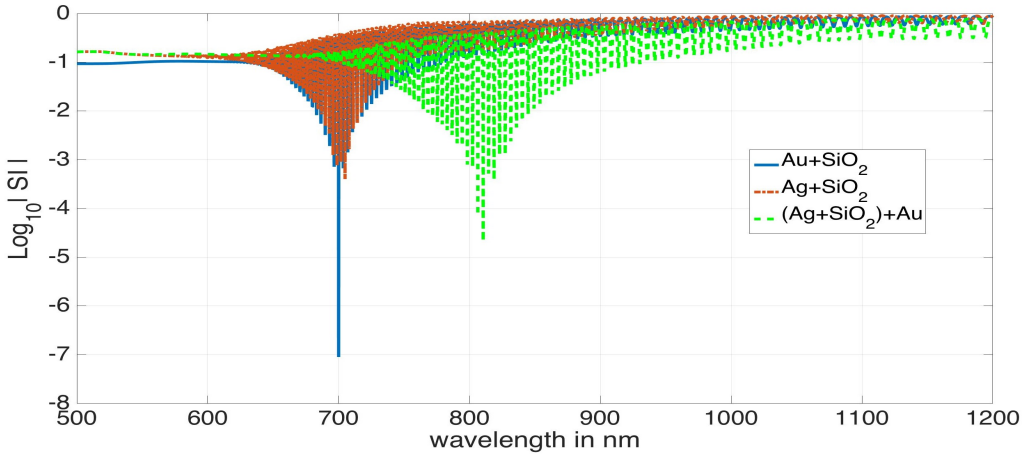

Figure 4.3: Log of scattering amplitude measured with respect to wavelengths. Solid $(-)$, dash dot dash $(-\cdot-)$ dash $(--)$ and lines are for CPA in GC $(Au + SiO_2)$, SC $(Ag + SiO_2)$ and GSC $(Au + Ag + SiO_2)$ respectively.

Using these optimized volume filling fraction values a three-component gold-silver-silica composite medium was constructed.

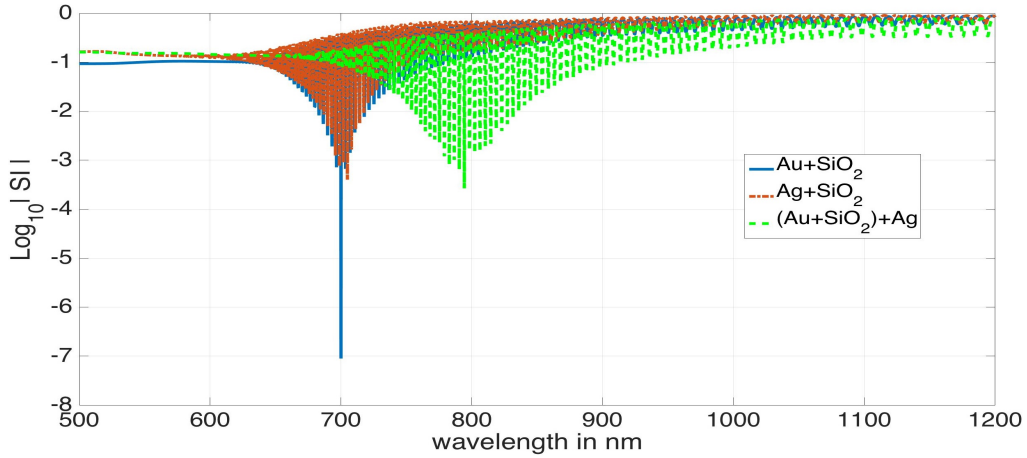

Figure 4.4: Log of scattering amplitude measured with respect to wavelengths. Solid $(-)$, dash dot dash $(-\cdot-)$ dash $(--)$ and lines are for CPA in GC $(Au + SiO_2)$, SC $(Ag + SiO_2)$ and GSC $(Au + Ag + SiO_2)$ respectively.

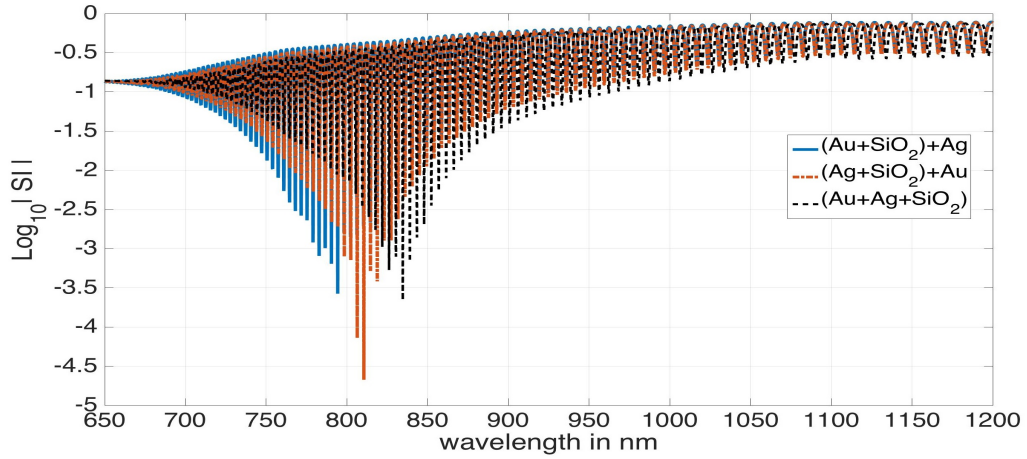

Figure 4.5: Log of scattering amplitude calculated with respect to wavelength for comparison between CPA of three distinct method of constructing three-component composite. Solid $(-)$, dash dot dash $(-\cdot-)$ dash $(--)$ and lines are for CPA in GC+S $((Au + SiO_2) + Ag)$, SC+G $((Ag + SiO_2) + Au)$ and GSC $(Au + Ag + SiO_2)$ respectively.

Fig.(4.2) illustrates the results for CPA studied in the three-component gold-silver-silica (denoted GSC) composite medium. For comparison purpose,

results for two-component gold-silica (denoted GC) and silver-silica (denoted SC) composites are also displayed in this figure. These results for plane-wave CPA show that for three component composite, the width of the CPA profile is broadened and the wavelength at which maximum absorption dip occurs,undergoes drastic red shift (120 nm) compared to that of the two-component, GC and SC composites. This increase can be attributed to enhanced interaction between localized surface plasmons of different metals.

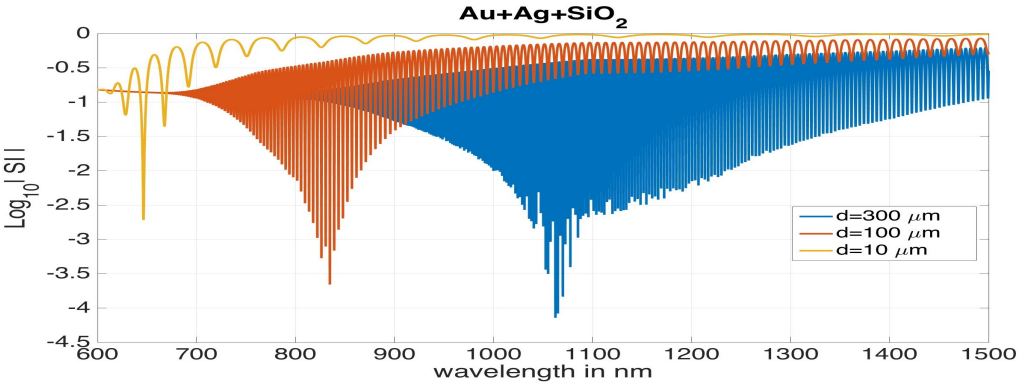

Figure 4.6: Log of scattering amplitude calculated with respect to the wavelength for different thickness 'd' of the three-component (GSC) composite. Yellow, brown and blue curves respectively, correspond to d = 10, 100 and 300 μm.

To investigate the origin of multiple CPA peaks in a three-component composite, we now study the influence of the thickness by varying the thickness 'd' from 10 μm to 300 μm. The results depicted in Fig.(4.6) reveal that the distance between adjacent resonance peaks increases with decreasing 'd' as is expected in a CPA resonator cavity (see ref.([4]). For this reason we observe many absorption resonances around the central resonance wavelength in a thicker medium that can be utilized as broadband absorber. However there is large blue shift of the (central) resonance wavelength of the CPA, with decreasing thickness of the composite medium.

The other two possibilities for construction of a three-component composite are: (ii) by adding silver to the two-component gold-silica composite, (iii) by adding gold to the two-component silver-silica composite. The result for CPA studied in the three component composites made by successive use of two-component composites mentioned above are displayed in the figures, fig(4.3) - fig(4.5).

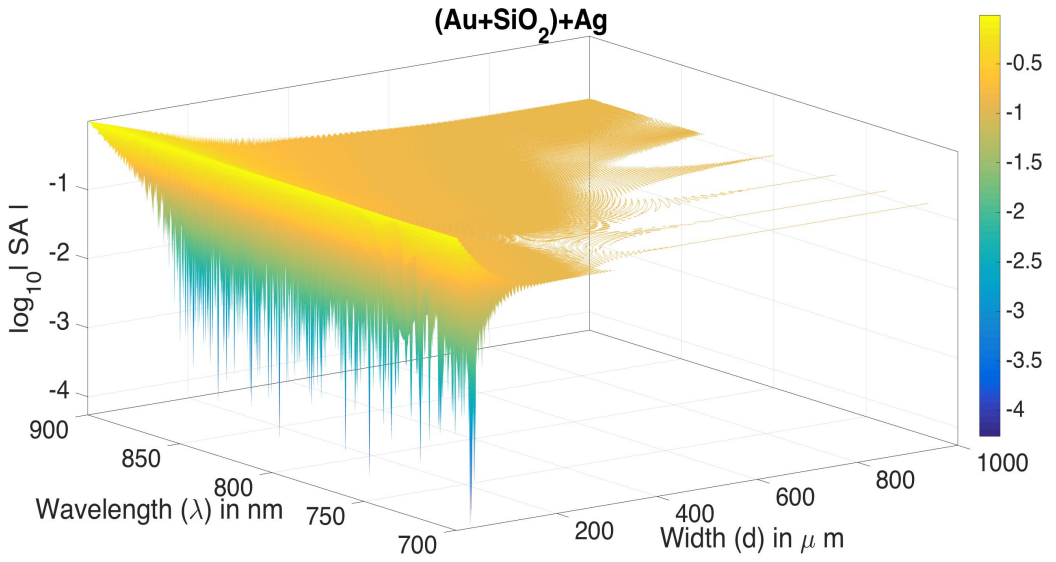

Figure 4.7: Log of scattering amplitude calculated as functions of width (d) of the medium and wavelength. The remaining parameters are constant.

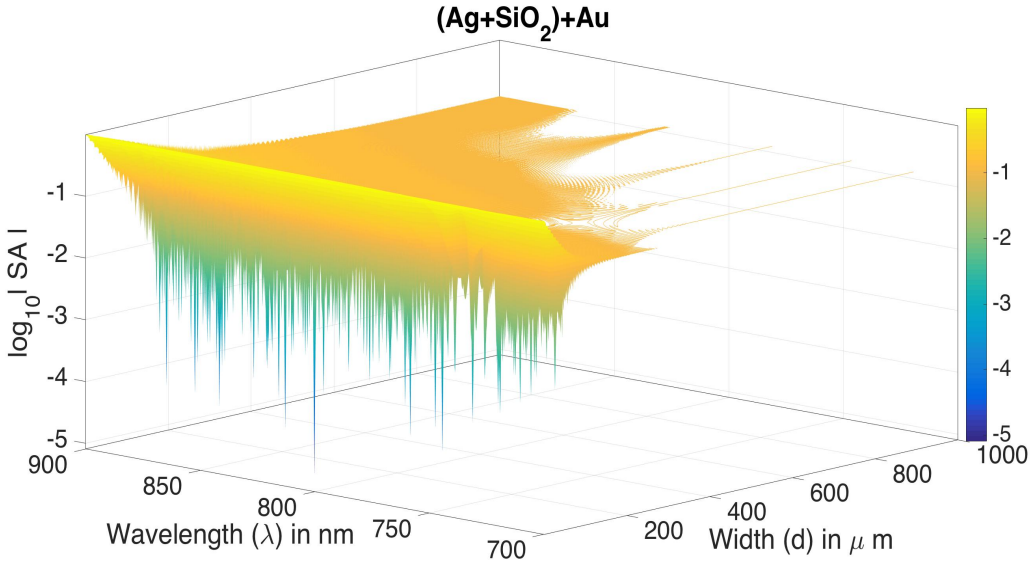

Figure 4.8: Log of scattering amplitude calculated as functions of width (d) of the medium and wavelength. The remaining parameters are constant.

A comparison of the plane wave results for CPA for the three cases of three component medium shown in fig.(4.5) reveals that except for a slight

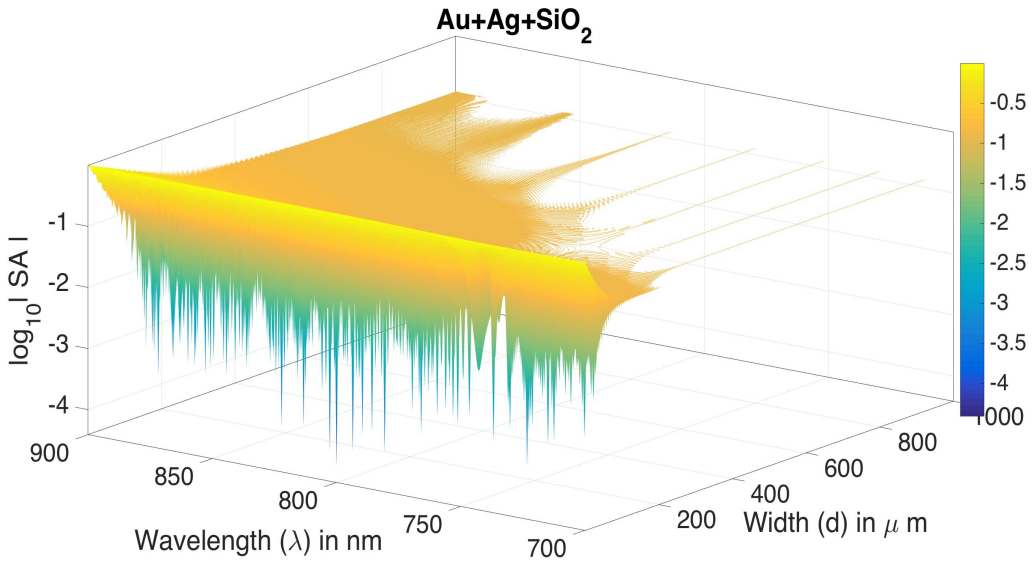

Figure 4.9: Log of scattering amplitude calculated as functions of width (d) of the medium and wavelength. The remaining parameters are constant.

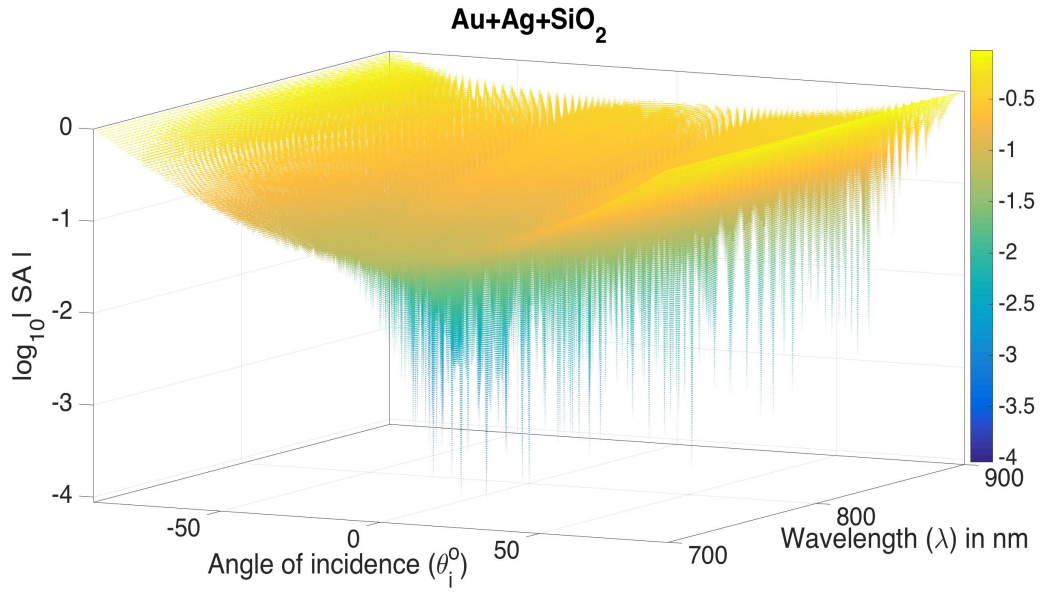

Figure 4.10: Log of scattering amplitude calculated as functions of angle of incidences (θ^o) and wavelength. The remaining parameters are constant.

difference in the peak position of the wavelength for the occurrence of CPA, other feature for all these three component composites are similar.

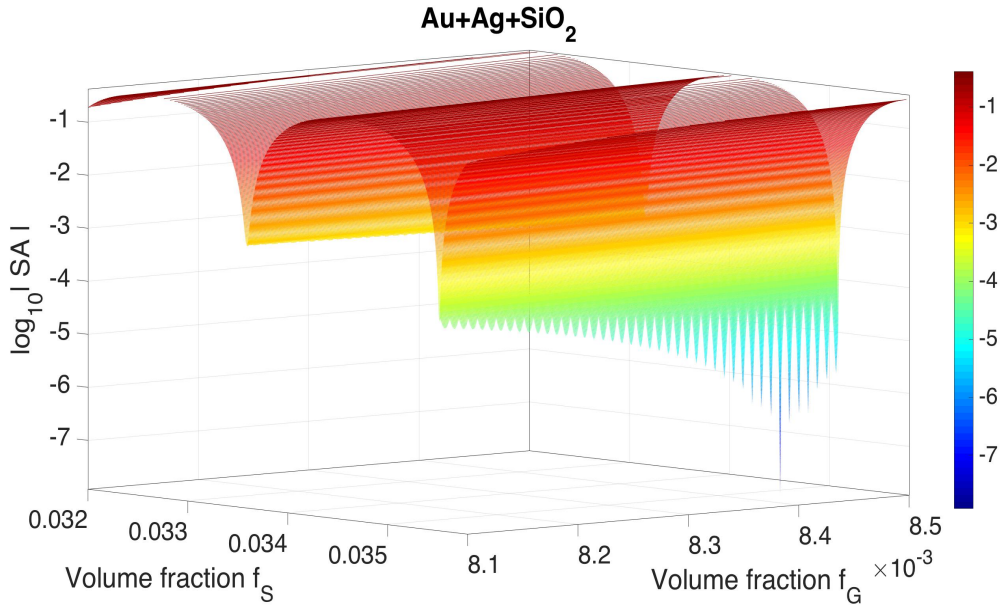

Figure 4.11: Log of scattering amplitude calculated as functions of Gold's and Silver's volume fraction, f_G and f_S. The remaining parameters are constant.

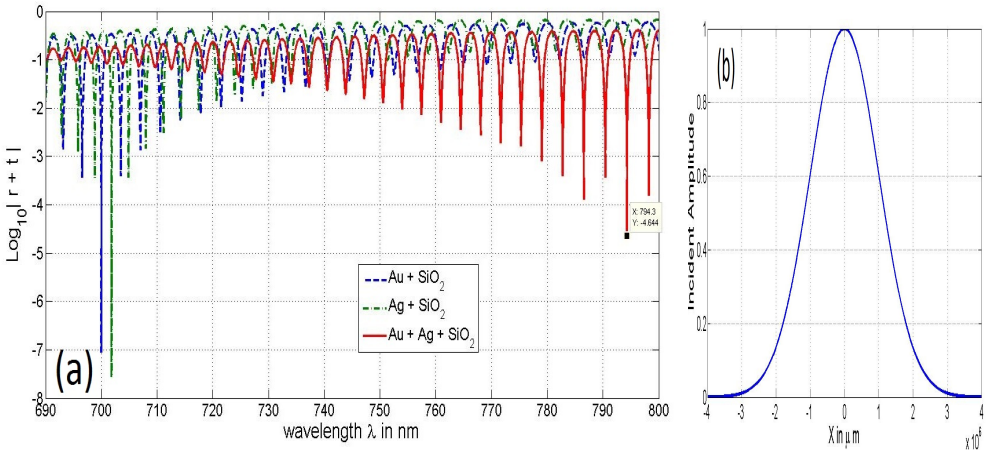

Figure 4.12: (a) Log of Scattering amplitude is measured with respect to wavelengths. Dash $(--)$, dash dot dash $(-\cdot-)$ and solid $(-)$ lines are for CPA in GC $(Au + SiO_2)$, SC $(Ag + SiO_2)$ and GSC $(Au + Ag + SiO_2)$ respectively. (b) Two identical incident beams profile.

The Gaussian beam results for CPA for the two and three component composites is displayed in fig.(4.12), fig.(4.13) and fig.(4.14) at various wavelengths at and around the (central) CPA wavelength. These reveal that perfect CPA

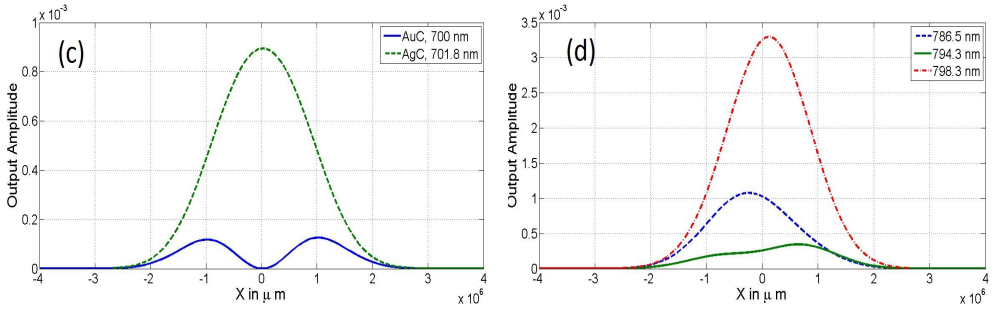

Figure 4.13: (c) Output beams profile for GC (−) and SC (−−) at 700 nm and 701.8 nm respectively. (d) Output beams profile for GSC at 786.5 nm (−−), 794.3 nm (−) and 798.3 nm (− · −) respectively.

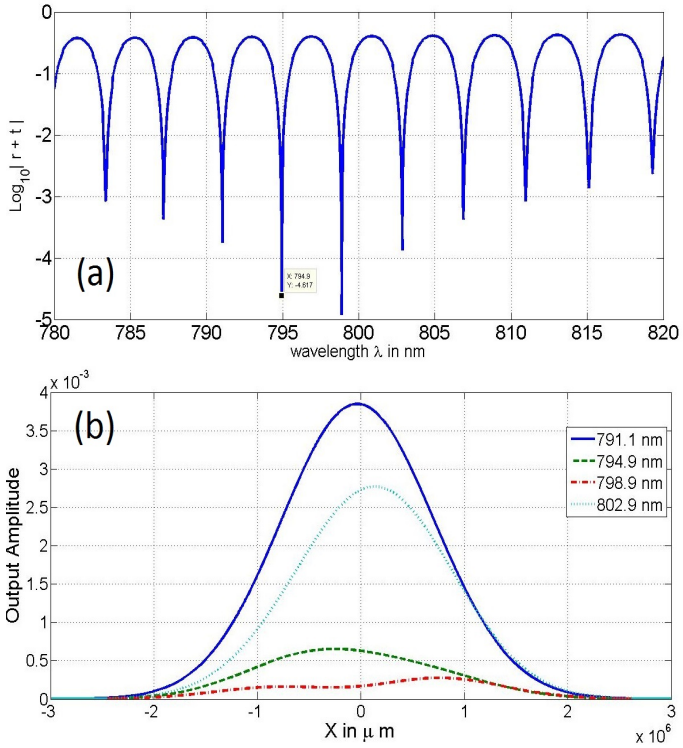

Figure 4.14: (a) Log of scattering amplitude measured as a function of wavelength on GSC when $Au : Ag : SiO_2 = f_G : f_S : (1-f_G)(1-f_S) = 0.008352251 : 0.035257 : 0.95668522$. (b) Output beams profile at the absorption peaks observed at 791.1, 794.9, 798.9 and 802.9 nm respected wavelengths.

occurs even for the realistic laser (Gaussian) beams specially at the central CPA wavelength.

4.4 Summary and conclusions :

In this chapter, we investigate CPA in a three-composite composite medium which is made of different combinations of Gold (Au), Silver(Ag) and Silica (SiO_2). We have shown results for three component composites by first optimizing all basic parameters to get CPA in $Au-SiO_2$ and $Ag-Sio_2$ composites for two very close wavelengths, say λ_1 and λ_2. We have then constructed a new three-component composite medium comprising $Au + Ag + SiO_2$ with similar volume fractions and have found CPA occurring at different (higher) wavelengths and broader widths. It is also shown that there are three ways in which this can be done. However comparison of CPA characteristics in these three cases reveals that except for a slight variation in the position of the wavelength where maximum CPA occurs other features are similar.

The most significant outcome of this study is the intriguing effect of the width of the composite on CPA. With increasing width of the composite, the CPA resonance shows red shift and number of absorption peaks increase around the central CPA wavelength which can be attributed to the CPA (resonant) cavity effect [4].

Bibliography

[1] Michael Quinten, "Optical Properties of Nanoparticle Systems", Wiley-VCH Verlag and Co. KGaA (2011) pp. 440.

[2] G. A. Niklasson, C.G. Granqvistand O.Hunderi, "Effective medium models for the optical properties of inhomogeneous materials", Appl. Opt. 20(1981)26–30.

[3] R. Luo, "Effective medium theories for the optical properties of three - component composite materials", . Appl. Opt. 36(1997) 8153 – 8158 .

[4] Y. D. Chong, L. Ge, H. Cao and A. D. Stone, "Coherent perfect absorbers:time reversed lasers", Phys. Rev. Lett. 105(2010)053901.

[5] W. Wan, Y. D. Chong, L. Ge, H. Noh, A. D.Stone and H. Cao, "Time-reversed lasing and interferometric control of absorption", Scnc. 331(2011)889–892.

[6] S. Longhi, "Coherent perfect absorption in a homogeneously broadened two level medium", Phys. Rev. A83(2011)055804.

[7] S. Thongrattanasiri, F. H. L. Koppens and F. J. GarciadeAbajo, "Complete optical absorption in periodically patterned graphene", Phys. Rev. Lett. 108(2012)047401.

[8] D. G. Sourya, O. J. F. Martin, S. DuttaGupta and G. S. Agarwal, "Controllable coherent perfect absorption in a composite film", Opt. Exp. 20(2012)1330.

[9] S. Dey, "Coherent perfect absorption using Gaussian beams", Opt. Comm. 356(2015)515-521

[10] S. Longhi, "PT-symmetric laser absorber", Phys. Rev. A 82(2010)031801(R).

[11] M. Cai, O. Painter and K. j. Vahala, "Observation of critical coupling in a fiber taper to a silica-microsphere whispering -gallery mode system", Phys. Rev. Lett. 85 (2000)74.

[12] J. R. Tischler, M. S. Bradley and V. Bulovic, "Critically coupled resonators in vertical geometry using a planar mirror and a 5 nm thick absorbing film", Opt. Lett. 31(13)(2006)2045.

[13] S. Balci, C. Kocabas and A. Aydinli, "Critical coupling in plasmonic resonator arrays", Opt. Letts. 36(Aug 1, 2011)15.

[14] S. Duttagupta, "Strong interaction mediated critical coupling at two distinct frequencies", Opt. Lett. 32(2007)1483–1485.

[15] H. Noh, Y. Chong, A. D. Stone and H. Cao, "Perfect coupling of light to surface plasmons by coherent absorption", Phys. Rev. Lett. 108(2012)186805.

[16] P. B. Johnson and R. W. Christy, "Optical constants of the noble metals", Phys. Rev. B 6 (1972)4370–4379.

[17] L. I. Perez, "Reflection and non-specular effect of 2D Gaussian beam in interfaces between isotropic and anisotropic media", J. Mod. Opt. 47(10)(2000)1645–1658.

[18] A. Yariv, "Quantum Electronics", 3rd ed., John Wiley & Sons, NewYork(1987), p.106.

[19] C. F. Bohren and D. R. Huffman, "Absorption and Scattering of Light by Small Particles", John Wiley & Sons, NewYork(1983), p.77.

[20] W. Cai and V. Shalaev, "Optical Metamaterials:Fundamentals and Applications", Springer, NewYork(2010), p.25.

[21] M. Born and E. Wolf, "Principle of Optics", 7th ed., Cambridge University Press, NewYork(2005), p.75.

[22] L. Novotny and B. Hecht, "Principle of Nano-Optics", Cambridge University Press, NewYork(2006), p.45.

[23] S. Duttagupta, "Nonlinear optics of stratified media", in:E.Wolf(Ed.), "Progress in Optics", vol.38, Elsevier Science, NewYork, 1998, p.1.

[24] E. D. Palik, "Handbook of Optical Constant of Solids", Academic Press, London, 1998.

Chapter 5

Coherent Perfect Absorption: an Electromagnetic perspective

5.1 Introduction

This chapter deals with theoretical formulation of coherent perfect absorption (CPA) for plane electromagnetic waves. Initially we review the usual derivation of reflection and transmission coefficients for an obliquely incident plane wave using Maxwell equations and boundary conditions at an interface. Next, we calculate reflection and transmission coefficients at the interfaces of a CPA medium and derive the condition for the occurrence of CPA. The theoretical formalism is then applied to the numerical CPA studies of the previous chapters.

5.2 Reflection and transmission coefficients

Consider a TE (s-polarized) plane wave incident at oblique angle θ_i upon an interface at $z = 0$ between two media of refractive indices n_1 (medium 1) and n_2 (medium 2) with $n_2 > n_1$ [1]. Part of the light is reflected back in medium 1 at an angle θ_r and transmitted in medium 2 at angle θ_t. As usual all the angles are measured with respect to the normal to the interface at z = 0. The amplitude of incident, reflected and transmitted waves are denoted A_i, A_r and A_t respectively. A TE (s-polarised) wave can be expressed as $\vec{E} = (0, E_y, 0)$ according to the geometry shown in the fig. (5.1).

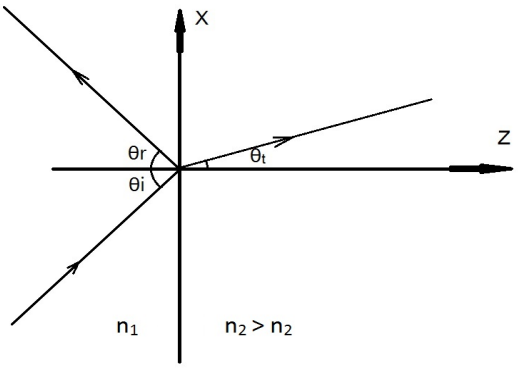

Figure 5.1: A plane wave incident on the interface between two media of refractive indices n_1 and n_2.

.

The, plane wave in medium I can be written as,

$$E_{1y} = (A_{in}e^{ik_{1z}z} + A_r e^{-ik_{1z}z})e^{i(k_{1x}x-\omega t)} \tag{5.1}$$

where first and second terms (inside bracket) respectively, are the incident and reflected parts with $k_{1z} = \sqrt{k_1^2 - k_{1x}^2} = \sqrt{k_0^2\epsilon_1 - k_{1x}^2}$ and $k_{1x} = k_0\sqrt{\epsilon_1}\sin\theta_i$.

As stated before at optical frequencies the medium is non-magnetic so that $\mu = 1$ and the corresponding magnetic field
$\vec{H}$=$(\hat{x}H_x + \hat{y}H_y + \hat{z}H_z)e^{i(k_x x-\omega t)}$
can be evaluated from the Maxwell's equation $-\frac{1}{c}\frac{\partial\vec{B}}{\partial t} = \vec{\nabla}\times\vec{E}$ as:

$$\begin{aligned} ik_0\vec{H} &= \vec{\nabla}\times\vec{E} \\ &= \begin{vmatrix} \hat{x} & \hat{y} & \hat{z} \\ \frac{\partial}{\partial x} & \frac{\partial}{\partial y} & \frac{\partial}{\partial z} \\ 0 & E_y & 0 \end{vmatrix} \\ &= -\hat{x}\frac{\partial E_y}{\partial z} + \hat{z}\frac{\partial E_y}{\partial x} \end{aligned} \tag{5.2}$$

where $k_0 = \frac{\omega}{c} = \frac{2\pi}{\lambda}$. Now equating the coefficients of x-axis in eq. (5.2) and using the expression for E_{1y} from eq. (5.1), we obtain

$$ik_0 H_{1x} = -\frac{\partial E_1 y}{\partial z} \tag{5.3}$$

$$= -(ik_{1z}A_{in}e^{ik_{1z}z} + ik_{1z}A_r e^{-ik_{1z}z})e^{i(k_{1x}x-\omega t)}$$

$$\Rightarrow H_{1x} = \frac{ik_{1z}}{ik_0}(-A_{in}e^{ik_{1z}z} + A_r e^{ik_{1z}z})e^{i(k_{1x}x-\omega t)} \tag{5.4}$$

$$\begin{bmatrix} E_{1y} \\ H_{1x} \end{bmatrix} = \begin{bmatrix} e^{ik_{1z}z} & e^{-ik_{1z}z} \\ -S_1 e^{ik_{1z}z} & S_1 e^{-ik_{1z}z} \end{bmatrix} \begin{bmatrix} A_{in} \\ A_r \end{bmatrix} \tag{5.5}$$

where we have set aside the term $e^{i(k_{1x}x-\omega t)}$ as it is currently not needed in our calculations and will ultimately vanish. Similarly the transmitted waves $E_{2y} = A_t e^{ik_{2z}z} e^{i(k_{2x}x-\omega t)}$ and $H_{2x} = A_t \frac{k_2 z}{k_0} e^{ik_{2z}z} e^{i(k_{2x}x-\omega t)}$ can be written in matrix form as follows :

$$\begin{bmatrix} E_{2y} \\ H_{2x} \end{bmatrix} = \begin{bmatrix} e^{ik_{2z}z} \\ -S_2 e^{ik_{2z}z} \end{bmatrix} A_t \tag{5.6}$$

where, $S_2 = \frac{k_2 z}{k_0}$. We keep the term $e^{i(k_{2x}x-\omega t)}$ aside for the same reason. According to the boundary conditions at the interface z = 0 we have $k_{1x} = k_0 \sin\theta_i = k_{2x}$ and $\begin{bmatrix} E_{1y} \\ H_{1x} \end{bmatrix}_{z=0} = \begin{bmatrix} E_{2y} \\ H_2 x \end{bmatrix}_{z=0}$ so,

$$\begin{bmatrix} 1 & 1 \\ -S_1 & S_1 \end{bmatrix} \begin{bmatrix} A_{in} \\ A_r \end{bmatrix} = \begin{bmatrix} 1 \\ -S_2 \end{bmatrix} A_t, \tag{5.7}$$

$$\Rightarrow \begin{bmatrix} A_{in} + A_r \\ -S_1 A_{in} + S_1 A_r \end{bmatrix} = \begin{bmatrix} A_t \\ -S_2 A_t \end{bmatrix} \tag{5.8}$$

Which straight away implies the following two equations :

$$\begin{aligned} 1 + r &= t, \\ S_1(1 - r) &= S_2 t. \end{aligned} \tag{5.9}$$

Here $r = \frac{A_r}{A_{in}}$ is the reflection coefficient and $t = \frac{A_t}{A_{in}}$ is the transmission coefficient. These are obtained by solving eq. (5.9) as

$$r = \frac{k_{1z} - k_{2z}}{k_{1z} + k_{2z}} = \frac{\sqrt{\epsilon_1} - \sqrt{\epsilon_2}}{\sqrt{\epsilon_1} + \sqrt{\epsilon_2}}, \tag{5.10}$$

$$t = \frac{2k_{1z}}{k_{1z} + k_{2z}} = \frac{2\sqrt{\epsilon_1}}{\sqrt{\epsilon_1} + \sqrt{\epsilon_2}}. \tag{5.11}$$

Here k_{jz} is wave number, where j=1 or 2. These can be evaluated using the relations, $k_{jz} = \sqrt{k_j^2 - k_{jx}^2}$, $k_j = k_0\sqrt{\epsilon_j}$ and $k_{1x} = k_0 \sin\theta_i = k_{2x}$. Hence from above equations (5.10) and (5.11) we can find reflection and transmission (or refraction) coefficients for any angle of incidence.

5.3 Reflection and transmission in CPA medium

In a typical CPA configuration, two identical electromagnetic waves are incident from opposite direction on the left (L) and the right (R) interfaces of the

CPA medium henceforth called slab. Both electromagnetic waves have the same angle of incidence θ. As shown in the fig. 5.2, the two air-slab interfaces are in the $x-y$ plane at $z=-d$ and $z=d$ so that the slab thickness is $2d$.

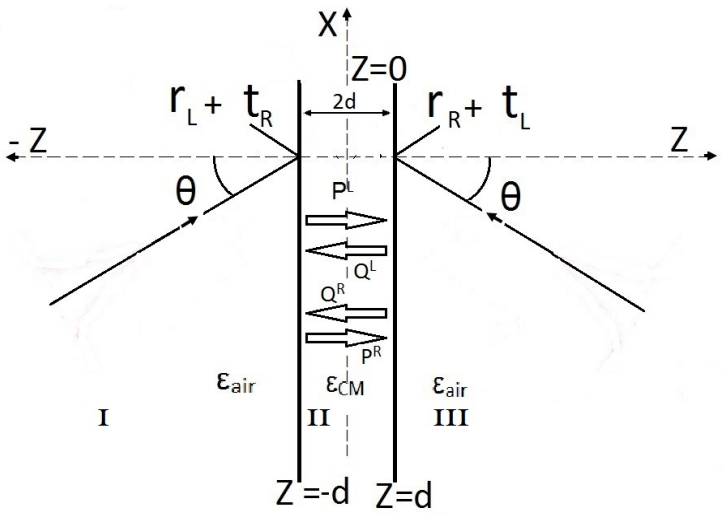

Figure 5.2: Two identical plane waves incident (at same angle θ) on the two air-CPA medium interfaces from both sides.

Owing to the symmetry of the CPA configuration and superposition principal we can consider the reflection and transmission characteristics of each electromagnetic wave separately and superpose them later to obtain the resultant transmission or reflectivity at any interface and deduce the CPA condition.

Therefore for the incident TE (s-polarized) plane wave from left (in medium 1) the expressions for the electric and magnetic field respectively, is the same as given by eqs.(5.1) and (5.4) which was written in matrix form as (5.5)

$$\begin{bmatrix} E_{1y} \\ H_{1x} \end{bmatrix} = \begin{bmatrix} e^{ik_{1z}z} & e^{-ik_{1z}z} \\ -S_1 e^{ik_{1z}z} & S_1 e^{-ik_{1z}z} \end{bmatrix} \begin{bmatrix} A_{in} \\ A_r \end{bmatrix} \tag{5.12}$$

Similarly, the expressions for the electric and magnetic field respectively, in medium II and III can be written in the matrix form as

$$\begin{bmatrix} E_{2y} \\ H_{2x} \end{bmatrix} = \begin{bmatrix} e^{ik_{2z}z} & e^{-ik_{2z}z} \\ -S_2 e^{ik_{2z}z} & S_2 e^{-ik_{2z}z} \end{bmatrix} \begin{bmatrix} P_L \\ Q_L \end{bmatrix} \tag{5.13}$$

and

$$\begin{bmatrix} E_{3y} \\ H_{3x} \end{bmatrix} = \begin{bmatrix} e^{ik_{1z}z} \\ -S_1 e^{ik_{1z}z} \end{bmatrix} A_t \tag{5.14}$$

Here P_L and Q_L are the amplitudes of the forward and backward moving waves (in medium II) as shown in fig.5.2. According to the electromagnetic boundary conditions at the interface $z = d$, $\begin{bmatrix} E_{2y} \\ H_{1x} \end{bmatrix} = \begin{bmatrix} E_{3y} \\ H_{3x} \end{bmatrix}$. So,

$$\begin{bmatrix} e^{ik_{2z}d} & e^{-ik_{2z}d} \\ -S_2 e^{ik_{2z}d} & S_2 e^{-ik_{2z}d} \end{bmatrix} \begin{bmatrix} P_L \\ Q_L \end{bmatrix} = \begin{bmatrix} e^{ik_{1z}d} \\ -S_1 e^{ik_{1z}d} \end{bmatrix} A_t \tag{5.15}$$

The above eq.5.15. yields the solutions for P_L and Q_L in terms of A_t as follows:

$$\begin{bmatrix} P_L \\ Q_L \end{bmatrix} = \begin{bmatrix} (1+\frac{S_1}{S_2})\frac{e^{ik_{1z}d}}{e^{+ik_{2z}d}} \\ (1-\frac{S_1}{S_2})\frac{e^{ik_{1z}d}}{e^{-ik_{2z}d}} \end{bmatrix} \frac{A_t}{2} \tag{5.16}$$

Again, the electromagnetic boundary condition at the interface $z = -d$ yields:

$$\begin{bmatrix} e^{-ik_{1z}d} & e^{ik_{1z}d} \\ -S_1 e^{-ik_{1z}d} & S_1 e^{ik_{1z}d} \end{bmatrix} \begin{bmatrix} A_{in} \\ A_r \end{bmatrix} = \begin{bmatrix} e^{-ik_{2z}d} & e^{ik_{2z}d} \\ -S_2 e^{-ik_{2z}d} & S_2 e^{ik_{2z}d} \end{bmatrix} \begin{bmatrix} P_L \\ Q_L \end{bmatrix} \tag{5.17}$$

Substituting the value of P_L and Q_L from eq.(5.16) in the above eq. (5.17) we obtain

$$\begin{bmatrix} \frac{e^{ik_{1z}d}}{2}\{(1+\frac{S_1}{S_2})e^{-2ik_{2z}d} + (1-\frac{S_1}{S_2})e^{2ik_{2z}d}\} & -e^{ik_{1z}d} \\ \frac{e^{ik_{1z}d}}{2}\{(1+\frac{S_1}{S_2})e^{-2ik_{2z}d} - (1-\frac{S_1}{S_2})e^{2ik_{2z}d}\} & \frac{S_1}{S_2}e^{ik_{1z}d} \end{bmatrix} \begin{bmatrix} \frac{A_t}{A_{in}} \\ \frac{A_r}{A_{in}} \end{bmatrix} = \begin{bmatrix} e^{-ik_{1z}d} \\ \frac{S_1}{S_2}e^{-ik_{1z}d} \end{bmatrix} \tag{5.18}$$

Here, $t_L = \frac{A_t}{A_{in}}$ and $r_L = \frac{A_r}{A_{in}}$ respectively, are the transmission (t_L) and reflection (r_L) coefficient that can be obtained from the solution of the following matrix equation

$$\begin{bmatrix} t_L \\ r_L \end{bmatrix} = D^{-1} \begin{bmatrix} e^{-ik_{1z}d} \\ \frac{S_1}{S_2}e^{-ik_{1z}d} \end{bmatrix} \tag{5.19}$$

where $D = \begin{bmatrix} \frac{e^{ik_{1z}d}}{2}\{(1+\frac{S_1}{S_2})e^{-2ik_{2z}d} + (1-\frac{S_1}{S_2})e^{2ik_{2z}d}\} & -e^{ik_{1z}d} \\ \frac{e^{ik_{1z}d}}{2}\{(1+\frac{S_1}{S_2})e^{-2ik_{2z}d} - (1-\frac{S_1}{S_2})e^{2ik_{2z}d}\} & \frac{S_1}{S_2}e^{ik_{1z}d} \end{bmatrix}$. The determinant of D is $|D| = \frac{e^{2ik_{1z}d}}{2}\{(1+\frac{S_1}{S_2})^2 e^{-2ik_{2z}d} - (1-\frac{S_1}{S_2})^2 e^{2ik_{2z}d}\}$.
Therefore, the inverse of D can be written as follows :
$D^{-1} = \frac{1}{|D|} *$

$$\begin{bmatrix} \frac{S_1}{S_2}e^{ik_{1z}d} & e^{ik_{1z}d} \\ \frac{e^{ik_{1z}d}}{2}\{(1-\frac{S_1}{S_2})e^{2ik_{2z}d} - (1+\frac{S_1}{S_2})e^{-2ik_{2z}d}\} & \frac{e^{ik_{1z}d}}{2}\{(1+\frac{S_1}{S_2})e^{-2ik_{2z}d} + (1-\frac{S_1}{S_2})e^{2ik_{2z}d}\} \end{bmatrix} \tag{5.20}$$

From the eq.s (5.19) & (5.20) the solution for t_L and r_L are

$$t_L = \frac{4\frac{S_1}{S_2}e^{-2ik_{1z}d}}{\{(1+\frac{S_1}{S_2})^2e^{-2ik_{2z}d} - (1-\frac{S_1}{S_2})^2e^{2ik_{2z}d}\}} \tag{5.21}$$

and

$$r_L = \frac{e^{-2ik_{1z}d}(1-\frac{S_1^2}{S_2^2})(e^{2ik_{2z}d} - e^{-2ik_{2z}d})}{\{(1+\frac{S_1}{S_2})^2e^{-2ik_{2z}d} - (1-\frac{S_1}{S_2})^2e^{2ik_{2z}d}\}} \tag{5.22}$$

respectively. Similarly one can obtain the solutions for an electromagnetic wave from RHS incident on interface d and these are as follows:

$$t_R = \frac{4\frac{S_1}{S_2}e^{-2ik_{1z}d}}{\{(1+\frac{S_1}{S_2})^2e^{-2ik_{2z}d} - (1-\frac{S_1}{S_2})^2e^{2ik_{2z}d}\}} \tag{5.23}$$

and

$$r_R = \frac{e^{-2ik_{1z}d}(1-\frac{S_1^2}{S_2^2})(e^{2ik_{2z}d} - e^{-2ik_{2z}d})}{\{(1+\frac{S_1}{S_2})^2e^{-2ik_{2z}d} - (1-\frac{S_1}{S_2})^2e^{2ik_{2z}d}\}} \tag{5.24}$$

Now we have all reflection (r_L & r_R) and transmission (t_L & t_R) coefficients for both left and right sides. In the next section we analyze the condition of CPA.

5.4 CPA conditions

As shown in fig.(1.2) the fields exiting the medium at either interface have contributions from both forward (wave on LHS) and the backward (wave on RHS). Thus for CPA to occur the coefficient of the field at the interface z = -d (or z = d) given by $r_L + t_R$ (or $r_R + t_L$) must vanish, that is:

$$\frac{e^{-2ik_{1z}d}(1-\frac{S_1^2}{S_2^2})(e^{2ik_{2z}d} - e^{-2ik_{2z}d})}{\{(1+\frac{S_1}{S_2})^2e^{-2ik_{2z}d} - (1-\frac{S_1}{S_2})^2e^{2ik_{2z}d}\}} + \frac{4\frac{S_1}{S_2}e^{-2ik_{1z}d}}{\{(1+\frac{S_1}{S_2})^2e^{-2ik_{2z}d} - (1-\frac{S_1}{S_2})^2e^{2ik_{2z}d}\}} = 0 \tag{5.25}$$

The above equation reduces to a much simpler form as

$$4\frac{S_1}{S_2} + (1-\frac{S_1^2}{S_2^2})(e^{2ik_{2z}d} - e^{-2ik_{2z}d}) = 0 \tag{5.26}$$

Using the relations $S_1 = \frac{k_{1z}}{k_0}$ and $S_2 = \frac{k_{2z}}{k_0}$ in eq.5.26 and after simplification we arrive at the final expression

$$2k_{1z}k_{2z} + i(k_{2z}^2 - k_{1z}^2)sin(2k_{2z}d) = 0 \tag{5.27}$$

it is obvious from above eq.(5.27) obtained under CPA conditions that the solution for propagation constant k_{2z} (or $\sqrt{\epsilon 2}$) will be complex or in other words, the CPA medium is required to be dissipative. Thus to fulfil the CPA condition in the eq.(5.27), both real and imaginary part simultaneously have to be zero.

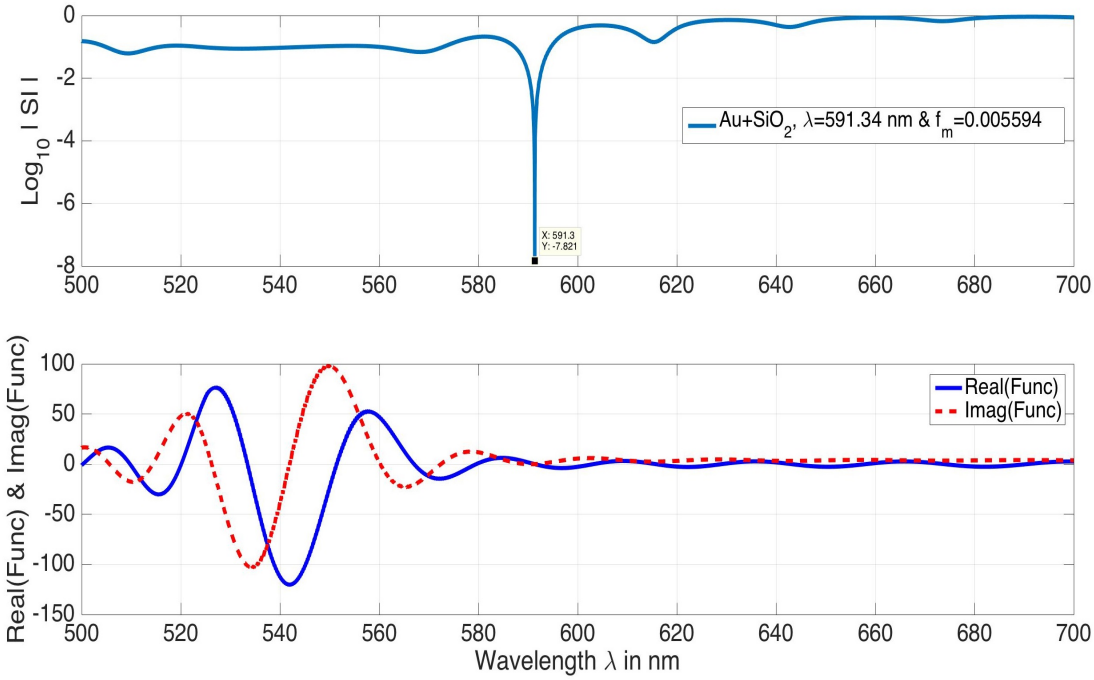

Figure 5.3: Top figure depicted CPA as a function of wavelength for Gold-Silica composite and the bottom figure shows at CPA frequency, real and imaginary part of the function become zero. Thickness of medium $d = 10\ \mu m$ and angle of incidences $\theta_i = 45^o$.

5.5 Results and discussion

We now apply the theory to CPA results computed numerically in preceding chapters 2 and 3. It may be noted that eq.(5.27) is a function of various parameters like wavelength 'λ', thickness 'd' and dielectric constants 'ϵ_2' of the CPA as well as that 'ϵ_1' of the media surrounding it. Taking these parameters from Chapter 2 and 3 and using them in eq.(5.27) we plot the variation of real and imaginary parts of the same as a function of the wavelength. The results are shown in Figures 5.3, 5.4, 5.5, 5.6, 5.7 and 5.8 respectively. It is observed

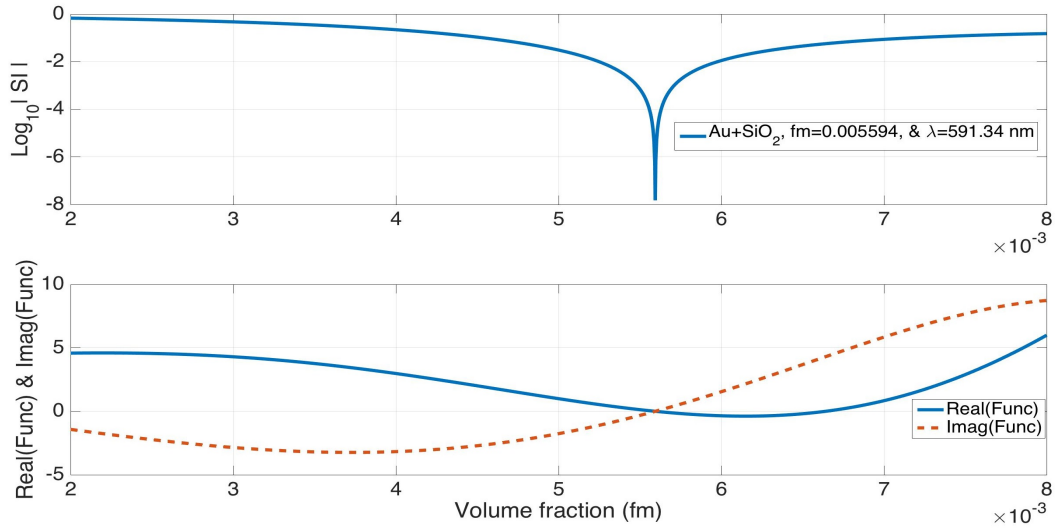

Figure 5.4: Top figure depicted CPA as a function of volume fraction (f_m) for Gold-Silica composite and the bottom figure shows at CPA frequency, real and imaginary part of the function become zero. Thickness of medium $d = 10$ μm and angle of incidences $\theta_i = 45^o$.

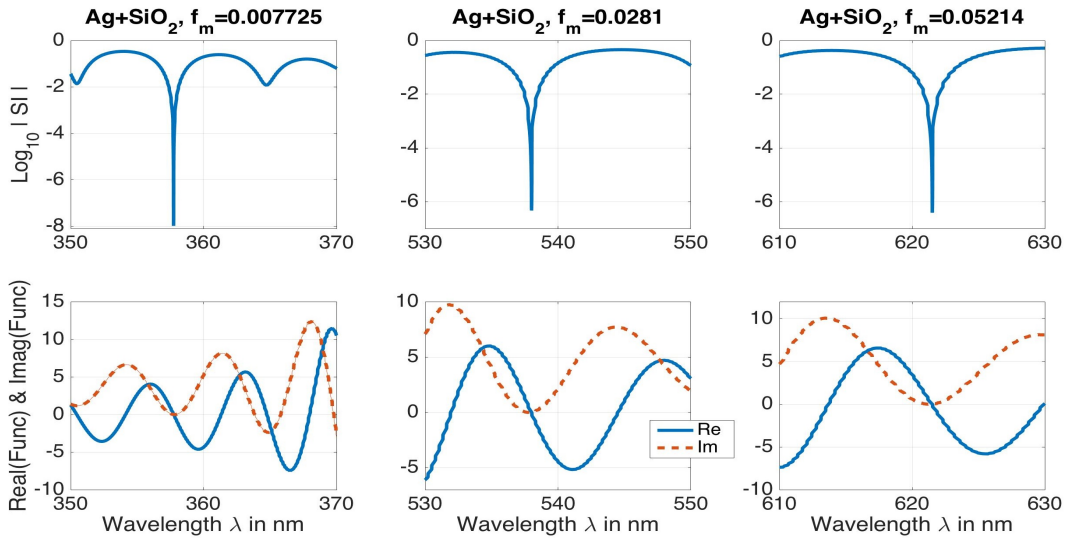

Figure 5.5: Top row shows CPA for different volume fraction as a function of wavelengths for Silver-Silica composite and the bottom row shows at CPA frequency, real and imaginary part of the function become zero. Here, thickness of the medium $d = 10\mu m$ and angle of incidences $\theta_i = 45^o$.

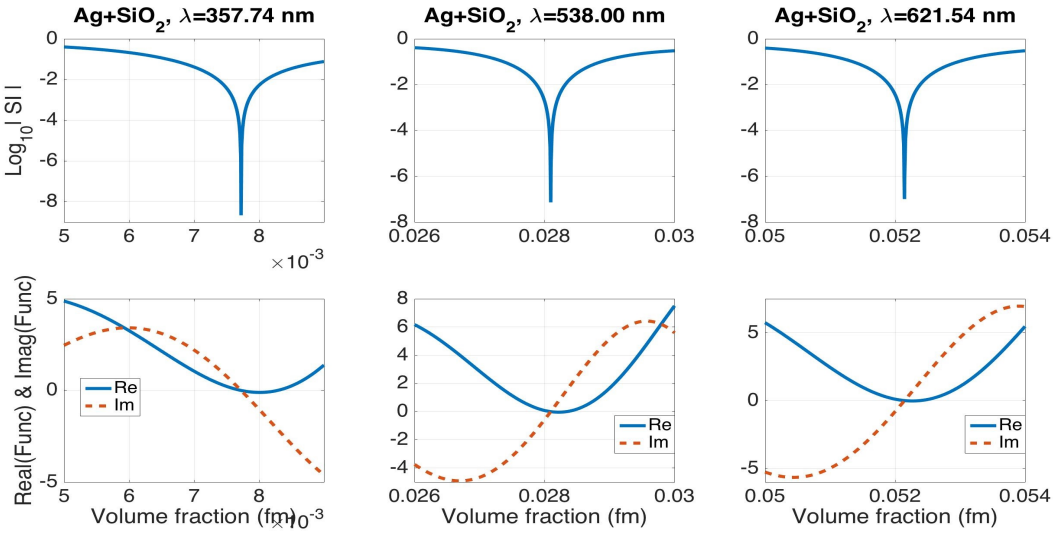

Figure 5.6: Top row shows CPA for different frequencies as a function of volume fraction (f_m) for Silver-Silica composite and the bottom row shows at CPA frequency, real and imaginary part of the function become zero. Here, thickness of the medium $d = 10\mu m$ and angle of incidences $\theta_i = 45^o$.

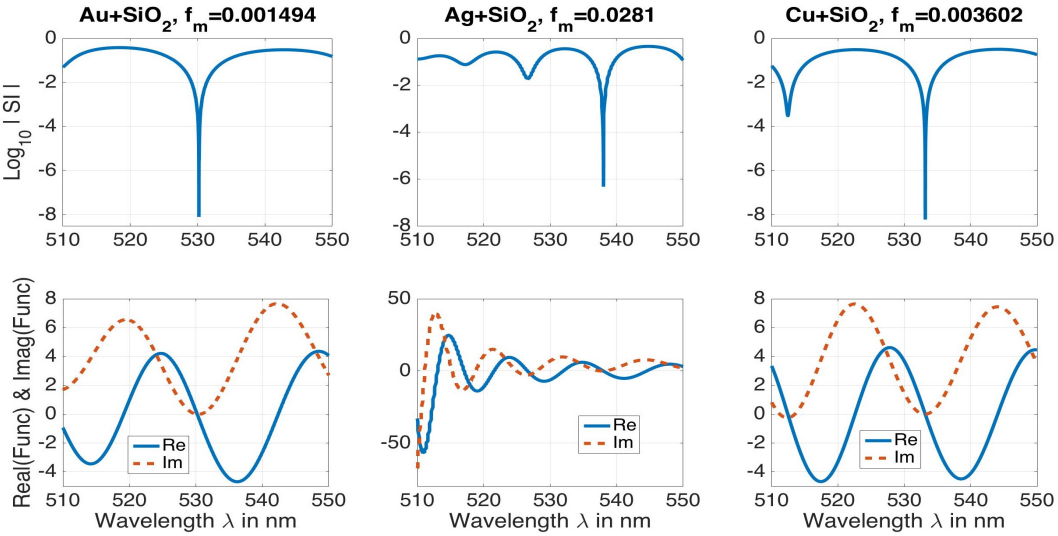

Figure 5.7: Top row shows CPA for different volume fraction as a function of wavelengths for different metal-dielectric composite and the bottom row shows at CPA frequency, real and imaginary part of the function become zero. Here, thickness of the medium $d = 10\mu m$ and angle of incidences $\theta_i = 45^o$.

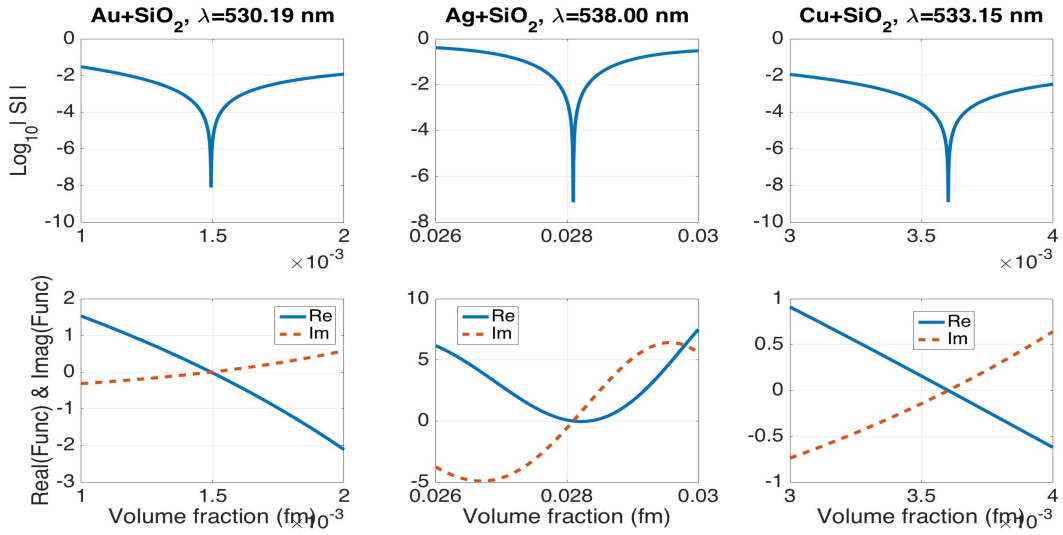

Figure 5.8: Top row shows CPA for different frequency as a function of volume fraction (f_m) for different metal-dielectric composite medium and the bottom row shows at CPA frequency, real and imaginary part of the function become zero. Here, thickness of the medium $d = 10\mu m$ and angle of incidences $\theta_i = 45^o$.

that real and imaginary parts of the eq.(5.27) are both simultaneously zero at all values of the wavelength where CPA is found to occur in numerical results of Chapters 2 and 3. Thus this agreement between the theory and numerical results clearly show that CPA occurs due to destructive interference between the contributions of the two oppositely directed waves incident on the medium.

Owing to the transcendental nature of the above equation (5.27) it is not possible to solve it exactly except in certain limiting cases. Let us now consider a very thin medium of thickness much less compared with the incident wavelength. Indeed in this limiting case it is possible to approximate $sin(2k_{2z}d)$ by $2k_{2z}d$ in (5.27) to arrive at the result:

$$2k_{1z}k_{2z} + i(k_{2z}^2 - k_{1z}^2)2k_{2z}d = 0 \tag{5.28}$$

which can be simplified further to obtain

$$k_{2z}^2 = k_{1z}^2 + ik_{1z}/d \tag{5.29}$$

Using the relation $k_{iz}^2 = k_o^2\epsilon_i$, i=1, 2 the above equation simplifies further to yield the required dielectric constant of the CPA medium as

$$\epsilon_2 = \epsilon_1 + i\frac{\sqrt{\epsilon_1}}{(k_o d)}\cos\theta_i \tag{5.30}$$

Note that this expression is derived in the limit $k_o d$ much smaller than unity hence the imaginary part which contains the term $\frac{1}{(k_o d)}$ will be very large in order to fulfill the CPA criterion.

5.6 Conclusion

In this chapter we have developed a theoretical formulation of CPA in order to gain insight into the complicated process of coherent perfect absorption and to explain the numerical results of CPA in composite mixtures of metals and dielectric. Excellent agreement between the results obtained from the theoretical expression and the numerically computed results for CPA of previous chapters is observed.

Although due to complicated form of the theoretical CPA eq.(5.27)) exact solutions cannot be obtained, analytical results are extracted in the limit of ultra-thin (sub-wavelength) film and it is seen that the imagingary part of the medium is inversely proportional to the thickness of the CPA medium and hence is expected to be very high. This is in accordance with previous numerical deductions wherein it was shown that large filling fractions for metal (which enhances absorption) are needed at lower thickness of the CPA medium [5]. Recent technological advancements particularly in the field of nanotechnology has made it feasible to fabricate such sub-wavelength thin film structures [14].

Bibliography

[1] P. Yeh, "Optical waves in layered media", (John wiley and sons, New York (1988)) pp. 83.

[2] D. G. Sourya, O. J. F. Martin, S. Dutta Gupta, G. S. Agarwal, "Controllable coherent perfect absorption in a composite film", Opt. Exp. 20, 1330(2012).

[3] S. Dey, "Coherent perfect absorption using Gaussian beams", Opt. Comm. ,Vol.356 , pp. 515-521(2015).

[4] S. Dey and S. Singh, "Coherent perfect absorption with Gaussian beams", IIT-Delhi-WRAP2013-10.10.131111.

[5] P. B. Johnson and R. W. Christy, "Optical constants of the noble metals", Phys. Rev. B, Vol.6, pp. 4370–4379(1972).

[6] W. Cai and V. Shalaev, "Optical Metamaterials:Fundamentals and Applications", Springer, NewYork(2010), pp. 25.

[7] C. F. Bohren and D. R. Huffman, "Absorption and Scattering of Light by Small Particles", John Wiley & Sons, New York (1983) pp.77.

[8] G. L. Fischer, R. W. Boyd, R. J. Gehr, S. A. Jenekhe, J. A. Osaheni, J. E. Sipe, and L. A. Weller-Brophy, "Enhanced nonlinear optical response of composite materials", Phys. Rev. Lett. Vol.74, pp. 1871 (1995).

[9] G. S. Agarwal, and S. Dutta Gupta, "T-Matrix approach to the nonlinear susceptibilities of heterogeneous media", Phys. Rev. A, Vol.38, pp. 5678 (1988).

[10] S. Dutta Gupta, "Nonlinear optics of Stratified media", Progress in Optics, E.Wolf, ed.(Elsevier Science, 1998), Vol. 38, pp.1-84.

[11] M. Born and E. Wolf, "Principle of Optics", 7th ed., Cambridge University Press, New York(2005), pp.75.

[12] L. Novotny and B. Hecht, "Principle of Nano-Optics", Cambridge University Press, New York(2006), pp.45.

[13] H. Noh, Y. Chong, A. D. Stone, and H. Cao "Perfect coupling of light to surface plasmons by coherent absorption", Phys. Rev. Lett. Vol.108, 186805 (2012).

[14] P. Feng, W. D. Li and W. Zhang, "Dispersion engineering of plasmonic nanocomposite for ultrathin broadband optical", Opt. Exp. Vol. 23, No. 3, 2329 (2015).

Chapter 6

Coherent Perfect Absorption in Layered Medium

6.1 Introduction

In this chapter a study of CPA in a layered medium consisting of a few layers of composite and spacer medium is presented. Here, initial and final layers are fixed but the middle layers can be shifted to create symmetric and asymmetric situations. In such situations, we have calibrate all basic parameters for which it is possible to get CPA.

The organization of the chapter is as follows: The next section deals with definition of geometry of the system and formulation of the problem. Third section contains numerical results and discussions. In the final section we summarise our results and draw conclusions. Here we draw some of the major results and indicate their possible uses for displacement sensing.

6.2 Geometry and formulation

Consider a layered structure made of metal-dielectric composite mediums (CM) and spacer (or air) layers as shown in the fig. 6.1. Faire intention to choose such a structure to create symmetrical and asymmetrical situation on the structure. Lets we describe the structure from a symmetric position. Here, d_1, d_2, d_3, d_4 and d_5 are the width of five layers and their respective per-

mittivities are ϵ_{CM}, ϵ_{Air}, ϵ_{CM}, ϵ_{Air} and ϵ_{CM} respectively in the system, where, $d_1 = d_5 = d_{CM}$ and $d_2 = d_4 = d_{sp}$ ('sp' stands for space). A small asymmetry can be achieved by shifting the d_3 layer on space layers (i.e. on d_2 and d_4) by shifting a small distance δ to the left or right and making $d_2 = d_{sp} \mp \delta$ and $d_4 = d_{sp} \pm \delta$ respectively but the total optical path in the structure is constant. The whole system we assume to be non magnetic.

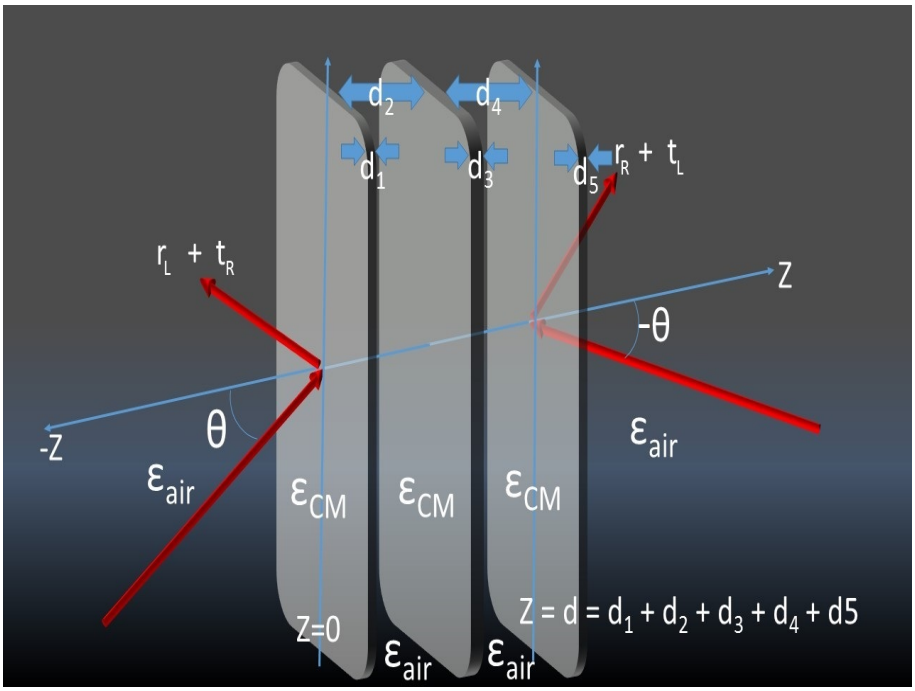

Figure 6.1: Schematic view of the layered medium. Two identical light waves focus (or incident) on opposite interfaces of the system on CM and air layered medium. Here, r_L (t_L) and r_R (t_R) are reflection (transmission) coefficient at the left and right side interface respectively. Various coordinate systems are also shown in the figure.

Two similar s-polarised (TE) light incident on the outer most CM parallel slabs from opposite directions with equal angles of incidence θ and $-\theta$ with the normal at Z = 0 and Z = d respectively as shown in the fig.6.1. We use the label L and R for left and right side respective incident waves. Hence, the resulting reflected (transmitted) waves are denoted as r_L (t_L) and r_R (t_R) respectively. Here we have monitor only the attenuated scattering intensity (SI). So that total SI at $Z = 0$ and $Z = d$ are square of scattering amplitude (SA) i.e. $r_L + t_R$ and $r_R + t_L$ respectively. Consider CM is a homogeneous

mixture of metal and dielectric. The effective permittivity of CM is calculating from Bruggeman effective medium theory (BEMT) [11, 12] which is described in the following equation.

$$\epsilon = \frac{1}{4}\{(3f_1 - 1)\epsilon_1 + (3f_2 - 1)\epsilon_2 \pm \sqrt{[(3f_1 - 1)\epsilon_1 + (3f_2 - 1)\epsilon_2]^2 + 8\epsilon_1\epsilon_2}\} \tag{6.1}$$

Here, ϵ_1, $\{f_1\}$ and ϵ_2, $\{f_2 = (1 - f_1)\}$ are permittivity {volume fraction} of metal and dielectric respectively. The sign of the above equation is to be chosen in such a way that the imaginary part of the effective permittivity is positive. The optical constant or permittivity of metals are obtained by interpolating the experimental data from et. al. Johnson and Christy [16] for all optical wavelength range. Dielectric's permittivity was taken constant on the visible wavelengths ranges. The reflection coefficient (r_L or r_R) and transmission coefficient (t_L or t_R) for the layered medium for each spatial harmonic was calculated using the characteristics matrix method [13, 14, 15].

The reflection and transmission coefficient for a system shown in fig. 6.1 can be calculated using the standard characteristic matrix formula. The general expression of the amplitude of reflection (r) and transmission (t) coefficients are given by following .

$$r = \frac{(m_{11} + m_{12}p_f)p_i - (m_{21} + m_{22}p_f)}{(m_{11} + m_{12}p_f)p_i + (m_{21} + m_{22}p_f)} \tag{6.2}$$

$$t = \frac{2p_i}{(m_{11} + m_{12}p_f)p_i + (m_{21} + m_{22}p_f)} \tag{6.3}$$

Where m_{ij} $(i, j = 1, 2)$ are the elements of the total characteristic matrix of the structure (expressions for m_{ij} , $i, j = 1, 2$ can be found) and

$$p_{i,f} = \sqrt{\epsilon_{i,f}/\mu_{i,f}}\cos\theta_{i,f}, \quad \text{for} \quad TE\text{- polarisation} \tag{6.4}$$

$$p_{i,f} = \sqrt{\mu_{i,f}/\epsilon_{i,f}}\cos\theta_{i,f}, \quad \text{for} \quad TM\text{- polarisation} \tag{6.5}$$

and $\theta_{i,f}$ are the angles of incidence and emergence in the first and the last medium respectively.

6.3 Numerical results and discussion

In this section we present numerical results pertaining to the reflection and transmission coefficients for left (L) and right (R) of oblique incidence with

TE polarized light. For calculating $|r_L|$, (t_L) and r_R, (t_R) we use characteristic matrix method [13, 14, 15] parameters as follows. Initial and final medium's permittivities are $\epsilon_i = \epsilon_f = 1$, because these are space or air medium. The width of the layers are $d_1 = d_5 = 3000$ nm, $d_2 = d_4 = 1180.06$ nm and $d_3 = 4000$ nm for the structure in symmetric position. Here d_1, d_3 and d_5 are made of same Gold (Au) − Silica (SiO_2) composite and there permittivities ware calculated using BEMT eq. 6.1. From the interpolated data of Au [16]

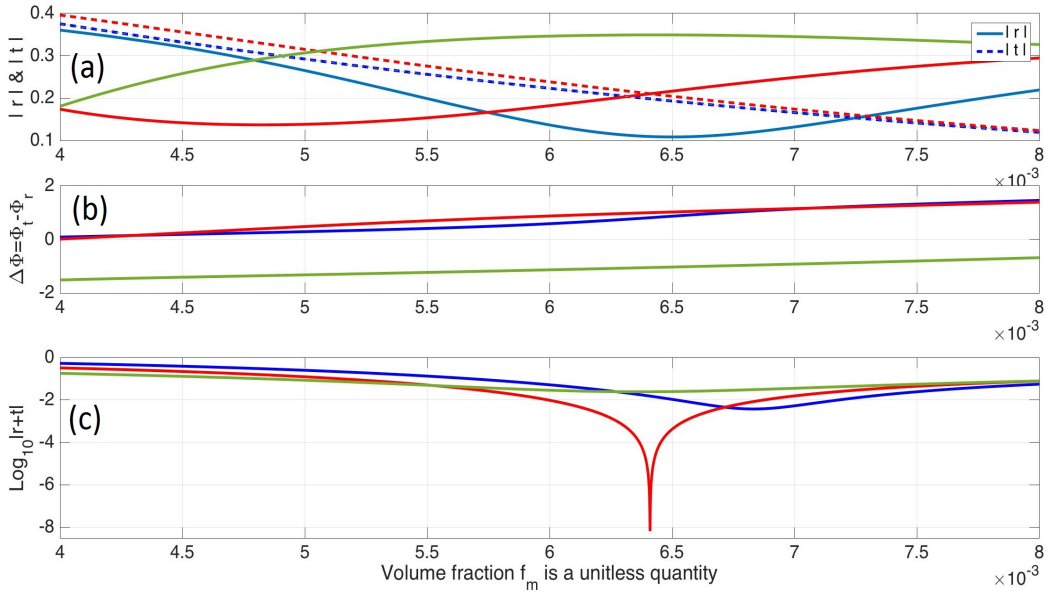

Figure 6.2: (a) Absolute values of reflected (solid line) and transmitted (dash line) amplitudes $|r_L|$ and $|t_R|$, (b) phase difference, $\Delta\phi$ (scale of π) between the right transmitted $(\Phi_{t_R})$and left reflected (Φ_{r_L}) plane waves of scale of π and (c) $log_{10}|SI|$ as a function of volume fraction (f_m) for $\lambda = 590.03$ nm.

one can find permittivity at 590.03 nm wavelength is $\epsilon_{Au} = -8.3421 + 1.6348i$, permittivity of Silica as $\epsilon_{SiO_2} = 2.25$ and angle of incidence $\theta_i = 45^o$. From the fig. 6.2, it is observed that the maximum absorption is recorded at the volume fraction $(f_m = 0.00641)$.

So, using eq. 6.1 at volume fraction, $f_m = 0.00641$ and wavelength, $\lambda = 590.03$ nm the permittivity of CM is calculated and that to be $\epsilon_{CM} = 2.3667 + 0.0371i$. The reflection coefficient from left hand side (r_L) and transmission coefficient from right hand side (t_R) are calculated from eqs. 6.2 and 6.3 respectively. There after $log_{10}|SI|$ is calculated. Now, the d_3 layer is shifted

a small amount i.e. $\delta = 59.03$ nm to the left and right side into the adjacent spacer layers (i.e. d_2 and d_4) with respect to the symmetric structure of the system.

The fig. 6.2(c) shows that absorption of incidence lights is calculated by

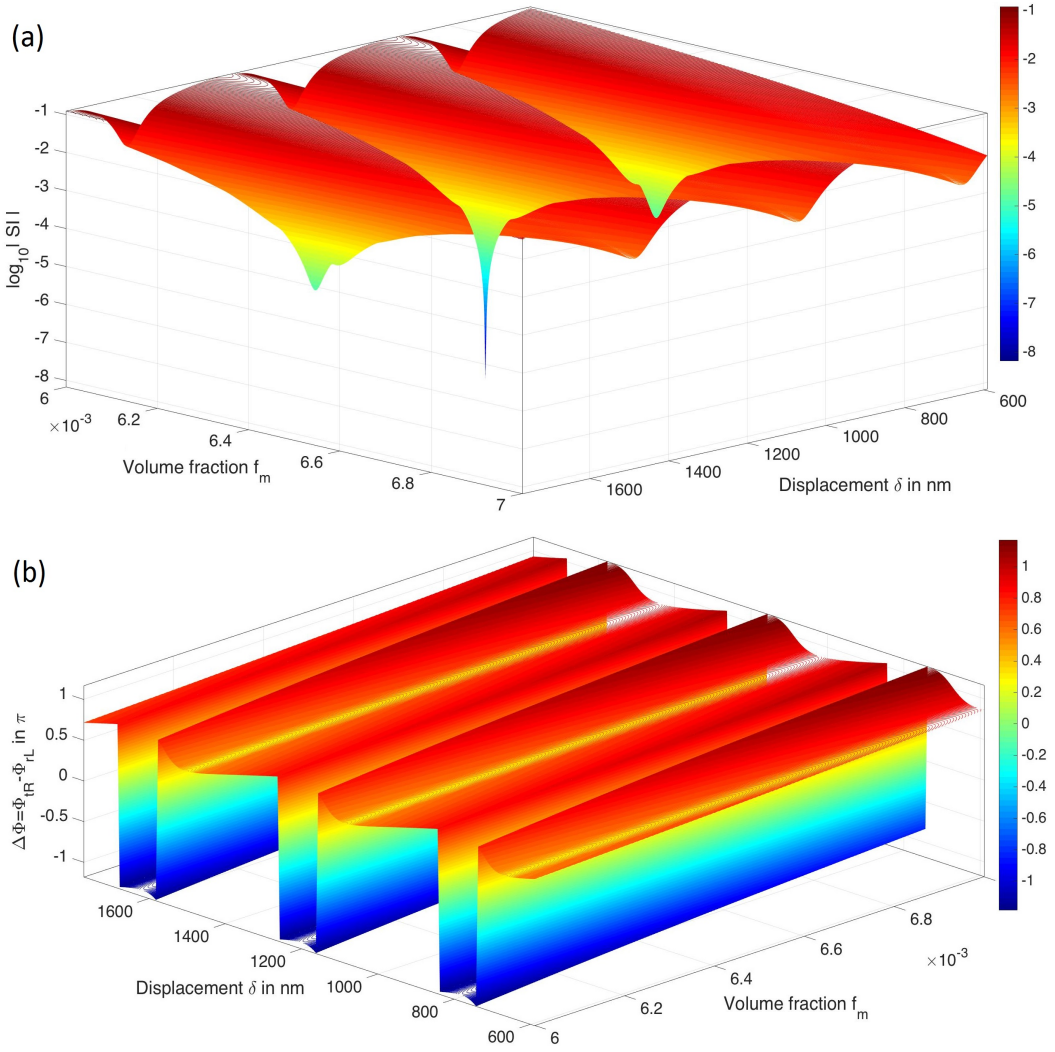

Figure 6.3: (a) $log_{10}|SI|$ and (b) corresponding phase $\Delta\phi$ (scale of π) as functions of volume fraction (f_m) and space of d_2 layer for δ displacement

evaluating $log_{10}|SI|$ as a function of volume fraction (f_m) for different positions of d_3 layer's which may be classified by left(asymmetric), middle(symmetric) and right(asymmetric) side and shown with solid blue, red and green lines respectively. We only noted the spacing of d_2 layers is given in the figure(fig. 6.2(c)), for the shifting of d_3 layers. We must remind that due to moving of

d_3 layer, both d_2 and d_4 layers will be affected.

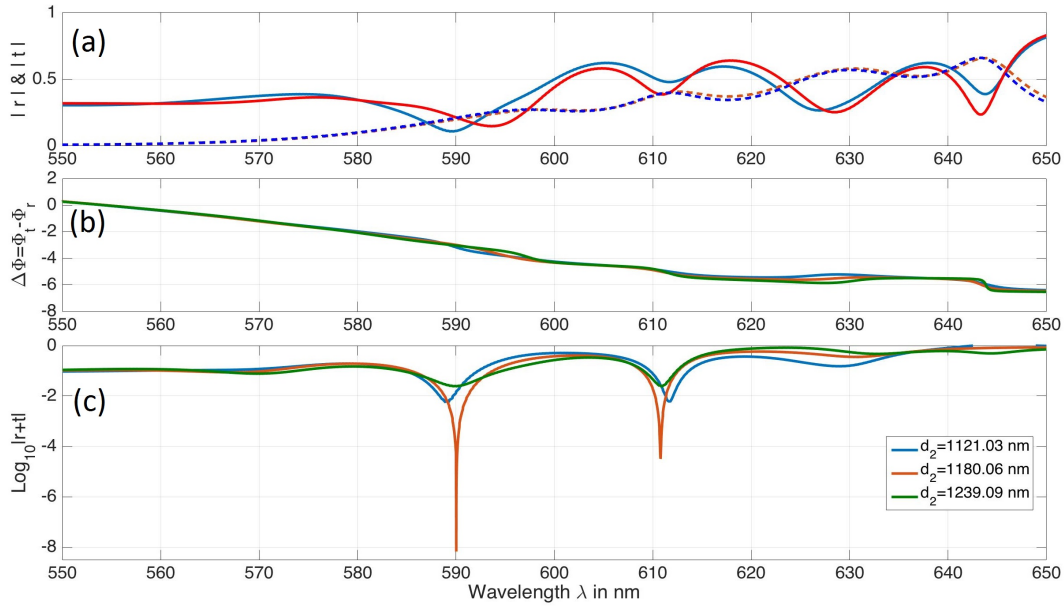

Figure 6.4: (a) Absolute values of reflected (solid line) and transmitted (dash line) amplitudes $|r_L|$ and $|t_R|$, (b) phase difference, $\Delta\Phi$ (scale of π) between the right transmitted (Φ_{t_R})and left reflected (Φ_{r_L}) plane waves of scale of π and (c) $log_{10}|SI|$ as a function of wavelength (λ) for volume fraction $f_m = 0.00641$.

Fig. 6.2(a) shows the reflection (solid line) coefficient of LHS and transmission (dash line) coefficient RHS are plotted as a function of volume fraction (f_m) when simultaneously light is shining in the structures and their corresponding phase difference are plotted in the fig. 6.2(b) as function of volume fraction (f_m). All these respective colour lines represent above mentions structural conditions. More extensive and explanatory figure is fig. 6.3(a), where $log_{10}|SI|$ is plotted under both functions, volume fraction (f_m) and position of d_3 (spacing of d_2 is only given in the figure). Here, spacing of d_2 goes from 600 nm to 1600 nm and where as correspondingly d_4 goes from 1600 nm to 600 nm respectively. A wide area of volume fraction (f_m) can be chosen to achieve CPA for $\lambda = 590.03$ nm wavelength which are shown by the region from orange to blue colour in the fig. 6.3(a). The variation of corresponding phase difference ($\Delta\Phi$) between r_L and t_R is plotted in the fig. 6.3(b) under the same functions of variables.

Now we have observed in the fig. 6.4, reflection coefficient ($|r_L|$), transmission coefficient ($|t_R|$), their phase difference ($\Delta\Phi$) and $Log_{10}|SI|$ as a function

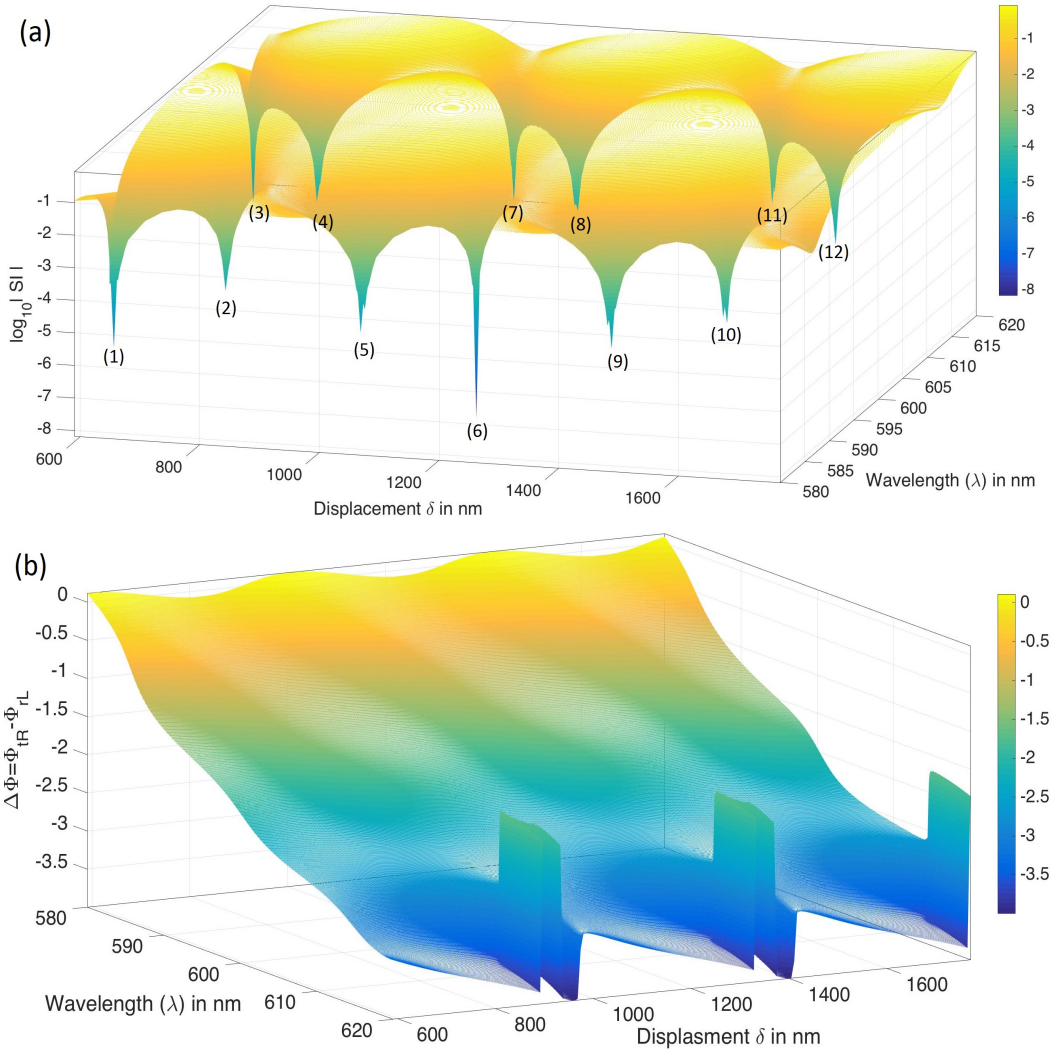

Figure 6.5: (a) $log_{10}|SI|$ and (b) corresponding phase $\Delta\phi$ (scale of π) as functions of wavelength (λ) and space of d_2 layer for δ displacement

of wavelengths (λ) where the volume fraction is fixed at $f_m = 0.00641$ for all CM layers. These also indicate new possibilities to get CPA at two distinct wavelengths for the same symmetric and asymmetric structures (fig. 6.4(c)) under oblique angle of illumination i.e. at 45^o of incidence. The magnitude of the $|r_L|$, $|t_R|$ curves and their corresponding phase difference imply amplitude attenuation which leads to destructive interference or CPA at more than one frequency for all of the different structures.

In figure 6.5 we have studied that the Log_{10} of SI and phase difference

between r_L and t_R as a function of wavelengths (λ) and width of d_2 due to continuously moving the d_3 layers. Obviously, d_4 layer is also affected reverse way to the d_2 layer. Figure 6.5(a) have several islands with sharp dips indicates that CPA is occurring for several pairs of parameter values, where the third parameter, volume fraction ($f_m = 0.00641$) is constant for all CM layers. And the fig. 6.5(b) shows that corresponding phase difference between r_L and t_R of the above figure which implies always equal or closer to π when the parameters shows CPA on the structure of the system. From the fig. 6.5(a), all absorption dips are numbered and their corresponding data values are in the following table.

Absorption Picks of fig.6.5(a)				
Dip No.	d_2 in nm	d_4 in nm	Wavelength (λ) (in nm)	$Log_{10}\|SI$
1	595.9	1764.1	587.4	-6.3
2	761.1	1598.9	590	-4.8
3	607.7	1752.3	614.4	-5.4
4	743.4	1616.6	610.8	-4.7
5	1009	1351	587.4	-5.4
6	1180	1180	590	-8.2
7	1044	1316	614.4	-4.8
8	1180	1180	610.8	-4.5
9	1428	932	587.4	-5.4
10	1599	761	590	-4.8
11	1475	885	614.5	-4.4
12	1611	749	610.8	-4.9

We can group them in four sets of absorption picks are as {(1), (5) & (9)}, {(2), (6) & (10)}, {(3), (7) & (11)} and {(4), (8) & (12)} have CPA at 587.4 nm, 590.03 nm, 614.4 nm and 610.8 nm wavelengths respectively for different position of the structure. From fig. 6.4 and 6.5 (picks no. (6) and (8)) shows CPA in two discrete wavelengths (i.e. 590.03 nm and 610.8 nm respectively) for any fixed position of the structure. similarly, One can shows for other distinct position also have such absorption [5] after plotting entire wavelength range.

6.4 Summary and conclusion

We have presented a study of the coherent perfect absorption (CPA) in a system of composite and spacer layered medium with symmetric and asymmetric structures. The structure was illuminated by two identical coherent light waves from opposite side with same angle of incidence with the normal. Here, we achieved symmetric and asymmetric structures by moving the middle CM layer into the spacer layers to the left and right to show some more possibilities to obtain CPA. The composite medium's permittivity was calculated by the Bruggeman effective medium theory (BEMT). The reflection and transmission coefficients of the multi-layered system ware calculated using characteristic matrix methods. A detailed analysis of the CPA dips as a function of the volume fraction (fig. 6.2) and the wavelengths (fig. 6.4) for multi-layers (of CM and spacer layers) was carried out. Figure 6.3 state that CPA can be possible in the whole orange to blue colour region for corresponding volume fraction and structural position. Again CPA could be achieve in two different frequencies for any fix position (figs. 6.4 & 6.5) in the structure of the multi layer Composite medium dispersion. And farther, three distinct structural configuration shows CPA at a discrete wavelength for a fixed volume fraction in the system The main results of this study is that the controllability of the frequency in symmetric / asymmetric layer structure and the possibility of CPA at more than one frequency in the dispersive sample.

Bibliography

[1] C. F. Gmachl, "Suckers for light" Nature 467, 37–39 (2010).

[2] W. Wan, Y. D. Chong, L. Ge, H. Noh, A. D. Stone, and H. Cao, "Time-reversed lasing and interferometric control of absorption", Science 331, 889-892 (2011).

[3] H. Noh, Y. Chong, A. D. Stone, and H. Cao, "Perfect coupling of light to surface plasmons by coherent absorption" Phys. Rev. Lett. 108, 186805 (2012).

[4] M. Pu, "Ultra thin broadband nearly perfect absorber with symmetrical coherent illumination" Opt. Express 20, 2246–2254 (2012).

[5] D. G. Sourya, O. J. F. Martin, S. Dutta Gupta, G. S. Agarwal, "Controllable coherent perfect absorption in a composite film", Opt.Express 20(2012)1330.

[6] J. Zhang, "Coherent perfect absorption and transparency in a nano structured graphene film", Opt. Express 22, 12524 (2014).

[7] Y. Fan, "Tunable mid-infrared coherent perfect absorption in a graphene meta-surface", Sci. Rep. 5, 13956 (2015).

[8] S. Dey, "Coherent perfect absorption using Gaussian beams", Opt. Comm. 356(2015)515-521.

[9] H. Noh, Y. Chong, A. D. Stone, and H. Cao "Perfect coupling of light to surface plasmons by coherent absorption", PRL 108, 186805 (2012).

[10] S. Duttagupta, "Strong interaction mediated critical coupling at two distinct frequencies", Opt Lett, Vol. 32, 11, pp. 1483-1485 (2007).

[11] C. F. Bohren and D. R. Huffman, "Absorption and Scattering of Light by Small Particles", John Wiley & Sons, NewYork(1983), p.77.

[12] W. Cai and V. Shalaev, "Optical Metamaterials:Fundamentals and Applications", Springer, NewYork(2010), p.25.

[13] S. Dutta Gupta, "Nonlinear optics of Stratified media", Progress in Optics, E.Wolf, ed.(Elsevier Science, 1998), Vol. 38, p.1

[14] M. Born and E. Wolf, "Principle of Optics", 7th ed., Cambridge University Press, NewYork(2005), p.75.

[15] L. Novotny and B. Hecht, "Principle of Nano-Optics", Cambridge University Press, NewYork(2006), p.45.

[16] P. B. Johnson and R. W. Christy, "Optical constants of the noble metals", Phys. Rev. B 6 (1972)4370–4379.

Chapter 7

Summary and Conclusions

In this work it is demonstrated that by employing metal-dielectric composites instead of just pure dielectrics or bulk metals, one can develop a tunable (or broadband) coherent perfect absorber that can operate at any desired visible or near-infrared wavelength with the frequency controlled by the metal filling factor of the metal (s) in the metal-dielectric composite.

Chapter 1 dealt with an introduction to the interesting and important phenomenon of coherent perfect absorption (CPA), wherein we presented earlier developments, progress made in this field, current status, the concept and motivation for taking up this study. A brief overview of metal-silica composite was also presented since it is seen as a potential medium for investigation of the CPA.

Chapter 2 dealt with designing and characterization of various types of composite materials using metals (Au, Ag etc.) and dielectric (SiO_2). The effective permittivity of two-component (metal-dielectric) composite medium was estimated using the more versatile Bruggeman effective medium theory. Next using the extended Bruggeman effective medium theory, the effective permittivity of three-component (metal-metal-dielectric) composite medium was also estimated. It may be noted that three-component composite can be made in three distinct ways, these are: (i) by direct use of three-component Bruggeman effective medium theory and (ii) by successive application of two-component Bruggeman effective medium theory in the following manner: (a) a two-component (metal-dielectric) composite is first constructed using metal

'A' and SiO_2. Next using the above composite, and metal 'B' another two-component (metal-composite) mixture is constructed. (b) The process of (a) is repeated by using metal 'B' first and then metal 'A' that is, interchanging metals 'A' and 'B' in the components. The effective dielectric constants (permittivities) are plotted to highlight the difference between the bulk and composite materials.

In chapter 3, CPA in a two-component metal-dielectric heterogeneous medium is investigated by illuminating, (at oblique incidence) the opposite sides of the medium with two laser beams of Gaussian intensity profile. The effective permittivity of the two-component (metal-dielectric) composite medium was estimated using the Bruggeman effective medium theory. The dependence of CPA on various parameters: the filling fraction, the thickness of the slab and wavelength was explored in detail and is noted that a little absorption is necessary for the occurrence of CPA. The major finding of this study is that CPA effects still persists for Gaussian beams.

In chapter 4, the characteristics of CPA were investigated in a three-component composite medium which is made of different combinations of Gold (Au), Silver(Ag) and Silica (SiO_2). We have shown results for three component composites by first optimizing all basic parameters to get CPA in $Au - SiO_2$ and $Ag - SiO_2$ composites very close to a single wavelength say around λ_1. We have then constructed a new three-component composite medium comprising $Au + Ag + SiO_2$ with similar volume fractions and have found CPA occurring at different (higher) wavelengths and with broader widths. It is also shown that there are three ways in which one can construct a three-components composite using two metals and a dielectric. However comparison of CPA characteristics in these three distinct cases reveals that, except for a slight variation in the position of the wavelength where maximum CPA occurs other features are similar. The most significant outcome of this study is the intriguing effect of the width of the composite on CPA. With increasing width the CPA resonance shows red shift and number of absorption peaks are increased which can be attributed to the CPA (resonator) cavity effect.

In chapter 5 we have developed a theoretical formulation of CPA in order to gain insight into the complicated process of coherent perfect absorption and

to explain the numerical results of CPA in composite mixtures of metals and dielectric. Excellent agreement between the results obtained from the theoretical expression and the numerically computed results for CPA of previous chapters is observed.

In chapter 6, a study is presented of the coherent perfect absorption (CPA) in a system of composite and spacer layered medium with symmetric and asymmetric structures. The structure was illuminated by two identical coherent light waves from opposite side with same angle of incidence with the normal. The symmetric and asymmetric structures were obtained by moving the middle CM layer into the spacer layers to the left and right to show some more possibilities to obtain CPA. The permittivity of the composite medium was estimated through Bruggeman effective medium theory (BEMT). The reflection and transmission coefficients of the multi-layered system ware calculated using characteristic matrix methods. A detailed analysis of the CPA dips as a function of the volume fraction and the wavelength for multi-layers (of CM and spacer layers) was carried out. It was demonstrated that it is possible to attaining CPA in the whole orange to blue colour region for certain volume fraction and structural position. Again CPA could be achieved at two different frequencies for any fixed position in the structure of the multi layer Composite medium dispersion. And further, three distinct structural configuration shows CPA at a discrete wavelength for a fixed volume fraction in the system The main results of this study is that the controllabelity of the frequency in symmetric / asymmetric layer structure and the possibility of CPA at more than one frequency in the dispersive sample.

7.1 Future Scope

: The present study does not taken into account the shape and size of the metal particles. Particle shape is an important issue since the Bruggeman effective medium theory and other mean-field theories like Maxwell–Garnett Theory, Clausius–Mossotti relation are all based on the assumption that the metal particles (inclusions) are spherical particles. When the shape of the inclusion particles is notably non-spherical, modified forms of Maxwell–Garnett Theory or Bruggeman effective medium theory must be used with an additional depolarization or screening factor that accounts for the effect of particle shape.

Many other effective medium models are available that extend the original approach (of Maxwell - Garnett, Bruggeman) to take into account shapes, aggregation, sizes and shape distribution. These can be applied to calculate optical properties of the composite materials.

However to better understand and analyze the experimental data involving nano-particles, one has to address the fine features of the composite down to the sub-wavelength scale. For this purpose one has to employ more sophisticated effective medium approaches such as the Bergman–Milton representation which fully taken into account the micro- or nano-scale by defining geometrical functions whose analytical properties are quite general. It is usually felt that there is no general answer to which is the best effective medium approximation to characterize a composite material. Nevertheless, most of the time a thorough comparison between theory and optical experiments is the only possible means of determining which is the most suitable model under the given conditions of experiments and the material.

Chapter 8

Anti-Plagiarism Verification Reports and Certificate

This is certify that the thesis entitled
*"**Tunable coherent perfect absorption in single & multilayered metal-dielectric composite media**"*
submitted by **Sanjeeb Dey** bearing registration number **10PhPh17** has gone through anti plagiarism verification and is found to have 24% similarity index, among which 16% similarity is from his own published papers.

Hence, excluding the similarity index of 16% corresponding to his own published paper, the actual similarity index is found to be less than 10%. Whereas University of Hyderabad permits similarity index upto 15%. The anti plagiarism verification document issued by University of Hyderabad is attached.

Therefore, the thesis is recommended and forwarded for award of **Doctor of Philosophy**.

Supervisor

(Prof. Suneel Singh)

TUNABLE COHERENT PERFECT ABSORPTION IN SINGLE & MULTI LAYERED METAL DIELECTRIC COMPOSITE MEDIA

ORIGINALITY REPORT

%24	%2	%24	%1
SIMILARITY INDEX	INTERNET SOURCES	PUBLICATIONS	STUDENT PAPERS

PRIMARY SOURCES

1	Dey, Sanjeeb. "Coherent Perfect Absorption using Gaussian beams", Optics Communications, 2015. Publication	%16
2	W. Cai. "Optical Properties of Metal-Dielectric Composites", Optical Metamaterials, 2010 Publication	%2
3	Shourya Dutta-Gupta. "Controllable coherent perfect absorption in a composite film", Optics Express, 01/16/2012 Publication	%1
4	W. Cai. "Introduction", Optical Metamaterials, 2010 Publication	<%1
5	Dey, Sanjeeb, and Suneel Singh. "Coherent perfect absorption with Gaussian beams", Workshop on Recent Advances in Photonics (WRAP), 2013. Publication	<%1
6	Shourya Dutta Gupta. "Signature of strong	

	atom–cavity interaction on critical coupling", Journal of Optics, 07/01/2010 Publication	<%1
7	Subimal Deb. "Absorption and dispersion in metamaterials: Feasibility of device applications", Pramana, 11/2010 Publication	<%1
8	www.eng.yale.edu Internet Source	<%1
9	Submitted to The Hong Kong Polytechnic University Student Paper	<%1
10	Macleod, Angus. "Some aspects of absorption and gain", Optical Systems Design 2015 Advances in Optical Thin Films V, 2015. Publication	<%1
11	Stefano Longhi. "Coherent perfect absorption in a homogeneously broadened two-level medium", Physical Review A, 05/2011 Publication	<%1
12	pureapps2.hw.ac.uk Internet Source	<%1
13	Advanced Electromagnetics and Scattering Theory, 2015. Publication	<%1
14	M. J. Chester. "Grazing-incidence x-ray photoelectron spectroscopy from multilayer	<%1

	Physical Review B, 12/1993 Publication	
15	es.scribd.com Internet Source	<%1
16	Piyawattanametha, W, and T D Wang. "MEMS-Based Dual-Axes Confocal Microendoscopy", IEEE Journal of Selected Topics in Quantum Electronics, 2010. Publication	<%1
17	Kumari, M.. "Positive and negative giant Goos-Hanchen shift in a near-symmetric layered medium for illumination from opposite ends", Optics Communications, 20120301 Publication	<%1
18	physics.niser.ac.in Internet Source	<%1
19	Tianjie Chen. "Electrodynamics analysis on coherent perfect absorber and phase-controlled optical switch", Journal of the Optical Society of America A, 05/01/2012 Publication	<%1
20	www.ece.nus.edu.sg Internet Source	<%1
21	David C. Dobson. "Optimization of Periodic Composite Structures for Sub-Wavelength Focusing", Applied Mathematics and Optimization, 12/24/2008	<%1

Publication

22	Heeso Noh. "Perfect coupling of light to surface plasmons by coherent absorption", Physical Review Letters, 05/2012 Publication	<%1
23	Submitted to University of Southampton Student Paper	<%1
24	Quinten, . "Effective Medium Theories", Optical Properties of Nanoparticle Systems Mie and beyond, 2011. Publication	<%1
25	Kotlicki, Omer, and Jacob Scheuer. "Wideband coherent perfect absorber based on white-light cavity", Optics Letters, 2014. Publication	<%1
26	Chong, Y. D., Hui Cao, and A. D. Stone. "Noise properties of coherent perfect absorbers and critically coupled resonators", Physical Review A, 2013. Publication	<%1
27	M. Kulkarni. "Control of superluminal transit through a heterogeneous medium", Journal of Modern Optics, 3/1/2004 Publication	<%1
28	docslide.us Internet Source	<%1
29	www.me.iitb.ac.in Internet Source	<%1

30	A S Arnold. "Diffraction-limited focusing of Bose–Einstein condensates", Journal of Physics B Atomic Molecular and Optical Physics, 01/28/2004 Publication	<%1
31	www.ikb.poznan.pl Internet Source	<%1
32	par.nsf.gov Internet Source	<%1
33	Ben-Benjamin, J.S., and L. Cohen. "Snell's law and SOFAR channels: a particle view", Journal of Modern Optics, 2015. Publication	<%1
34	Rao Lian-Zhou. "Tightly Focusing of Circularly Polarized Vortex Beams through a Uniaxial Birefringent Crystal", Chinese Physics Letters, 09/2008 Publication	<%1
35	Joohyun Koh. "Correlation of real time spectroellipsometry and atomic force microscopy measurements of surface roughness on amorphous semiconductor thin films", Applied Physics Letters, 1996 Publication	<%1
36	Daniel Ross. "Effective medium theories in surface enhanced infrared spectroscopy: The pentacene example", The Journal of Chemical Physics, 2002 Publication	<%1

37	Yu, . "Introduction to the Parallel FDTD Method", VALU AVX and GPU Acceleration Techniques for Parallel FDTD Methods, 2013. Publication	<%1
38	Digital Media, 2014. Publication	<%1
39	David Langreth. "Derivation of the Landauer conductance formula", Physical Review B, 09/1981 Publication	<%1
40	researchbank.rmit.edu.au Internet Source	<%1
41	www.nickfieller.staff.shef.ac.uk Internet Source	<%1
42	repository.lib.polyu.edu.hk Internet Source	<%1
43	J. Ederth. "Characterization of porous indium tin oxide thin films using effective medium theory", Journal of Applied Physics, 2003 Publication	<%1
44	Bordo. "Linear Optical Properties of Surfaces and Interfaces", Optics and Spectroscopy at Surfaces and Interfaces, 08/08/2005 Publication	<%1
45	Roger, Thomas, Stefano Vezzoli, Eliot Bolduc, Joao Valente, Julius J. F. Heitz, John	<%1

Jeffers, Cesare Soci, Jonathan Leach, Christophe Couteau, Nikolay I. Zheludev, and Daniele Faccio. "Coherent perfect absorption in deeply subwavelength films in the single-photon regime", Nature Communications, 2015.
Publication

EXCLUDE QUOTES	ON	EXCLUDE MATCHES	< 5 WORDS
EXCLUDE BIBLIOGRAPHY	ON		